NASA Contractor Report 172278

P-93

Development of a Reduced Area Horizontal Tail for a Wide Body Jet Aircraft

Jerry J. Rising

LOCKHEED-CALIFORNIA COMPANY
BURBANK, CALIFORNIA

CONTRACT NO. NAS1-15326

FEBRUARY 1, 1984

National Aeronautics and Space Administration

Langley Research Center
Hampton, Virginia 23665

TABLE OF CONTENTS

LIST OF FIGURES

LIST OF FIGURES

LIST OF FIGURES

LIST OF TABLES

LIST OF SYMBOLS

b	Planform span length
c	Chord length
$\bar{c}$	Mean aerodynamic chord
C_D	Drag coefficient $\sim \frac{D}{\frac{1}{2}\rho V^2 S}$
C_L	Lift coefficient $\sim \frac{L}{\frac{1}{2}\rho V^2 S}$
C_{L_H}	Horizontal tail lift coefficient $\sim \frac{L_{TAIL}}{\frac{1}{2}\rho V^2 S_H}$
$C_{L_{TAIL}}$	Tail lift coefficient
$C_{L_{TRIM}}$	Airplane trim lift coefficient
$C_{L_{MAX}}$	Maximum lift coefficient
C_M	Pitching moment coefficient
$C_{M_{.25\bar{c}}}$	Pitching moment coefficient about $0.25\bar{c}$
$C_{M_{\delta_e}}$	Pitching moment versus elevator deflection gradient
$C_{M_{\delta_H}}$	Pitching moment versus horizontal tail deflection gradient
C_p	Pressure coefficient $\sim \frac{p - p_\infty}{\frac{1}{2}\rho V_\infty^2}$
c.g.	Center of gravity
C_{h_H}	Horizontal tail hinge moment coefficient $\sim \frac{h_H}{\frac{1}{2}\rho V^2 S_H \bar{c}_H}$
$C_{h_{H_o}}$	Horizontal tail hinge moment coefficient at zero angle of attack and zero elevator deflection

C_{h_H}/α_H	Horizontal tail hinge moment coefficient gradient with respect to angle of attack
C_{h_H}/δ_e	Horizontal tail hinge moment coefficient gradient with respect to elevator deflection
$C_{h_{e_o}}$	Elevator hinge moment coefficient $\sim \frac{h_e}{\frac{1}{2}\rho V^2 S_e \bar{c}_e}$
C_{h_e}/α_H	Elevator hinge moment coefficient gradient with respect to angle of attack
C_{h_e}/δ_e	Elevator hinge moment coefficient gradient with respect to elevator deflection
CAS	Curvature airfoil shaping procedure
e^X	Wind tunnel model component designation for elevator at X degrees deflection
H_{8C}^X, H_{18}^X	Wind tunnel model component designations of various horizontal tails at X degrees deflection
H_{8C}, H_{16}, H_{17}, H_{18}, H_{19}	Designations for various horizontal tails
KEAS	Knots equivalent airspeed
L/D	Lift to drag ratio
lbs	Pounds
LED	Leading edge down
LEU	Leading edge up
LH	Left hand side
$\frac{\ell_H}{\bar{c}}$	Horizontal distance of the 1/4 $\bar{c}_H$ of the horizontal tail to the 1/4 $\bar{c}$ of the wing in fraction of wing $\bar{c}$

M	Mach number
R_n	Reynold's number $\sim \frac{\rho V c}{\mu}$
R_N	Reynold's number $\sim \frac{\rho V \ell}{\mu}$
$R_{N_{\bar{c}_{H_{exp}}}}$	Reynold's number with the mean aerodynamic chord of the exposed horizontal tail as the characteristic length.
R_N/FT	Reynold's number per foot $\frac{\rho V}{\mu}$
RH	Right hand side
S_H	Horizontal tail area
S_H/S	Horizontal tail area to wing area ratio
S_{REF}	Reference area
sec	Second
SBL	Wind tunnel model butt line, spanwise location
SYM	Symbol
S_{25}	Wind tunnel model component designation for L-1011-1 model with standard wing (without extended tips) and without tail surfaces
TEU	Trailing edge up
TED	Trailing edge down
V_{ROT}	Takeoff rotation speed
V_{MC_A}	Air minimum control speed (speed minimum control speed during takeoff climb with the critical engine inoperative)
$V_{S_{FAA}}$	FAR stall speed (based on the minimum speed obtainable in Flight with a -1 kt/sec entry rate and a forward c.g.)
V_g	Wind tunnel model component designation for vertical tail
W_{27B}	Wind tunnel model component designation for standard wing

$X_{cg}/\bar{c}$	Longitudinal c.g. location aft of the $\bar{c}$ leading edge as a fraction of $\bar{c}$
X/C	Longitudinal location aft of the leading edge of the airfoil chord as a fraction of chord
$\frac{Y}{b/2}$	Spanwise location from the fuselage center line as a fraction of semi-span
Y/C	Vertical location from the airfoil chord line as a fraction of chord
α	Angle of attack
α_H	Angle of attack of horizontal tail
α_1, α_2, α_3	Designation used for angle of attack series used in wind tunnel test
ΔC_D	Drag coefficient increment
$\Delta C_{D_{TAIL}}$	Drag coefficient tail increment due to horizontal tail
δ_e	Elevator deflection angle
δ_H	Horizontal tail deflection angle
δ_F	Flap deflection angle
$\frac{\partial C_{M.25\bar{c}}}{\partial C_L}\Big\|_{C_L=0.3}$	Pitching moment coefficient versus lift coefficient gradient at a lift coefficient of 0.3
η	Dynamic pressure ratio of horizontal tail
$\ddot{\Theta}$	Pitch acceleration
$\Lambda_{.25\bar{c}}$	Planform sweepback angle of the quarter chord line
$\Delta C_{M_{STALL\ REcovery}}$	Pitching moment coefficient increment needed for stall recovery

SUMMARY

Commercial transport aircraft fuel consumption can be significantly reduced by decreasing the size of the horizontal tail. This report documents work accomplished for the NASA Aircraft Energy Efficiency program by Lockheed toward development of a reduced area horizontal tail for a commercial wide-body transport.

A discussion of the work accomplished to reduce the horizontal tail area of the L-1011 is given. The reduced area horizontal tail program consisted of design, fabrication, and wind tunnel testing of horizontal tails with reduced planform areas of 30 to 38 percent relative to the standard L-1011 tail. Profile changes evaluated included leading edge radius, camber, thickness to chord ratio, and high lift devices. Planform changes evaluated were tip configuration, leading edge sweep, aspect ratio, and taper ratio. Included in the report are results of the high-speed and low-speed wind tunnel tests. The total drag of the aircraft in cruise was reduced by approximately 2 percent. However, it was necessary to impose a forward c.g. limiations on the aircraft because the maximum lift goal of the reduced area tail was not achieved and sufficient aircraft nose-up control authority was not available. On a new design this problem could have been solved by moving the landing gear aft and enlarging the cut-out in the aft fuselage to allow for larger horizontal stabilizer deflections. However, since this is an existing design these modifications were unfeasible and resulted in the c.g. restriction.

1. INTRODUCTION

In a conventional airplane design the horizontal tail is sized to provide a specified level of static stability and the required longitudinal control by having an adequate C_{LMAX} in down lift. The requirement for a specific margin of static stability results in large stabilizer surfaces and a forward center-of-gravity (c.g.) range both of which penalize performance in terms of aerodynamic drag and vehicle weight. If an active control system were incorporated into the airplane in its initial design, to provide stability artificially, it is conceivable that the horizontal tail could be sized to provide the required airplane control by using the tail's maximum lift capability in both up and down lift. This would allow the size of the horizontal tail to be significantly decreased, thus decreasing drag and weight. This is shown conceptually in Figure 1.

Accepting the premise that large static margins are unnecessary with the introduction of a stability augmentation system, the aerodynamic objective of this program is to determine the maximum drag benefit that can be achieved by reducing horizontal tail size consistent with the airplane controllability requirements and by moving the airplane's c.g. range aft. This is accomplished by redesigning the surface to increase the low-speed maximum lift capability (thus maintaining longitudinal controllability) and simultaneously not increasing the horizontal tail drag coefficient at the cruise trim lift coefficient.

The following aerodynamic objectives are postulated for the new L-1011 small tail design. First, for good high-speed drag characteristics to ensure that a tail area reduction would result in a proportional drag decrease:

- Section drag characteristics similar to the standard L-1011 tail.
- No tail drag rise within the cruise Mach number region.
- Maximum tail lift-to-drag ratio occurring at nominal cruise trim C_L.

Second, at low speed to achieve a tail size with significantly reduced area:

- Achieve nose wheel liftoff at forward c.g. for prescribed nose wheel lift off speeds.
- Have sufficient control power to stall the aircraft at forward c.g.
- Have sufficient control power for stall recovery at aft c.g.

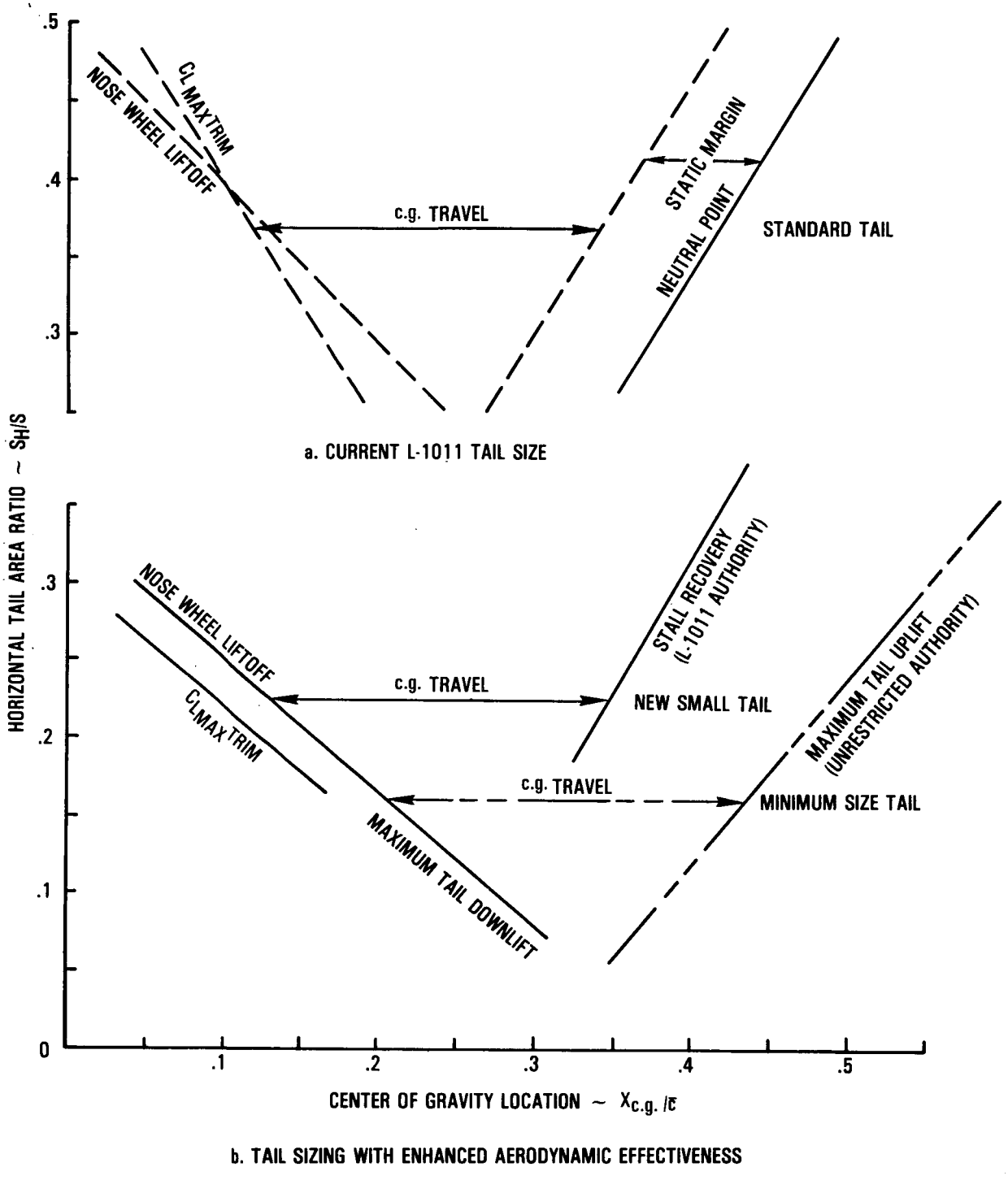

Figure 1. - Reduced area horizontal tail sizing summary.

2. SMALL TAIL INITIAL DESIGN

Early efforts to develop a small horizontal tail were performed under Lockheed Independent Development funding and were aimed at incorporation of the tail on a derivative L-1011 airplane. This work is summarized here, since it provides a foundation for what became a part of the NASA program. Much of the material presented here was previously documented in Reference 1.

In order to provide adequate longitudinal control power with a smaller horizontal tail area, it was necessary to redesign the L-1011's stabilizer/elevator surfaces and redefine their deflection limits to improve the aerodynamic effectiveness of the tail. It was premised that the smaller horizontal tail would be mounted on the same pivot bearings as the original L-1011 tail and would be actuated by the same power actuator arrangement as is currently used. The new horizontal would be an all flying surface, as is the original, and would also have a similar geared elevator revised to provide increased lift, both up and down as a function of tail plane angle. The smaller tail would have increased angular capability within the existing L-1011 fuselage cutout. Elevator travel would be increased and stabilizer/elevator gearing would be defined to achieve the design objectives.

2.1 Sizing Analysis

The goal of high lift production at low speed is in conflict with attaining the good transonic aerodynamics required for meeting the principal objective of low cruise drag. This conflict is similar in designing wings and thus the approach taken in horizontal tail definition is analogous to the method for wing design. The objective of the tail design definition was to select an airfoil which is a satisfactory compromise between high-speed and high lift objectives. A helicopter rotor blade airfoil section was chosen as an initial approximation for the tail airfoil. The wide range of aerodynamic conditions during a single cycle of a helicopter rotor at high forward speed and high Mach number on the advancing tip, and low speed/high angle of attack on the retreating blade, place constraints on rotor airfoil design similar to those faced in designing the relaxed stability tail. The airfoil section for the tail was selected from several advanced rotor airfoils, whose experimental characteristics are documented in Reference 2. The chosen section was modified slightly on the tail lower surface (convex side) to conform with thickness-to-chord ratio constraints for the tail. The airfoil section and its ordinates are presented in Figure 2 along with a comparison to standard horizontal tail airfoil characteristics.

2.2 Tail Sizing

The small horizontal tail sizing analysis was performed using what have been considered critical control criteria. With the center of gravity (c.g.) at the forward limit, the critical requirements are to be able to rotate the airplane for takeoff, and to control the airplane to stall in the landing configuration. With the center of gravity at the aft limit, the tail size for

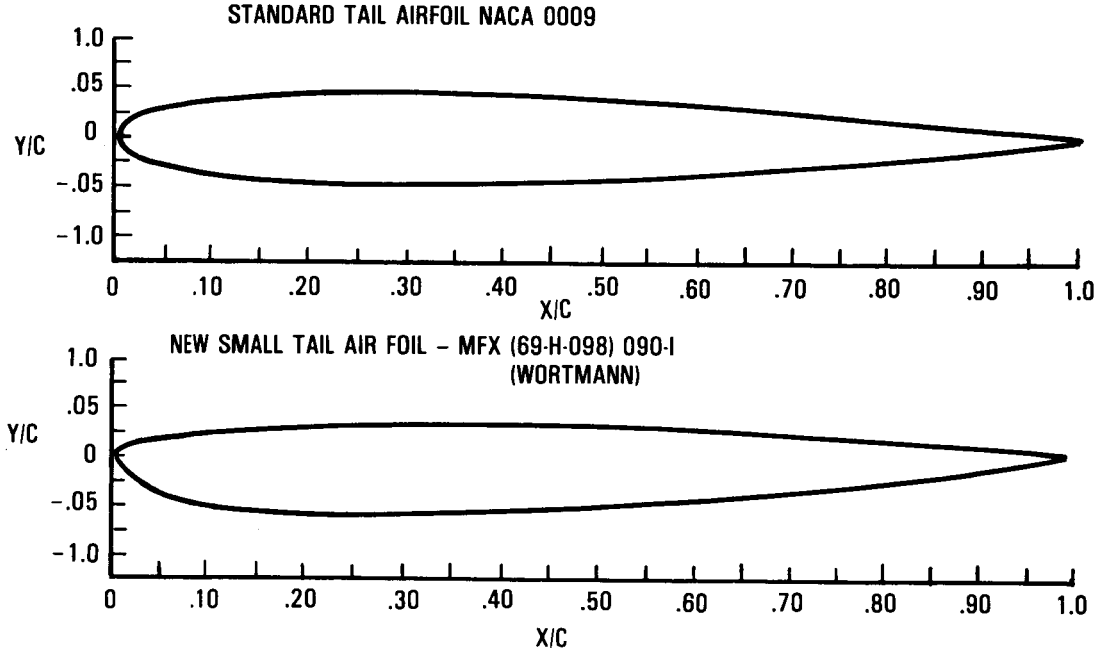

NACA 0009 (SYMMETRICAL)		MFX (69-H-098)		
X/C	Y/C	X/C	UPPER Y/C	LOWER Y/C
0	0	0	0	0
0.005	.....	0.0043	0.0069	-0.0096
0.0125	±0.01420	0.0096	0.0096	-0.0148
0.0250	±0.01961	0.0172	0.0122	-0.0204
0.050	±0.02666	0.0384	0.0171	-0.0320
0.075	±0.03150	0.0520	0.0192	-0.0374
0.100	±0.03512	0.0851	0.0231	-0.0470
0.150	±0.04009	0.1253	0.0264	-0.0534
0.200	±0.04303	0.1721	0.0292	-0.0567
0.250	±0.04456	0.2245	0.0313	-0.0579
0.300	±0.04501	0.2818	0.0323	-0.0577
0.400	±0.04352	0.3429	0.0324	-0.0571
0.500	±0.03971	0.4070	0.0317	-0.0564
0.600	±0.03423	0.4710	0.0305	-0.0551
0.700	±0.02478	0.5380	0.0288	-0.0524
0.800	±0.01967	0.6035	0.0267	-0.0486
0.900	±0.01086	0.6673	0.0242	-0.0435
0.950	±0.00605	0.7283	0.0215	-0.0374
1.000	±0.00095	0.7856	0.0186	-0.0311
		0.8379	0.0156	-0.0248
		0.8847	0.0126	-0.0185
		0.9579	0.0064	-0.0072
		1.0000	0.0013	-0.0009

LEADING EDGE RADIUS = 0.006c

Figure 2. - New small horizontal tail airfoil compared with the standard tail airfoil.

a relaxed stability airplane is determined by airplane nose-down stall recovery requirements evolved from flight data. The aft c.g. stall recovery criterion was obtained from a statistical study of stall time histories wherein less than full throw was used for recovery. This tends to define a recovery acceleration which feels comfortable to the pilot.

Specifically, the small horizontal tail was sized in accordance with the following requirements:

- Takeoff nose wheel liftoff at forward c.g. with maximum takeoff flaps at the lesser of 1.05 of the air minimum control speed or 1.1 of the FAA stall speed.
- Control-to-stall at forward c.g. with maximum landing flaps (42 degrees) and idle thrust.
- At least 4.58 deg/sec^2 nose-down pitch acceleration for stall recovery at aft c.g. and at the FAA stall speed for maximum landing weight.
- At least neutral stability at aft c.g.
- A c.g. range equal to that of the standard L-1011, 12 percent to 35 percent $\bar{c}$ (67.5 inches) for weights less than 338,000 lbs.

Within the physical constraints of the airplane geometry and actuating mechanisms, the stabilizer/elevator deflection limits were increased to expand the useable lift capability of the tail. By reducing the horizontal tail size, it was initially assumed that there would be sufficient space in the existing structure to expand the negative stabilizer deflection limit from -14 degrees to -18 degrees and the positive deflection limit from +1 degrees to 2 degrees. It was further assumed that the stabilizer/elevator gearing could be modified to widen the elevator deflection limits so that when the stabilizer deflected is -18 degrees the corresponding elevator angle is -30 degrees and at the positive stabilizer limit of +2 degrees the elevator is deflected +10 degrees.

Results of the initial tail sizing analysis are shown in Figure 1b, which shows the horizontal tail volume coefficient needed to satisfy the stability and control requirements for a specified c.g. range. This figure shows that the minimum size horizontal tail for an L-1011 is 800 square feet (23 percent of the wing area) compared to the standard L-1011 horizontal tail area of 1282 square feet (37 percent of the wing area). This represents a reduction in horizontal tail area of 38 percent.

What is surprising in Figure 1, is that the aft c.g. limit has not moved aft; it is still at 35 percent $\bar{c}$ due to the upthrow authority restrictions of the L-1011 tail. Thus this modification would be applicable to a derivative airplane. However, the tail lift coefficient to trim the airplane is going to be increased by the tail area ratio.

2.3 H_{16} Small Horizontal Tail

The following characteristics of the tail were assumed to differ from the standard L-1011 configuration to improve the low-speed lift capability of the surface:

- Cambered airfoil section
- Reduced planform sweep at mac/4
- Increased elevator chord ratio
- Increased tail incidence range
- Increased elevator angle range relative to FRL
- No dihedral
- Taper ratio

Other characteristics of the tail which were not changed were:

- Aspect ratio = 4.0
- Thickness/chord ratio = 9 percent

The new small horizontal tail planform is shown in Figure 3. The wind-tunnel model designation for this tail is H_{16}. For comparison the small tail is shown as an overlay to an image of the standard horizontal tail, designated H_{8c}.

The new small horizontal tail was designed according to the geometric specification in Table 1, which for comparison also lists characteristics of the standard tail.

The total horizontal tail area includes the imaginary or carry-through portion of the planform which is hidden within the fuselage. As a result, as tail size is decreased, a smaller fraction of the tail is exposed, which tends to degrade horizontal tail effectiveness somewhat.

2.4 Predicted Cruise Drag Reduction

The reduction in aerodynamic drag due to the smaller horizontal tail was estimated by using standard handbook methods for lifting surfaces. The particular technique which was employed applies a form factor for airfoil thickness to the planar surface compressible skin friction drag computed by the Sommer and Short T' method. The form factor was determined by a special Lockheed correlation of airfoil drag with thickness ratio.

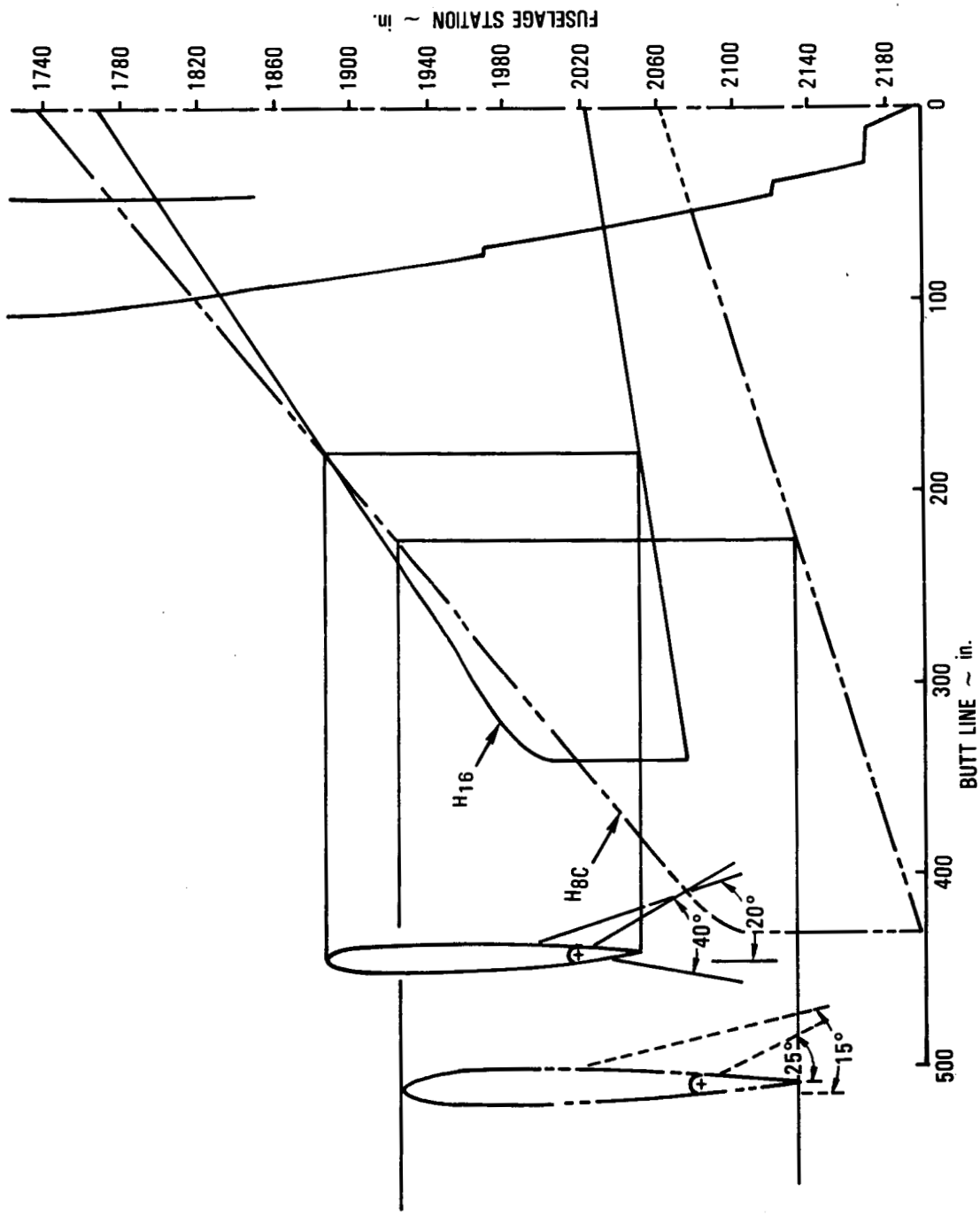

Figure 3. - H_{18} small horizontal tail compared with the H_{8c} standard tail.

TABLE 1. - COMPARISON OF SMALL TAIL AND STANDARD TAIL CHARACTERISTICS.

	H_{8c} Standard	H_{16} Small
Aspect ratio	4	4
Taper ratio	0.33	0.3
Leading-edge radius	0.0089c	0.006c
Camber	0	0.013c
Thickness ratio	0.09	0.09
Quarter chord sweep	35^0	28^0
Area, ft^2		
Total	1282	800
Exposed	960	565
Exposed/Total	0.75	0.71
Elevator chord ratio	0.25	0.3
Stabilizer throw	15^0 ($+1^0$ to -14^0)	20^0 ($+2^0$ to -18^0)
Elevator throw	25^0 (0^0 to -25^0)	40^0 ($+10^0$ to -30^0)

Results of these computations are shown in Figure 4. These data illustrate the potential drag advantages of the small tail compared to the standard configuration. The small tail offers a drag reduction of 11 counts at wind-tunnel test conditions and 7 counts at full-scale cruise conditions. This represents a potential drag savings of 2.7 percent at nominal cruise conditions.

The net improvement in cruise efficiency would approach 3 percent due to the slight weight reduction of the smaller horizontal tail.

2.5 Concept Verification

Initial concept verification wind-tunnel tests of the small horizontal tail were conducted under Lockheed Independent Development funding in 1976. Two sets were performed: in April, a high-speed test (N-307) in the Calspan Corporation 8-Foot Transonic Facility for cruise drag evaluation; and in November, a test (L-404) in the Lockheed-California Company Low Speed Wind Tunnel to determine the high-lift characteristics of the small horizontal tail.

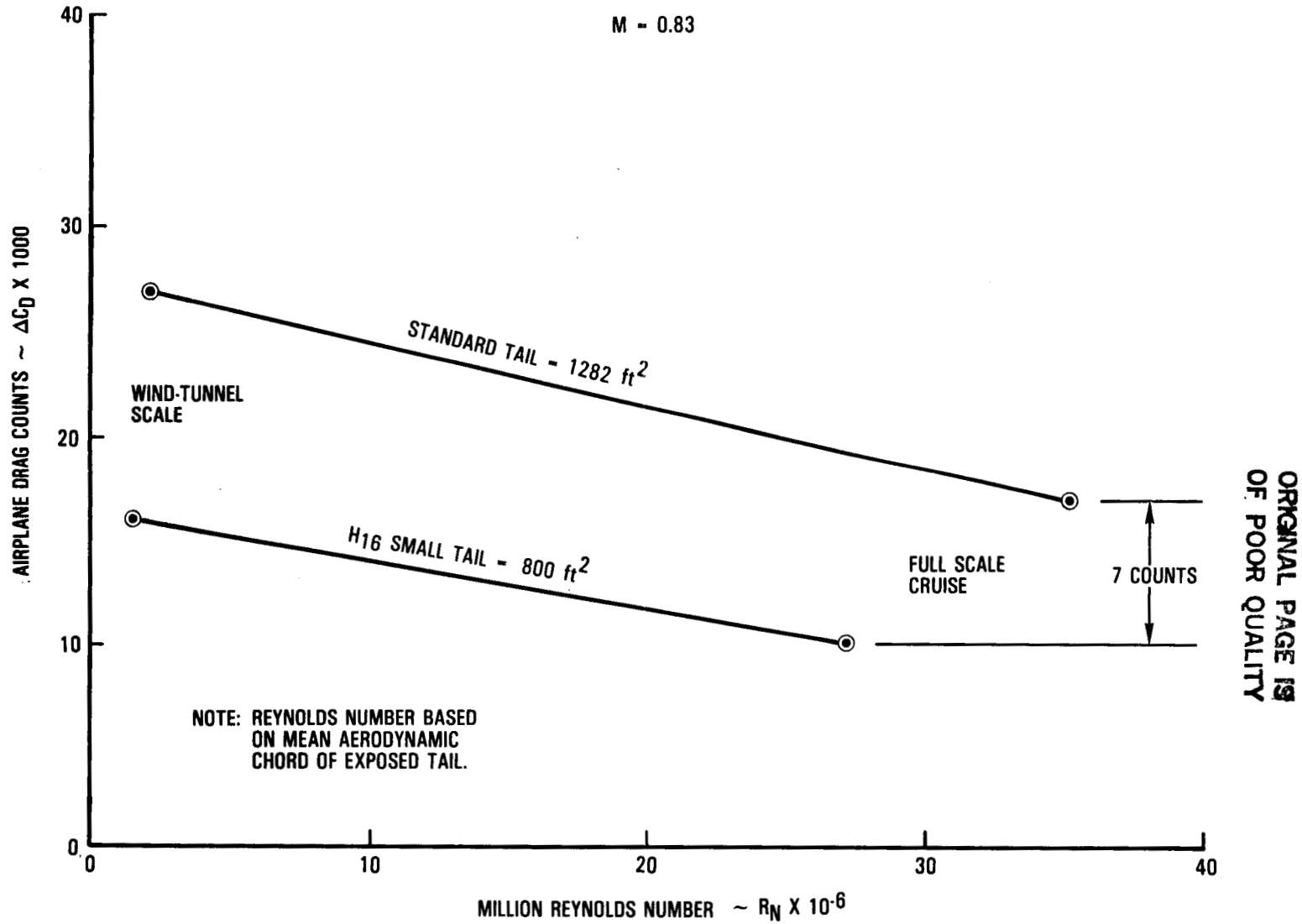

Figure 4. - Predicted zero-lift drag comparison of H_{16} small and H_{8c} standard horizontal tails at wind-tunnel test and full-scale cruise reynolds numbers.

A convenient method of evaluating horizontal tail drag characteristics is by a composite plot of tail-on and tail-off drag coefficient presented as a function of pitching moment for various trimmed lift coefficients. This type of plot for an L-1011 with H_{16} small horizontal tail is presented in Figure 5. This plot allows extraction of horizontal tail parasite drag, the drag at zero net lift on the tail, by determining the drag at points of intersection of the tail-off curve with tail-on drag for particular lift coefficients.

The technique illustrated by Figure 5 was used to extract horizontal tail zero-lift drag from the high-speed wind-tunnel test data. Zero lift drag is the difference in drag between tail off and on at the same total airplane C_L and $C_{m_{.25\bar{c}}}$. The results of this analysis show the potential drag reduction of the small tail compared to the standard tail L-1011. For a cruise Mach number of 0.84, Figure 6 shows the zero trim drag polar characteristics of the L-1011 with H_{16} small and H_{8c} standard horizontal tails. These data, along with similar data for Mach numbers 0.8 and 0.82, were used to extract the net, zero-lift drag characteristics of the small and standard horizontal tails as shown in Figure 7. The results show that there is a potential full scale drag benefit of 5.1 counts. The data in Figure 8 show that this translates into a net performance improvement of 2 percent, related to the cruise lift-to-drag ration characteristics of the airplane. This is 25 percent below the predicted drag reduction shown in Figure 4. The difference could be due to a number of reasons such as the effects of fuselage boattail, wing wake, etc.

The 2 percent improvement in cruise lift-to-drag ratio coupled with the estimated weight reduction of the smaller tail would result in about 2.5 percent overall improvement in long-range-mission fuel efficiency. These results were considered sufficiently promising to further pursue development of the small horizontal tail.

Stability and control data from the preliminary high-speed tests showed good agreement with predicted values of airplane neutral point and control power.

The horizontal tail high-lift characteristics from low-speed wind-tunnel test results are shown in Figure 9. These data reveal serious deficiencies in the initial airfoil choice at high angle of attack with the elevator deflected. Tail stall angle without elevator deflection was approximately -18 degrees tail angle of attack which was the expected angle for the test Reynolds number (about 10^6 referred to tail $\bar{c}$). However, as the elevator angle was set progressively higher, the stall angle dropped rapidly. Flow visualization by tufts showed leading edge separation, and disturbed and separated flow behind the elevator hinge. Appearance of leading-edge separation correlated well with measured stall angle of attack. The result was a maximum lift coefficient for the horizontal tail of -1.2, shown in Figure 9, 25 percent below the target value of -1.6 initially used to size the tail.

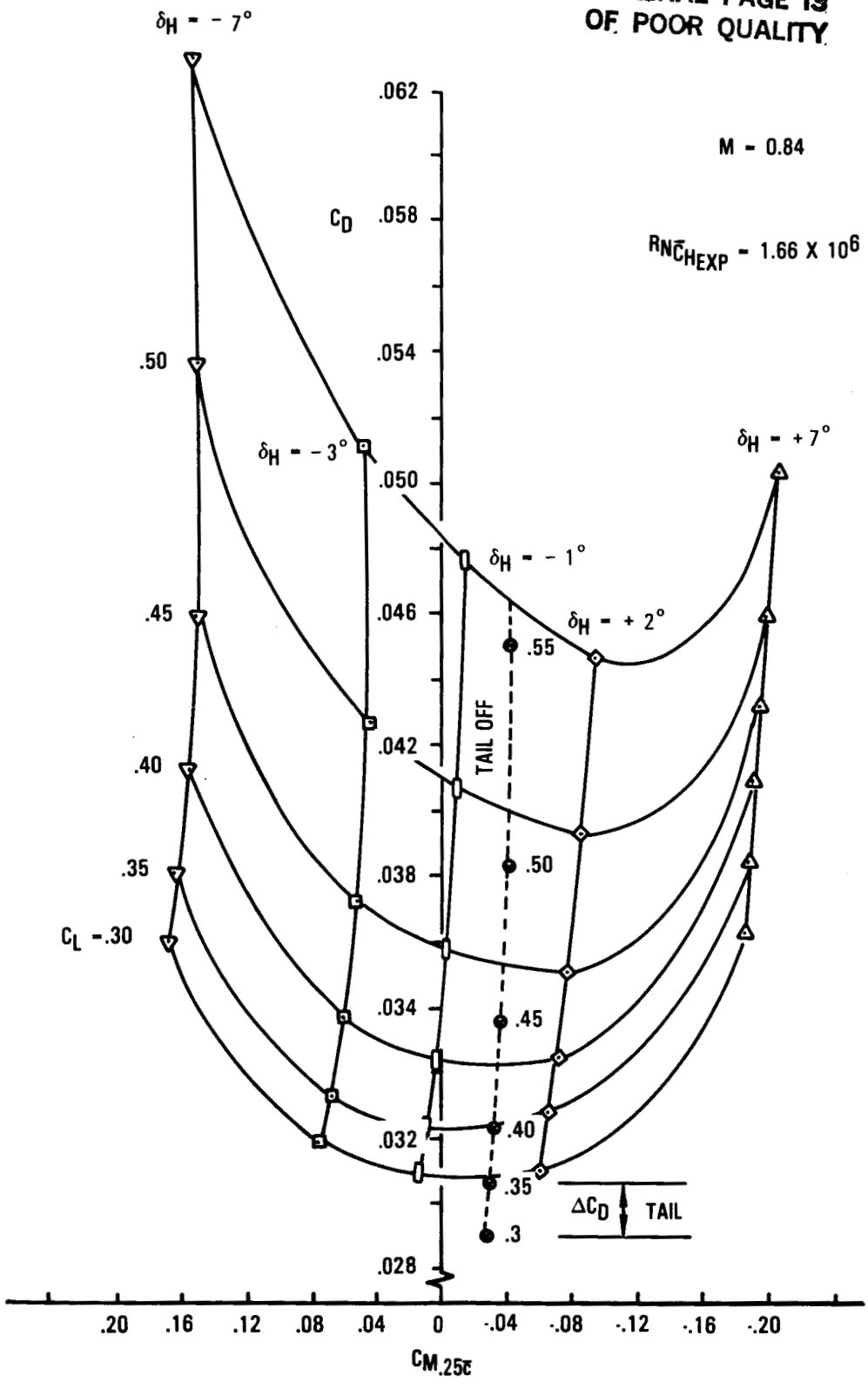

Figure 5. - Total airplane drag with and without the H_{16} small horizontal tail.

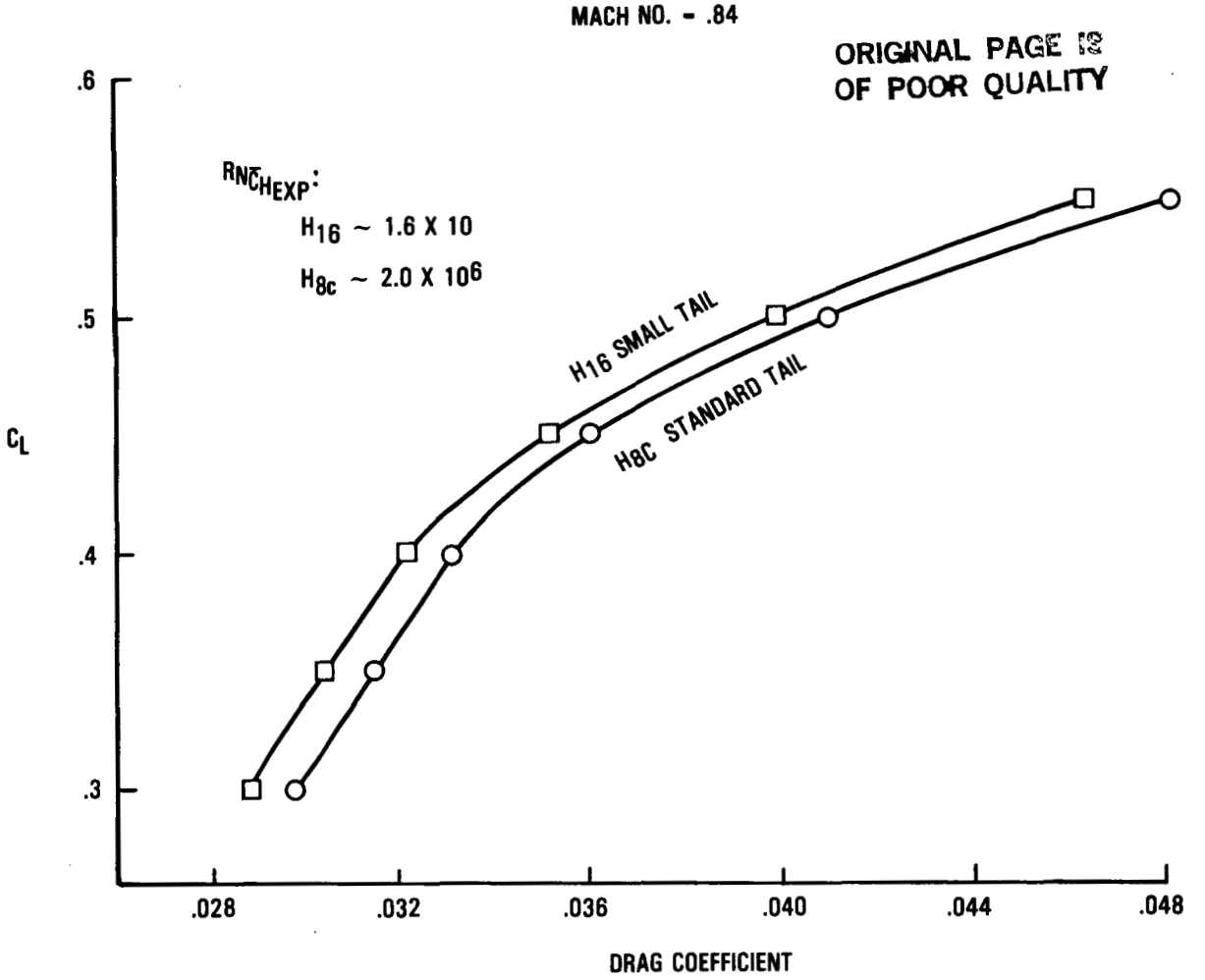

Figure 6. - Zero trim drag polar characteristics of the L-1011 with H_{16} small and H_{8c} standard horizontal tails.

In an attempt to improve these lift characteristics, three lift-enhancement devices were prepared for a second low-speed test entry. These were: a plain leading edge flap (or drooped leading edge), a Kreuger flap, and a second elevator hinge at the mid-point of the elevator chord allowing a double articulated motion to be simulated. The leading edge flap provided no benefit for this airfoil, but the Krueger flap effectively delayed leading edge stall. The combined Krueger and double elevator produced a maximum lift coefficient of -1.4 at 16 degrees angle of attack, as shown in Figure 10. If this value were scaled from wind-tunnel to flight Reynolds numbers (about 20 times higher), the design value of -1.6 might very well be realized.

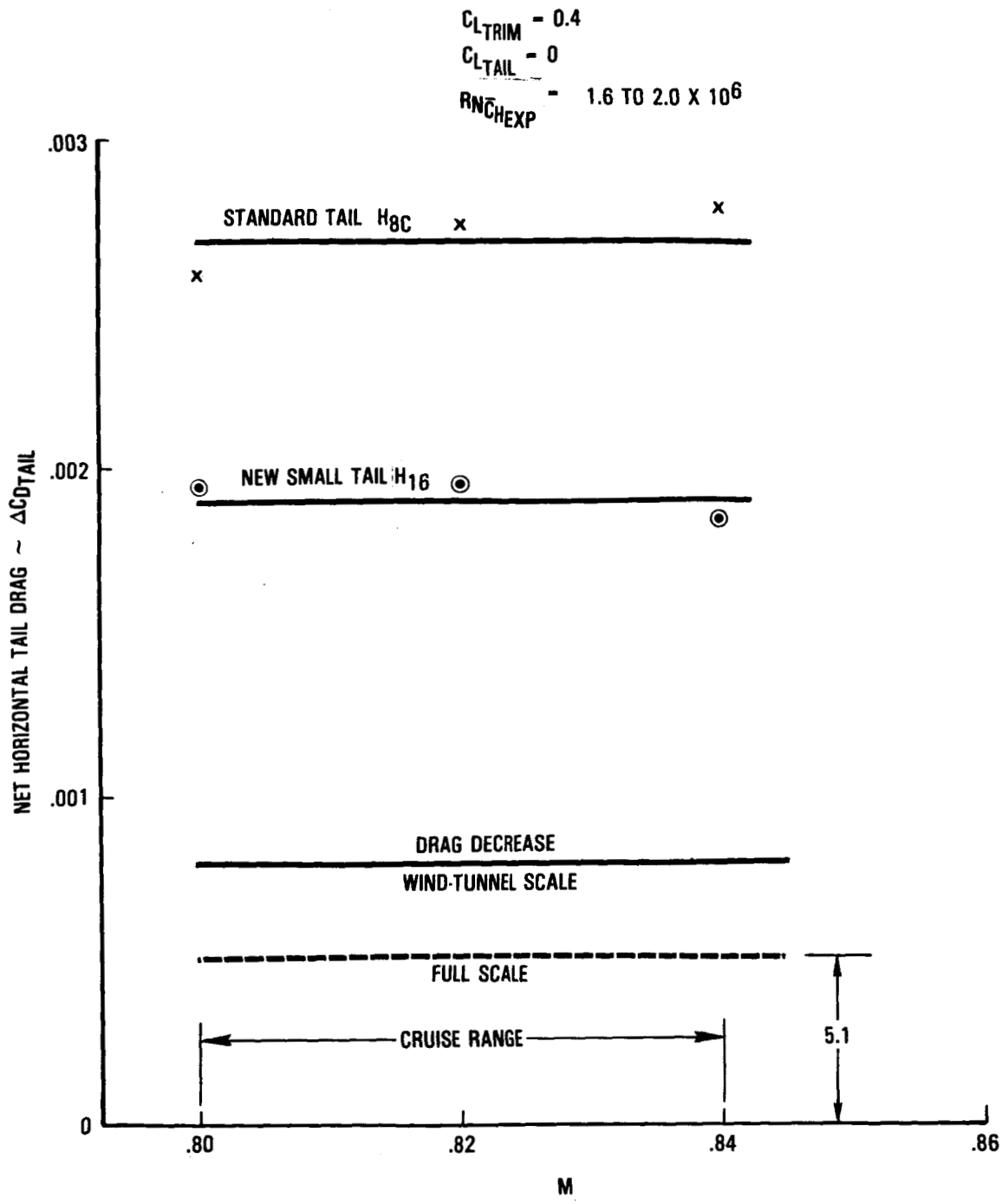

Figure 7. - Wind-tunnel test zero-lift drag characteristics of H_{16} small and H_{8c} standard horizontal tails.

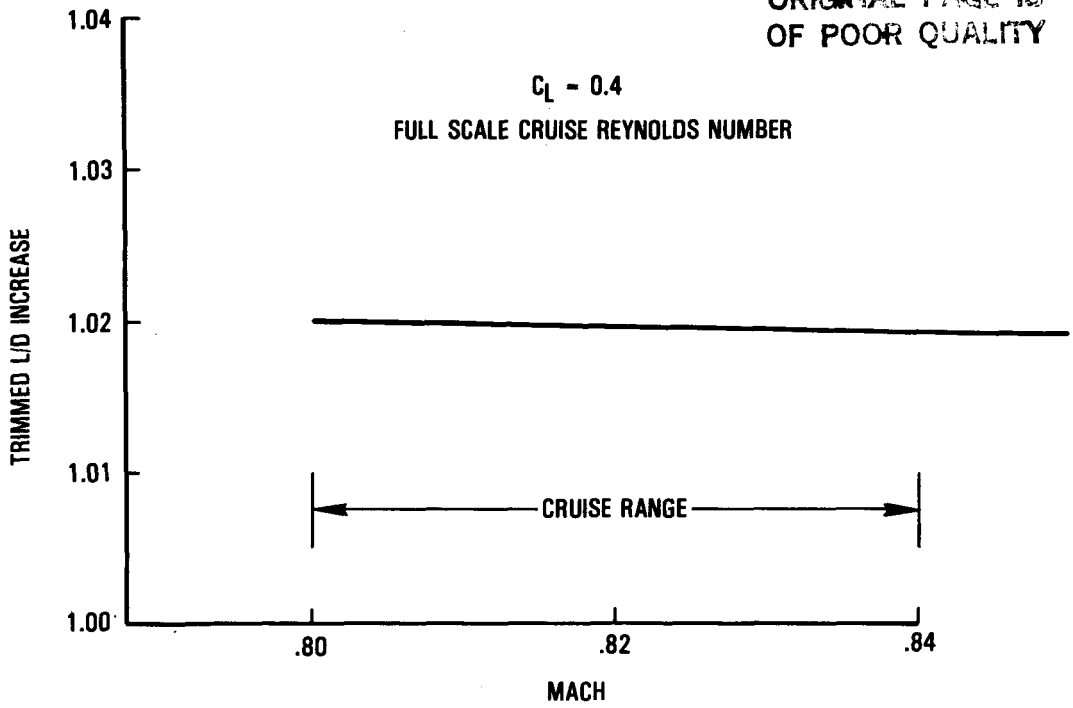

Figure 8. - H_{16} small horizontal tail cruise performance benefit.

The potential for significant cruise drag reduction was shown by the initial concept verification wind-tunnel tests of a 38 percent smaller horizontal tail. However, the smaller tail was found deficient in low-speed control capability without the introduction of complex high-lift devices. It was concluded that the design of a system with high-lift devices was too complex for production consideration, and further development of this initial tail design was abandoned in favor of a new design with improved airfoil characteristics.

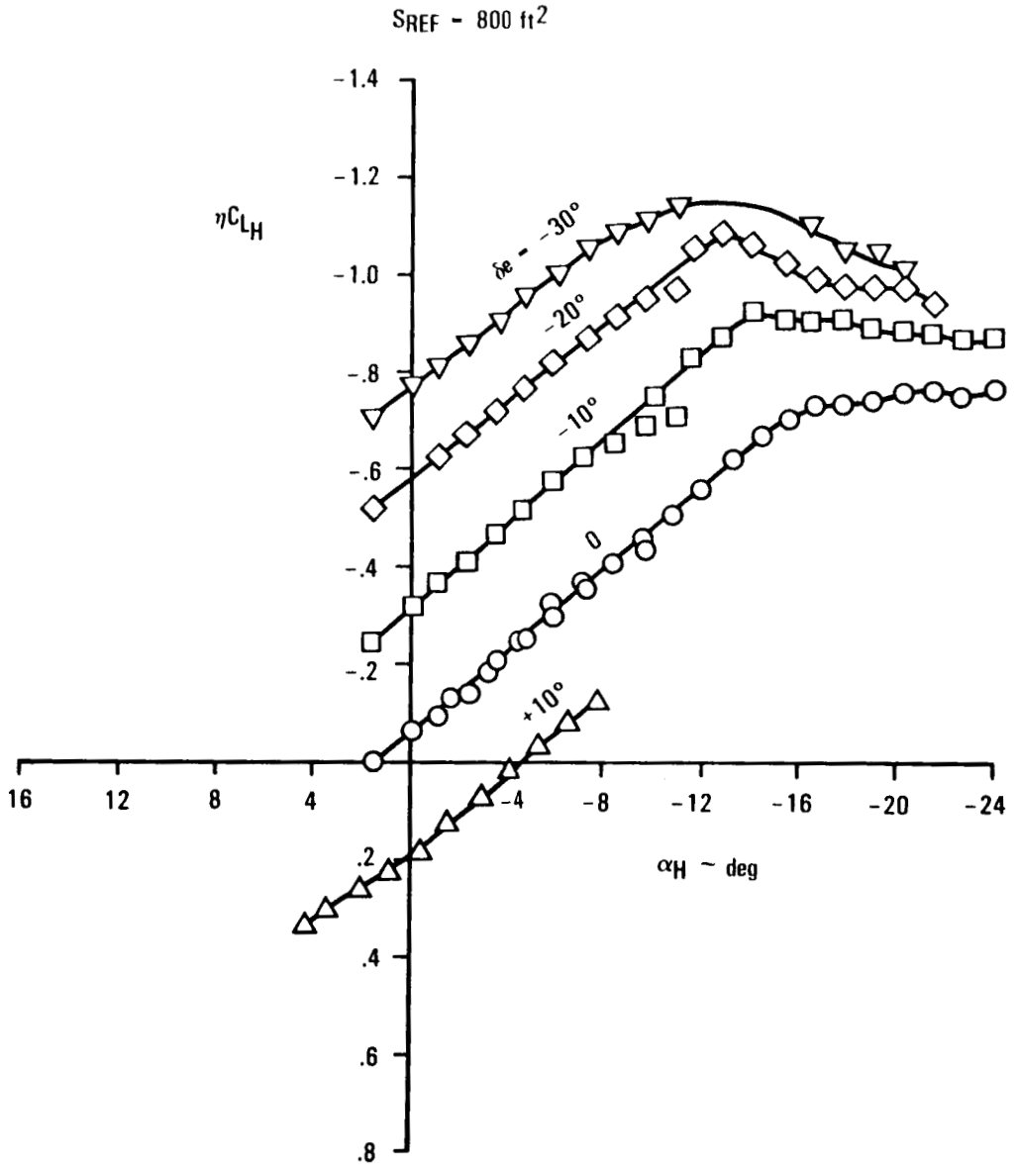

Figure 9. - H_{16} small horizontal tail high-lift characteristics - plain elevator.

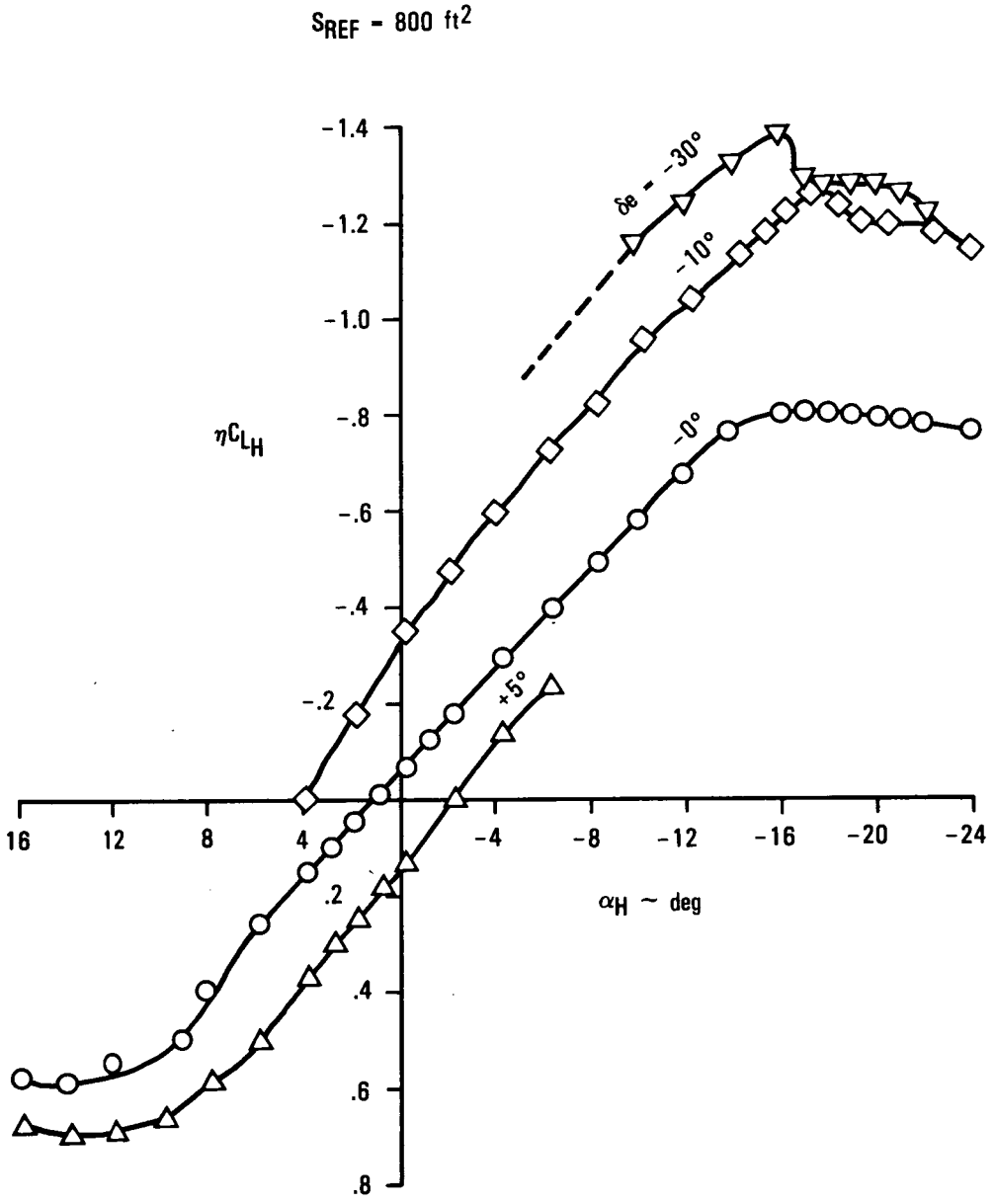

Figure 10. - H_{16} small horizontal tail high-lift characteristics - double segment elevator and Krueger flap.

3. SMALL TAIL REDESIGN

Advanced airfoil technology was utilized in the new design effort in an attempt to design a relatively thick section with large leading-edge radius to provide high lift at low speed for controllability while not significantly degrading high speed drag characteristics. Restated, the new tail redesign was to meet the specified design objectives for low-speed performance while duplicating the good high-speed characteristics demonstrated in wind-tunnel tests of the initial design. Undesirable separation and stall characteristics observed in preliminary tests of the initial tail design would be eliminated with minimal reliance on complex lift-enhancement devices.

3.1 RSS2 Airfoil Development

The RSS2 airfoil was developed by evolving a better trade-off between low-speed download capability, M = 0.2, tail C_L = -1.6, and low cruise drag, M = 0.84, tail C_L = -0.2, than the compromise offered by the helicopter blade section used in the initial work. This analysis at the initial section properties, the methods that have been used to improve the results, and the sequence of design evolution.

Pressure distribution on the tail surface was the primary evaluation basis in the design process. The pressure data were produced with the Jameson-Caughey exact potential inviscid flow analysis code, FLO-22 (Reference 1 and 2). This program solves the full potential flow equations for a wing (or tail panel) mounted on an infinite plate. Good operational reliability, ease of operation, and sound theoretical basis prompted the choice of this program. Force and moment coefficients were also obtained from the integrated pressure data.

Theoretically developed cruise and low-speed pressure profiles for the initial small horizontal tail airfoil section (Figure 1) are shown in Figures 11 and 12. These data were computed at a horizontal tail station of about 3/4 span. The cruise pressure distribution, Figure 11, is quite acceptable, showing a relatively weak shock. However, the sample low-speed case plot, Figure 12, shows a very peaky leading edge suction on the lower surface (as installed on the airplane) which will lead to separation and a leading edge type stall, as was discovered in the wind-tunnel test.

To start design evolution, a first redesign consisted of the initial airfoil upper surface (which performed well in wind tunnel tests) and a highly cambered lower surface to enhance low-speed download capability. This combination was fitted with an analytic description.

The results of the blend for the cruise condition, as analyzed with FLO-22 showed the lower surface pressure distribution clearly unacceptable due to a continuous supercritical expansion which terminated in a strong shock. The low-speed pressure distribution was not quite as peaky as Figure 12, but this section favors the low-speed case too strongly. Iterations to find a compromise used the Curvature Airfoil Shaping (CAS) tool described below.

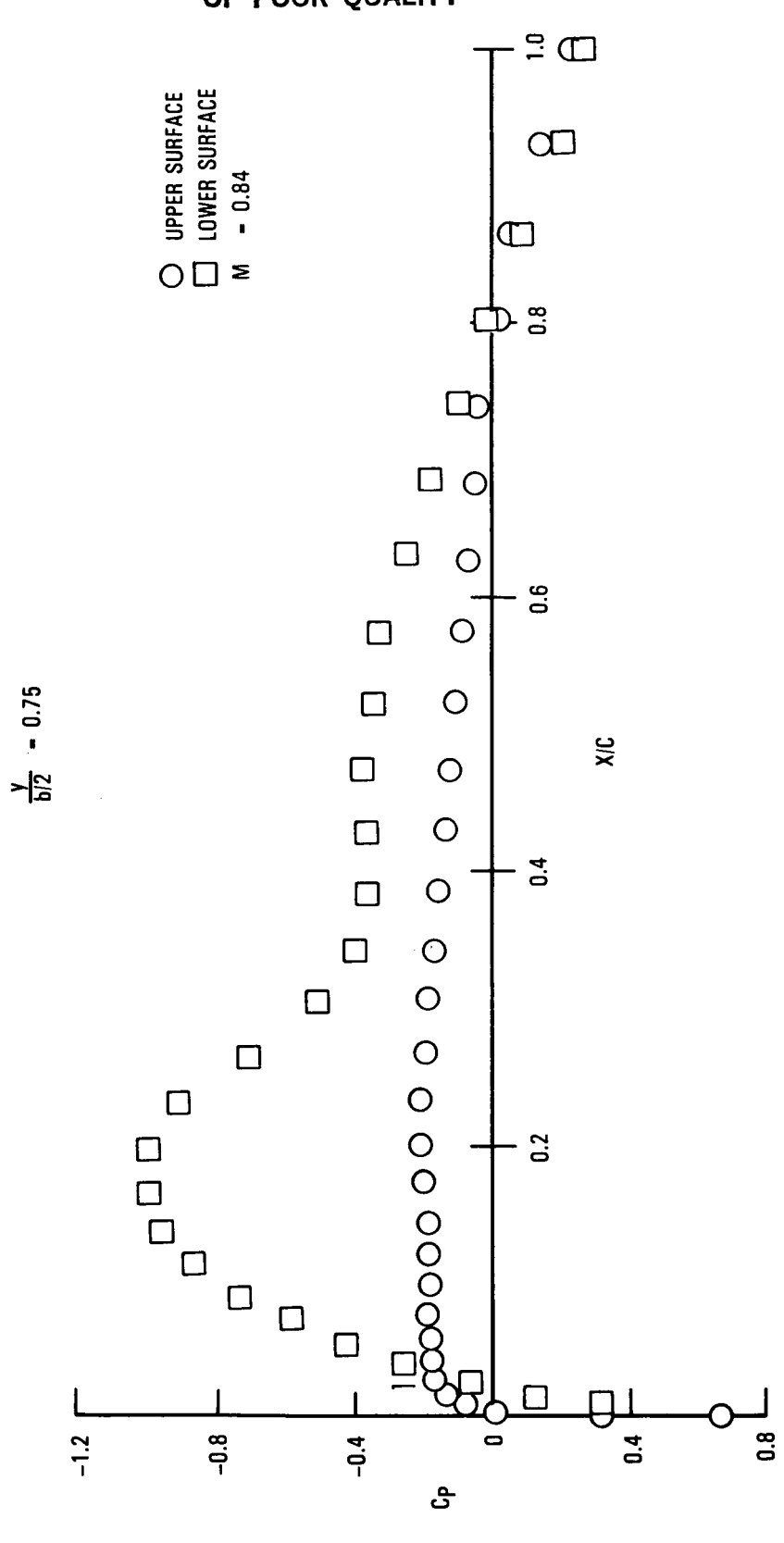

Figure 11. - Initial airfoil section cruise pressure distribution.

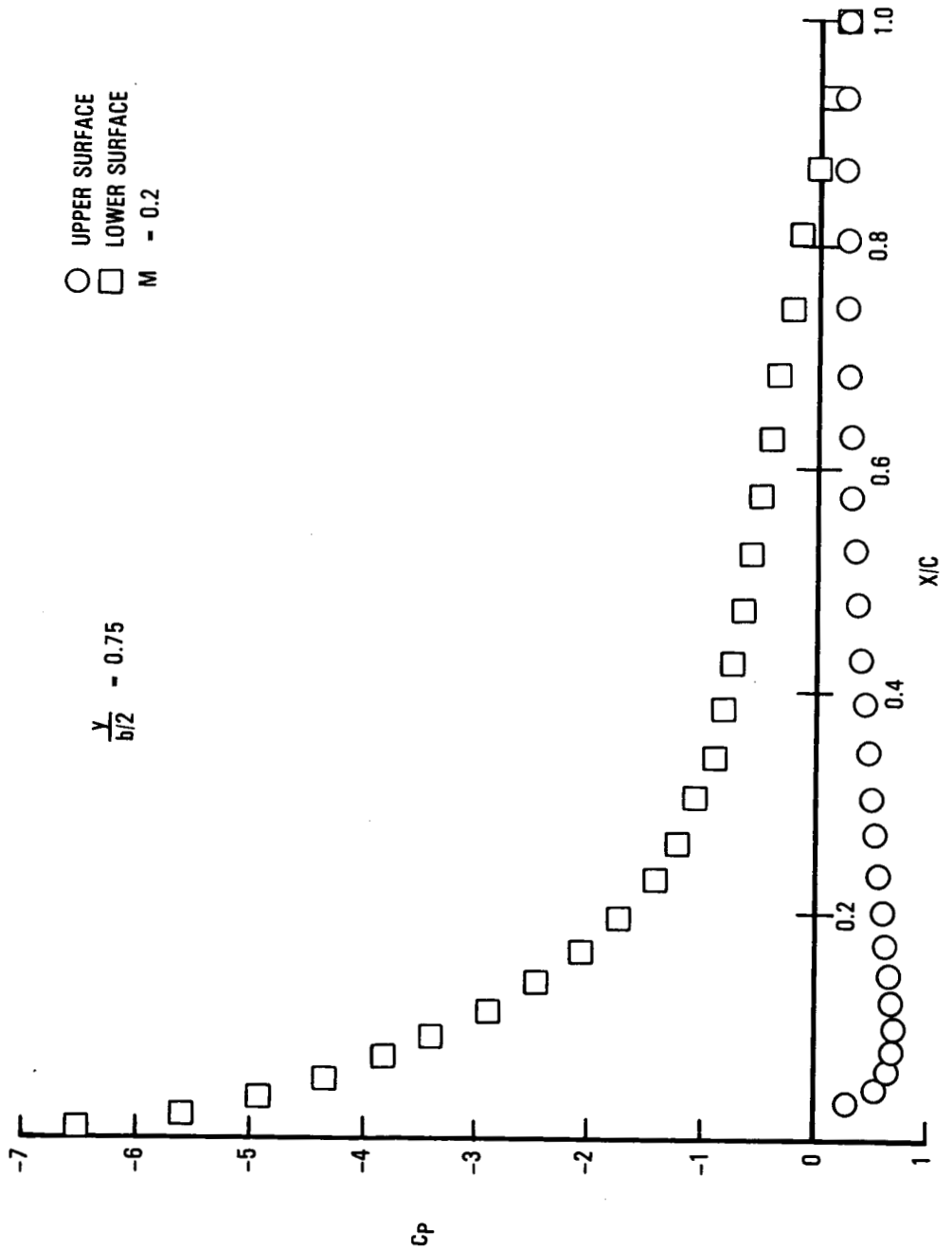

Figure 12. - Initial airfoil section low speed, high download pressure distribution.

The analytic description of the combination airfoil described above was produced using part of the iterative wing design CAS system which is depicted in the flow diagram given in Figure 13. This design system has been fully automated, as implied by the flow diagram. The cornerstone of the system is the ability to define the whole surface geometry by specifying a few key parameters at the surface control stations. The surface geometry generated by the CAS package satisfies a series of curvature conditions which tend to generate good transonic shapes. Thus, even though some amount of iteration may be required to arrive at the proper combination of parameters that will result in the desired type of pressure distribution, the actual number of iterations is usually very low. The rapid convergence rate is due to the inherent geometric properties of the CAS definition, as well as to the fact that the designer only has to operate with a relatively low number of parameters to describe the entire wing surface. This greatly helps the designer in quickly developing a feel for how to perturb these parameters in order to arrive at the desired type of pressure distribution while satisfying whatever constraints might have been imposed upon the design.

The analysis module of the system is the FLO-22 transonic swept wing full potential code. In addition to the automatic display of pressure distributions and other computed aerodynamic characteristics, the design system automatically generates, at the option of the user, data sets for air loads/structural analyses and comprehensive lofting of the wing including all required drawings for wind tunnel model fabrication.

The CAS program was used to improve the cruise pressure distribution while holding the low-speed/high-download case leading edge suction peakiness from going to excessive values. The first iteration using this tool reduced the airfoil thickness. Cruise performance was better, as shown by the data in Figure 14, but still exhibited shocked flow on the upper surface. The next iteration increased the radius of the leading edge to reduce peakiness. The results in Figure 15 show a reduced leading edge pressure gradient. However, the peak is into supercritical flow pressure coefficient values. On the third iteration, the thickness was further reduced, and the leading edge radius was reduced back to a prior iteration. These changes improved the upper surface pressure profile, but unfavorably affected the lower surface pressures (Figure 16).

The fourth change used the upper surface of the third iteration section for the inboard span stations. The outboard span stations used the lower surface of the first iteration section. The upper surfaces were modified for both locations to give a smaller leading edge radius. These changes resulted in an improved cruise performance as shown in Figure 17. Figure 18 shows that the low-speed suction recompression gradient was too high. More curvature was introduced into the upper surface of both outboard and inboard airfoil sections to help this problem by reducing the recompression rate. A reduction in the low-speed suction peakiness was accomplished with the fifth iteration as shown in Figure 19.

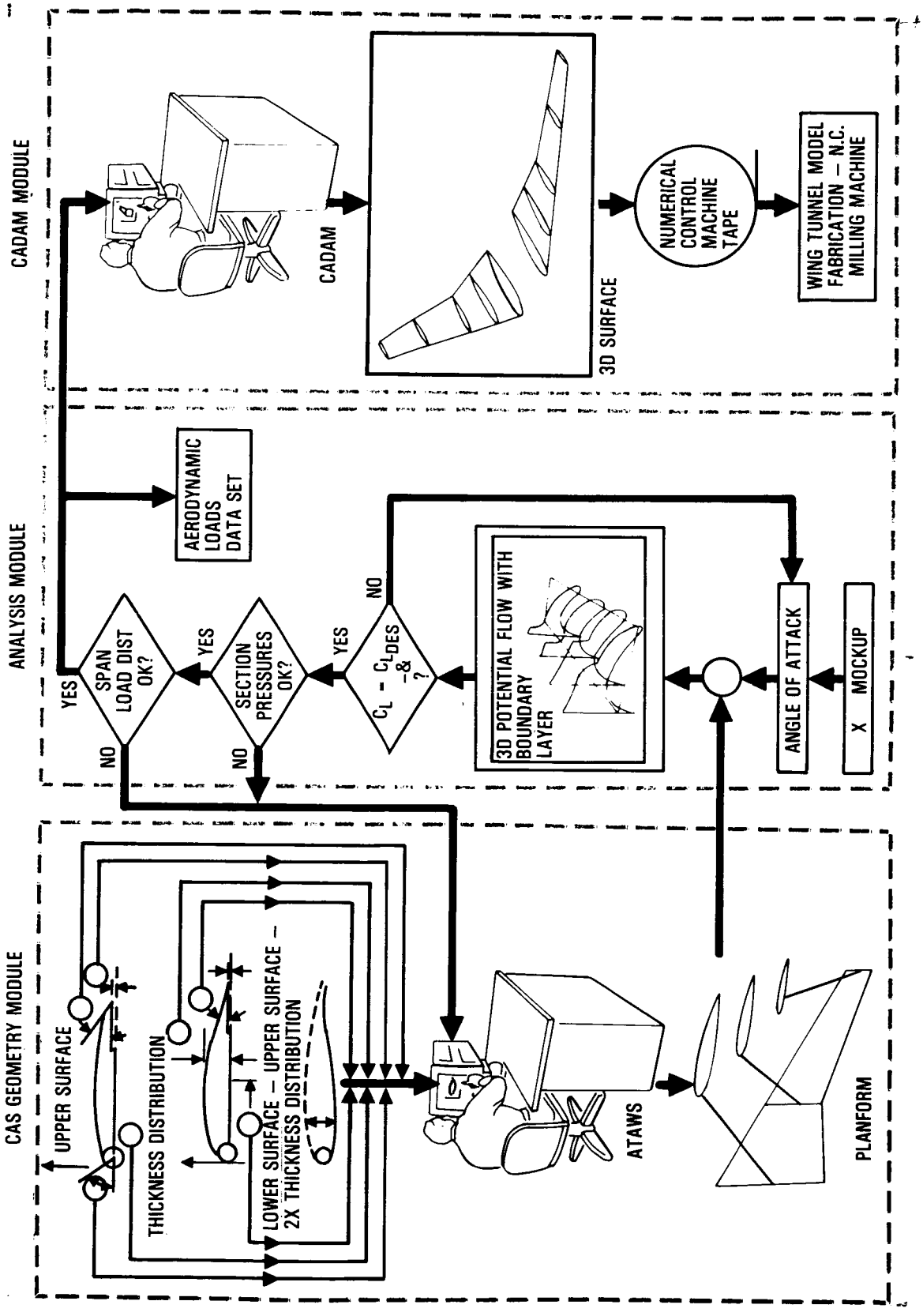

Figure 13. - CAS wing design system.

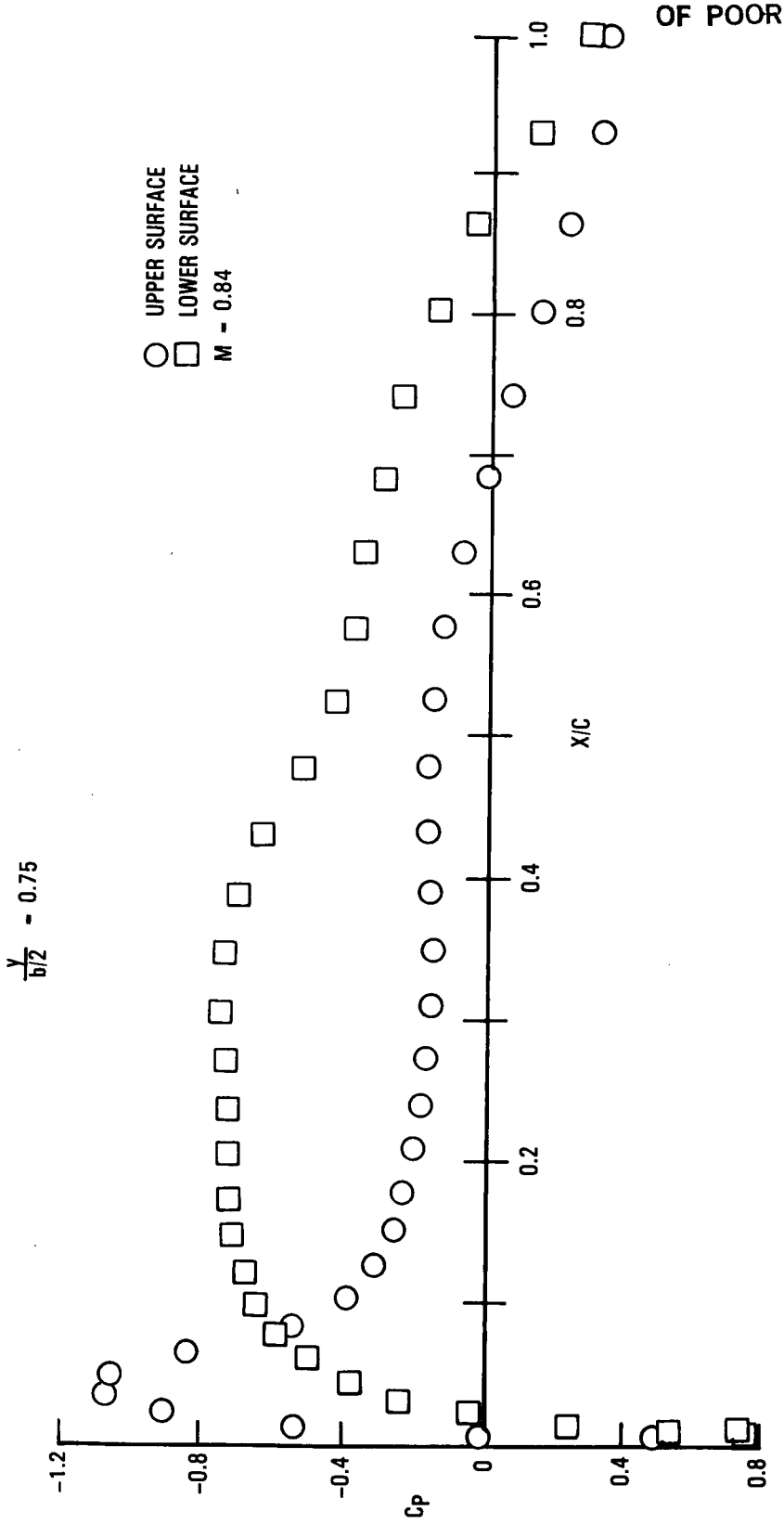

Figure 14. - First iteration cruise pressure distribution.

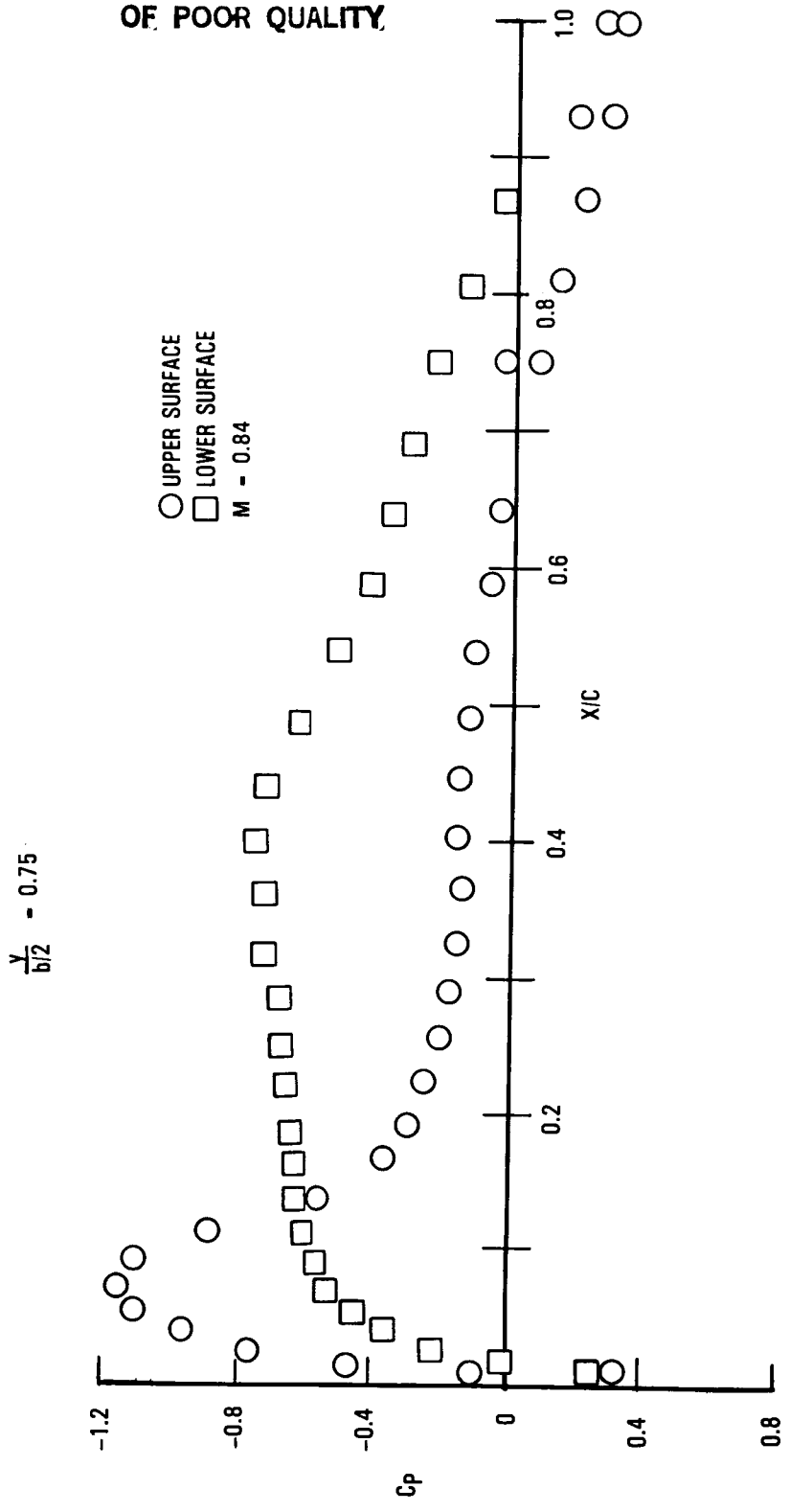

Figure 15. - Second iteration cruise pressure distribution.

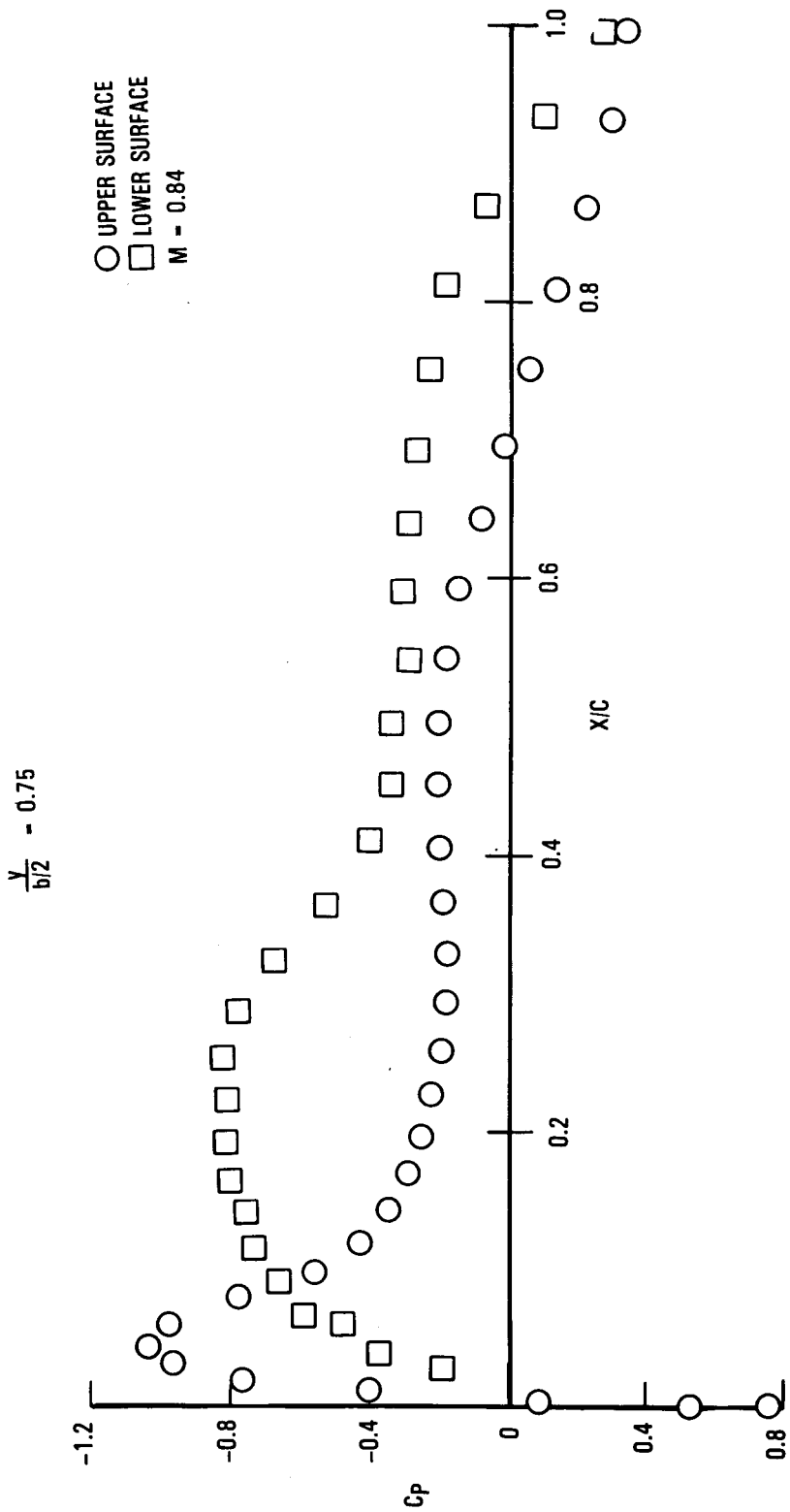

Figure 16. - Third iteration cruise pressure distribution.

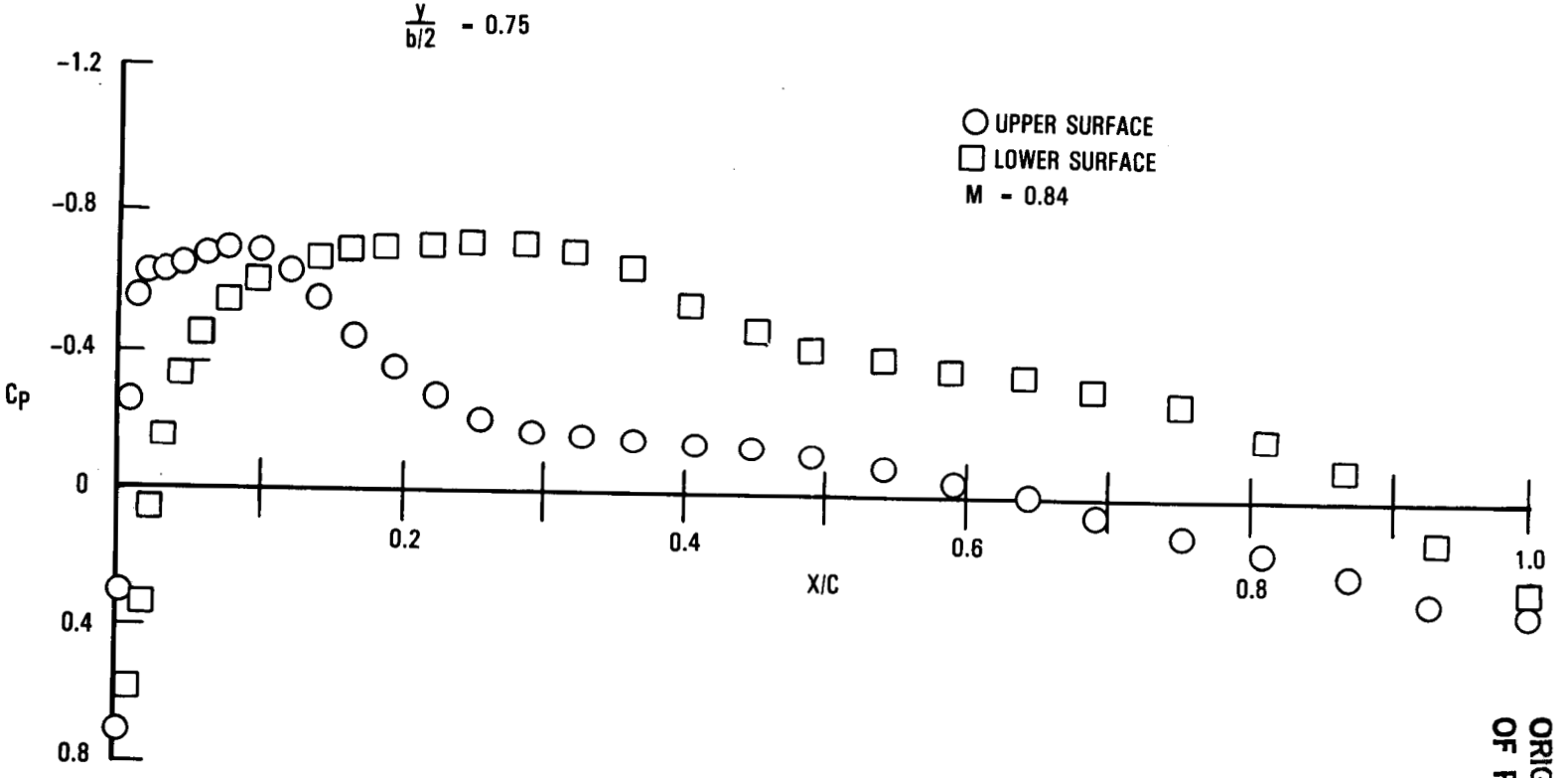

Figure 17. - Fourth iteration cruise pressure distribution.

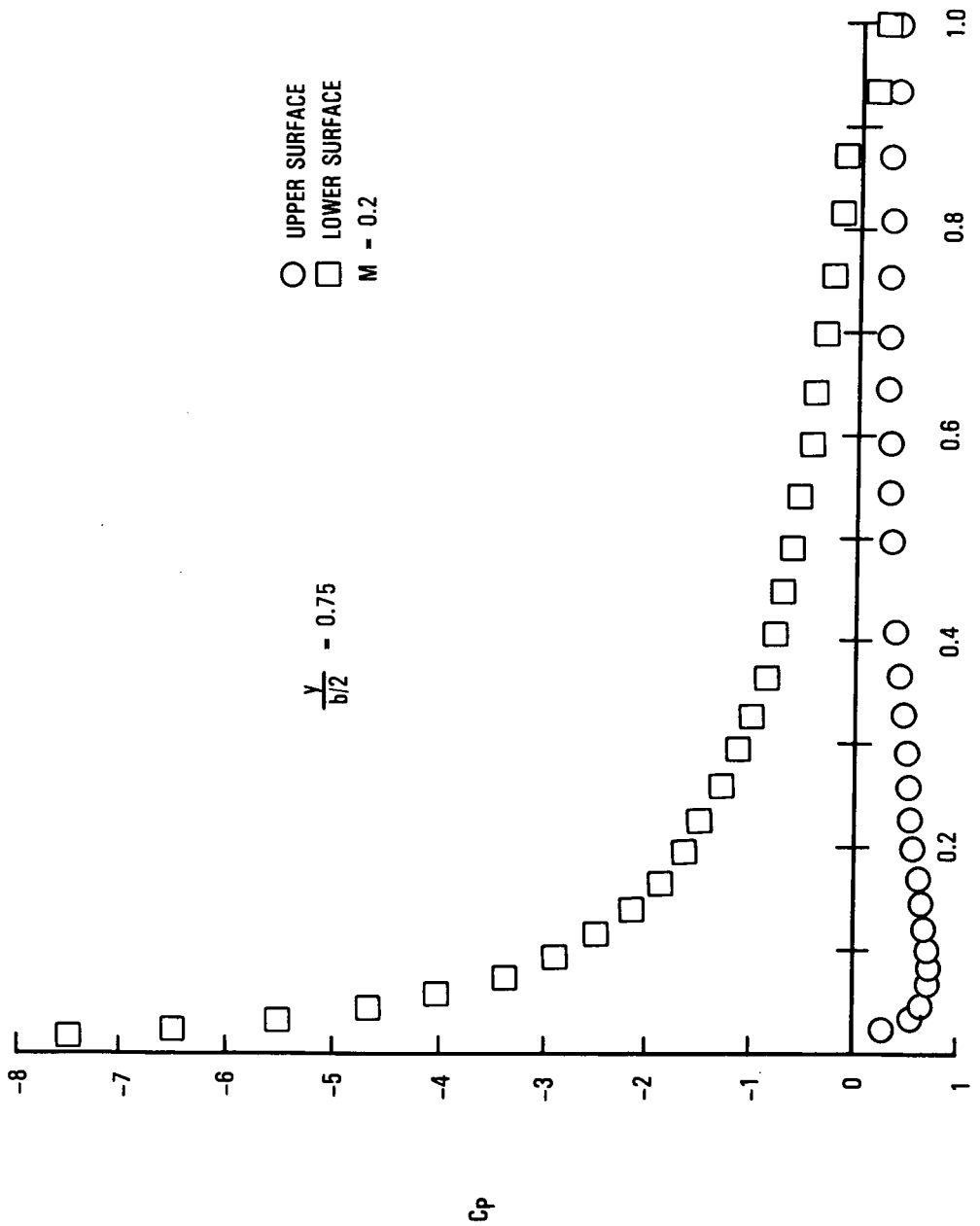

Figure 18. - Fourth iteration low speed, high download pressure distribution, high low-speed suction recompression gradient.

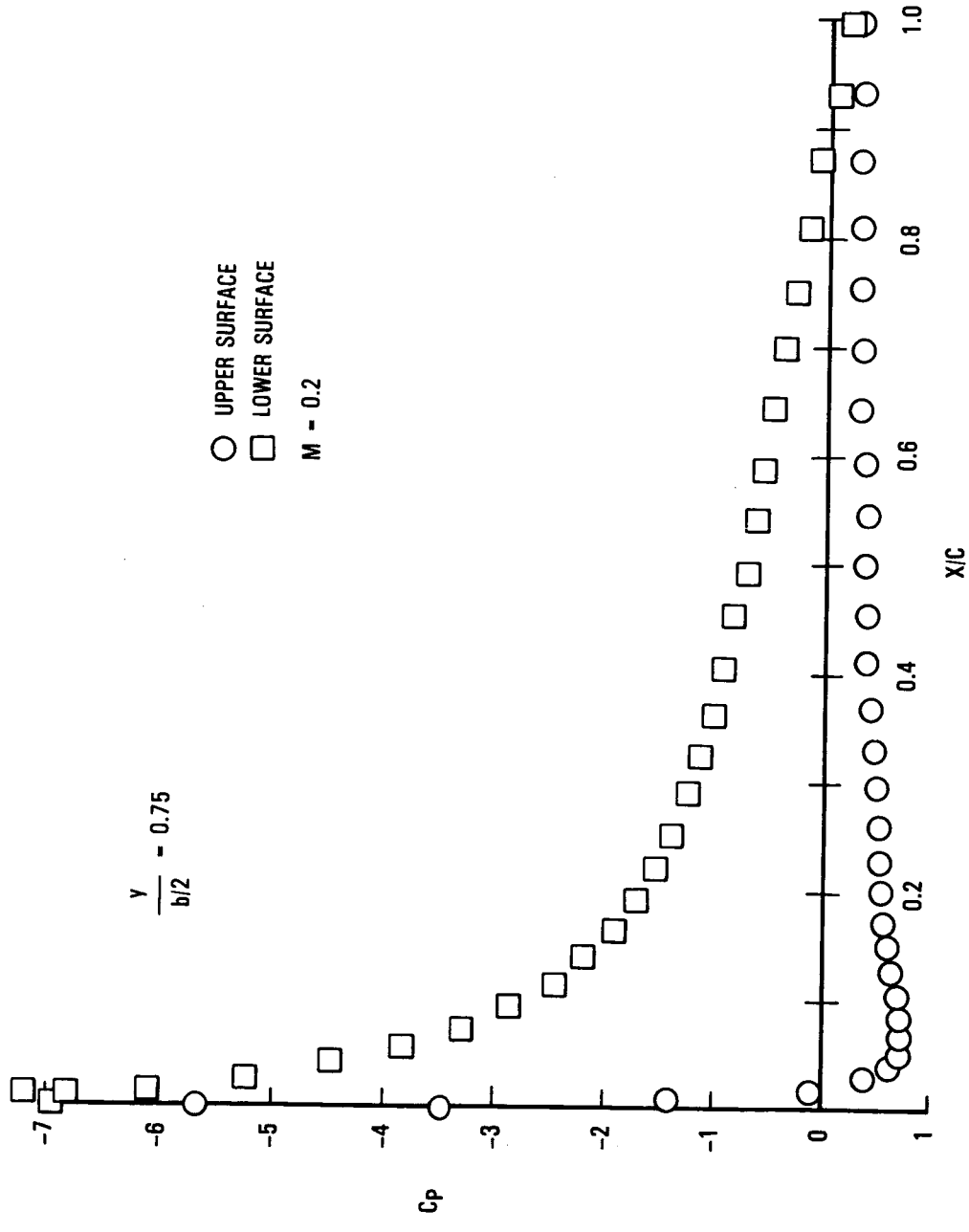

Figure 19. - Fourth iteration low speed, high download pressure distribution, reduced low-speed suction recompression gradient.

A final iteration used the inboard section from the fifth iteration design at all spanwise stations with a minor change to cusp the trailing edge to give more aft loading of the airfoil. The resulting final design RSS2 airfoil is shown in Figure 20. This airfoil section has a maximum thickness/chord ratio of 10.45 percent compared to 9 percent for the initial section (Wortman airfoil) and for the standard tail (NASA 0009). The leading-edge radius is 3.6 percent chord compared to 0.6 percent for the Wortman airfoil and 0.89 percent for the NACA 0009.

The pressure distribution characteristics of the RSS2 airfoil are shown in Figure 21. The data for cruise (Figure 21) show a relatively smooth lower surface pressure gradient, although the rooftop extent is short, and a weak shock recompression. The low-speed pressure data (Figure 22) show an acceptable suction peakiness. Also, from a low-speed standpoint, the generous leading-edge radius and lower surface development of the airfoil lends itself well to a leading-edge camber high-lift modification, if so desired. The lower surface curvature can be easily maintained when so modified, thus minimizing any adverse pressure gradient trends.

3.2 Modified Small Horizontal Tail - H_{17}

The small horizontal tail planform was modified slightly, based on the results of the RSS2 airfoil analysis, by reducing planform sweep from 28 degrees to 25 degrees. The wind-tunnel model designation for the modified small tail is H_{17}. Characteristics of this tail compare with the previous small tail and standard tail as shown in Table 2.

The H_{17} modified small horizontal tail planform is shown in Figure 23. A pressure instrumented model of the H_{17} small tail was constructed for low-speed wind-tunnel tests. Approximately 150 orifices were arranged in chordwise strips on both upper and lower surfaces at four spanwise stations.

Wind-tunnel measured pressure data were compared with the foregoing theoretically computed results. There was generally good correlation on these results as shown in Figure 24. This is particularly true for the section without elevator deflection. For the condition of 30 degrees up elevator (Figure 25), the inviscid potential theory predicts a suction peak somewhat higher than measured. Also, the low pressure recovery at the trailing edge was thought to be caused by the low test Reynolds number.

The force data from these tests for the H_{17} tail (Figure 26) show a maximum lift coefficient capability of -1.25, compared to a value of -1.2 for the H_{16} tail (Figure 9). The modest improvement in maximum lift capability of the modified tail leaves too large a deficiency to be made up by any other means than high-lift devices.

The conclusion once again was that a design with high-lift devices would be too complex for near-term production consideration. Therefore, in order to achieve the control requirements specified in Section 1.2, the size of the small horizontal tail was increased.

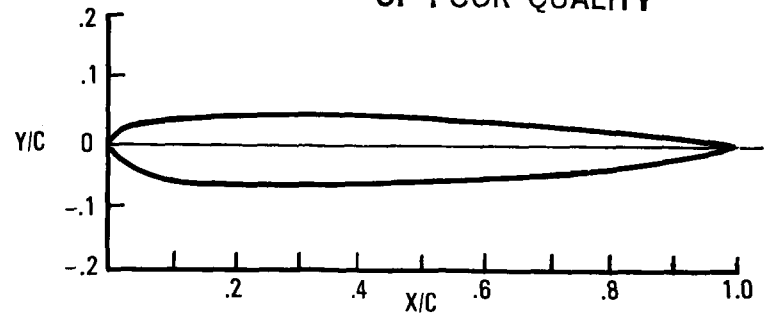

RSS2 AIRFOIL
SECTION COORDINATES

X/C	LOWER SURFACE Y/C	UPPER SURFACE Y/C
0.0	0.0	0.0
0.0015	-0.0104	0.0061
0.0062	-0.0202	0.0107
0.0138	-0.0290	0.0148
0.0245	-0.0368	0.0187
0.0381	-0.0438	0.0222
0.0545	-0.0497	0.0255
0.0737	-0.0548	0.0284
0.0955	-0.0589	0.0303
0.1198	-0.0622	0.0328
0.1464	-0.0647	0.0344
0.1753	-0.0664	0.0354
0.2061	-0.0675	0.0361
0.2388	-0.0679	0.0364
0.2730	-0.0679	0.0366
0.3087	-0.0674	0.0369
0.3455	-0.0666	0.0372
0.3833	-0.0654	0.0374
0.4218	-0.0640	0.0372
0.4608	-0.0624	0.0366
0.5000	-0.0606	0.0356
0.5392	-0.0587	0.0341
0.5782	-0.0566	0.0322
0.6167	-0.0543	0.0299
0.6545	-0.0517	0.0273
0.6913	-0.0490	0.0246
0.7270	-0.0460	0.0218
0.7612	-0.0428	0.0190
0.7939	-0.0393	0.0164
0.8247	-0.0356	0.0140
0.8536	-0.0317	0.0119
0.8802	-0.0277	0.0101
0.9045	-0.0237	0.0036
0.9263	-0.0198	0.0073
0.9455	-0.0161	0.0064
0.9619	-0.0127	0.0056
0.9755	-0.0098	0.0050
0.9862	-0.0073	0.0046
0.9938	-0.0055	0.0043
0.9985	-0.0044	0.0041
1.0000	-0.0040	0.0040

Figure 20. - RSS2 airfoil section.

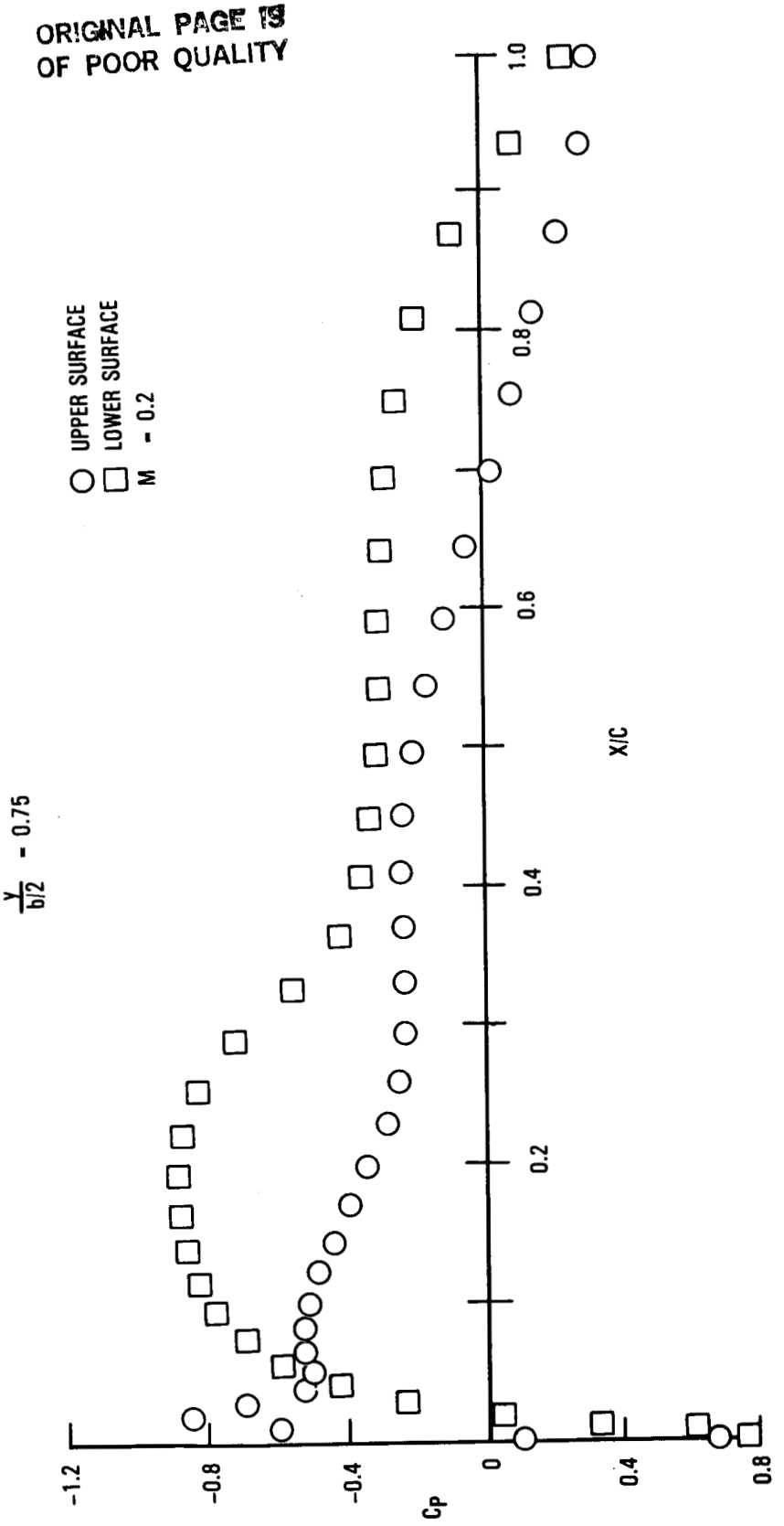

Figure 21. - Final redesign cruise pressure distribution.

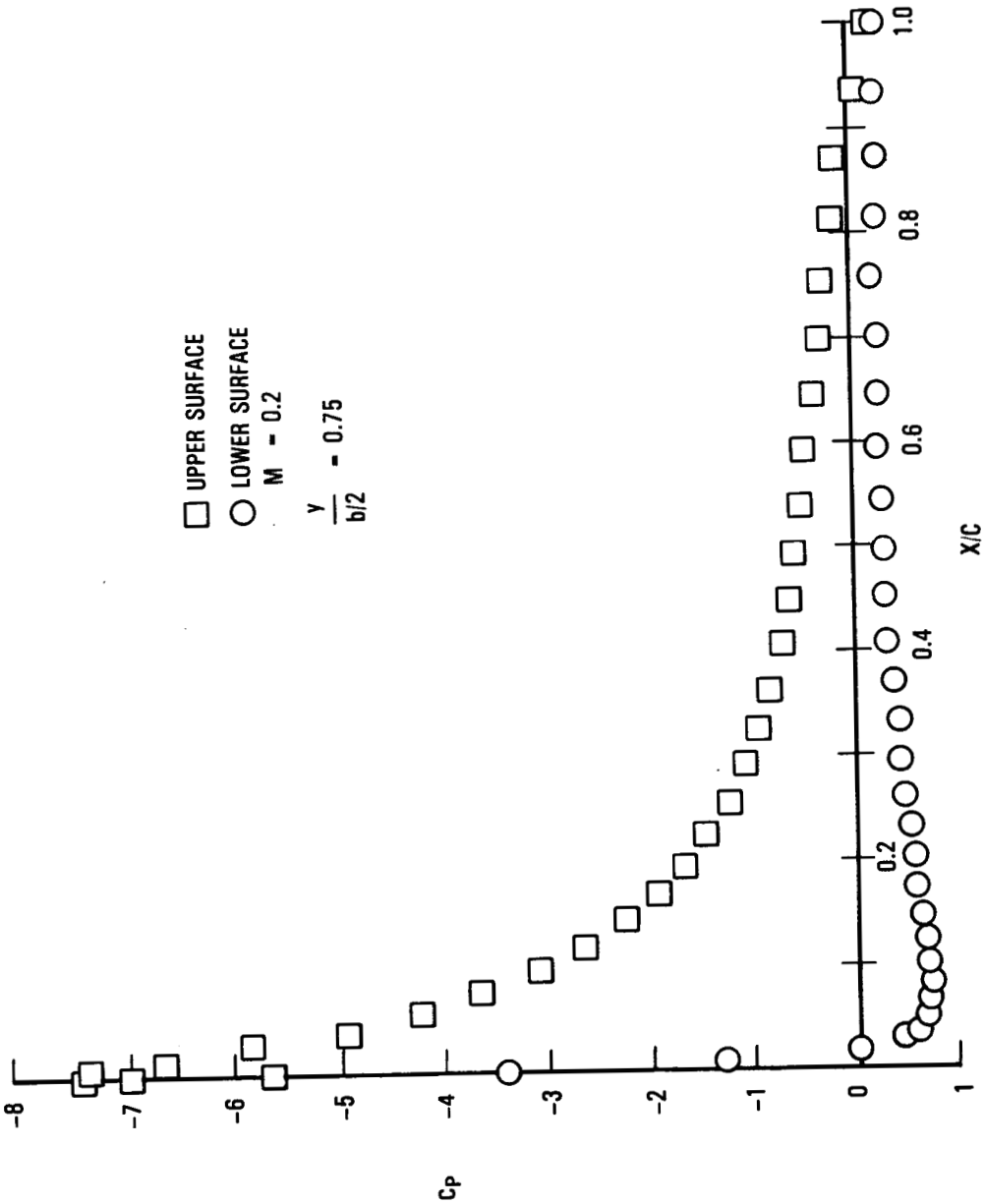

Figure 22. - Final redesign low speed, high download pressure distribution.

TABLE 2. - H_{17} SMALL TAIL COMPARATIVE DATA

	H_{8c} Standard	H_{16} Small	H_{17} Small
Aspect ratio	4	4	4
Taper ratio	0.33	0.33	0.33
Camber	0	0.013c	0.016c
Leading-edge radius	0.0089c	0.006c	0.036c
Thickness ratio	0.09	0.09	0.1045
Quarter chord sweep	35^0	28^0	25^0
Area, ft^2			
Total	1282	800	800
Exposed	960	552	552
Exposed/Total			
Elevator chord ratio	0.25	0.3	0.3
Stabilizer throw	15^0 ($+1^0$ to -14^0)	20^0 ($+2^0$ to -18^0)	20^0 ($+2^0$ to -18^0)
Elevator throw	25^0 (0^0 to -25^0)	40^0 ($+10^0$ to -30^0)	40^0 ($+10^0$ to -30^0)

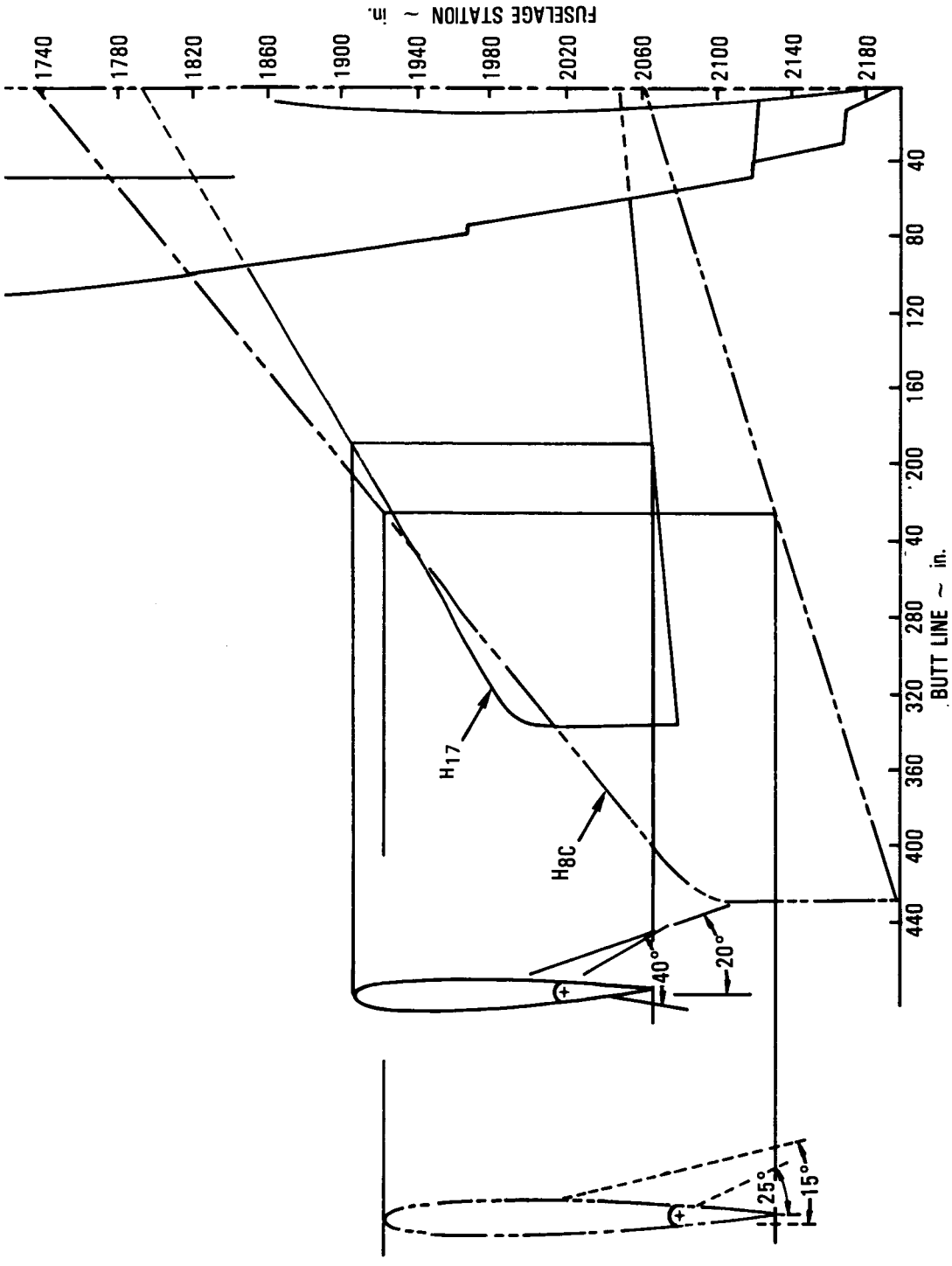

Figure 23. - H_{17} modified small horizontal tail compared with the H_{8c} standard tail.

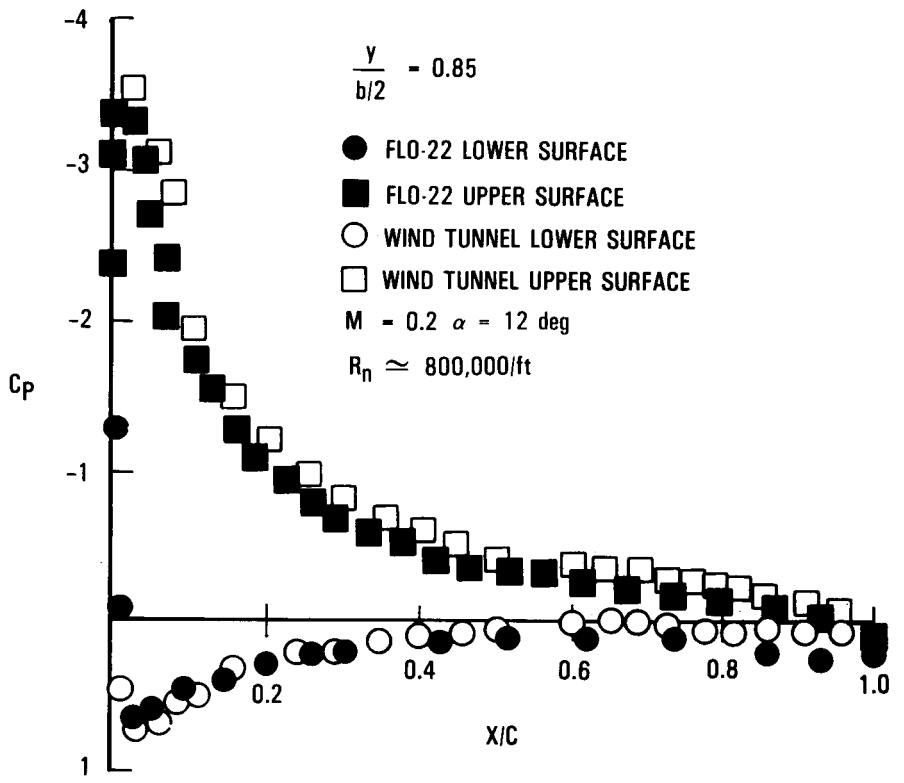

Figure 24. - Theory to experiment pressure distribution comparison.

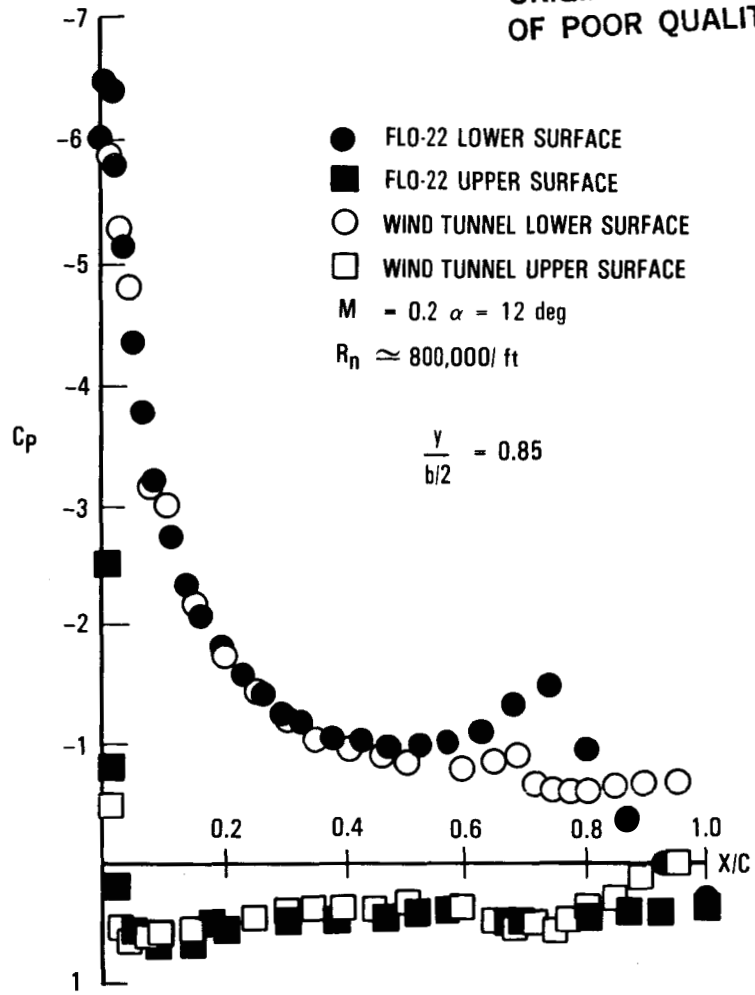

Figure 25. - Theory to experiment pressure distribution comparison - 30° up elevator.

Calculations were based on the same c.g. range used in the previous analysis: 0.12 to 0.35 $\bar{c}$ for weights less than 338,000 pounds.

SMALL HORIZONTAL TAIL LIFT COEFFICIENT

26° FLAPS

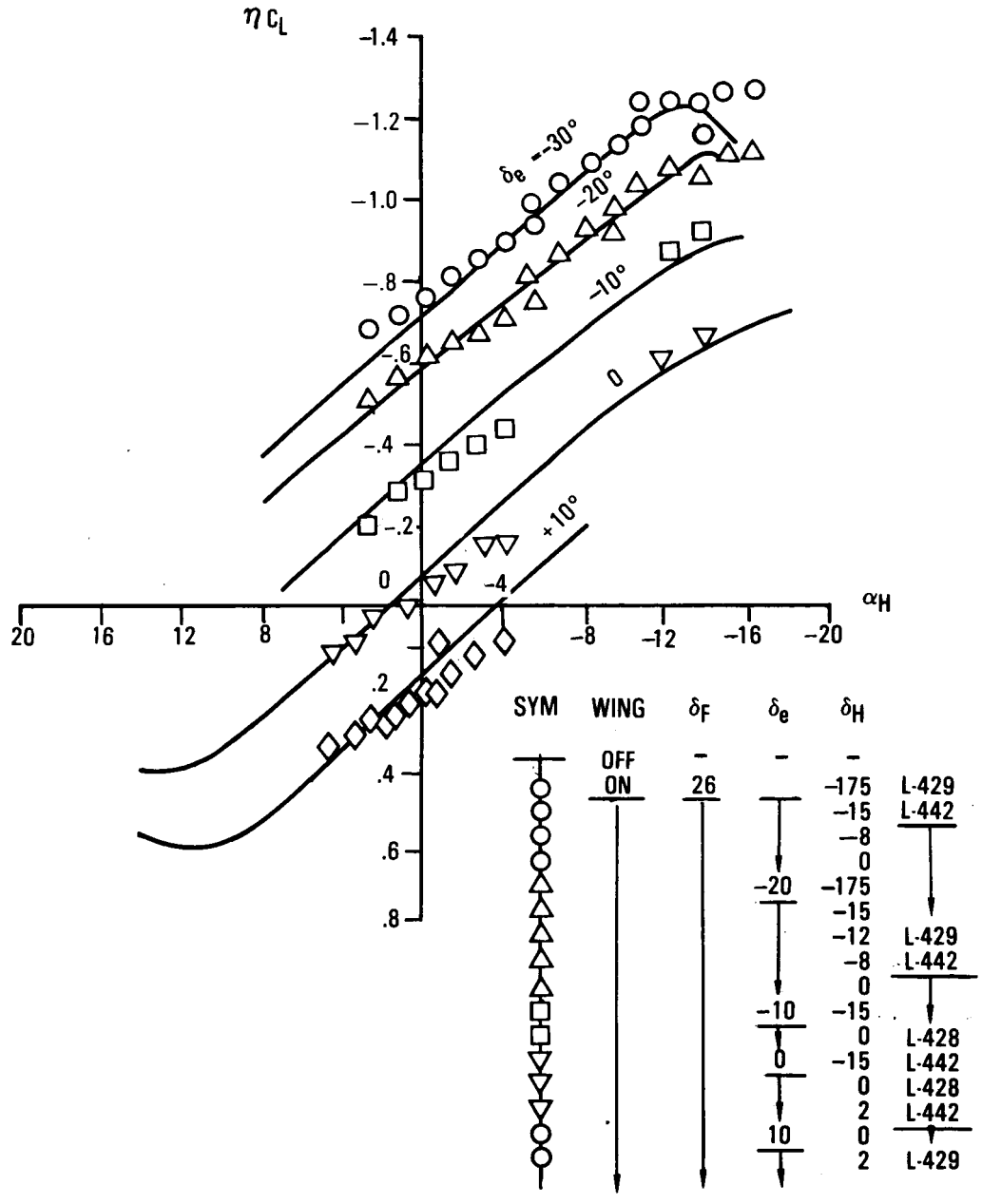

Figure 26. - H_{17} small horizontal tail high-lift characteristics.

4. COMMON-SIZE/NEAR-TERM SMALL TAIL

From the outset of the small tail development program, it was assumed that this sort of improvement would be incorporated into next generation derivative aircraft, which were expected to be of the long-body L-1011-1 type. Initial tail sizing was based on this assumption and also that it would be possible to employ leading-edge high lift devices on the small tail. This premise implied production application at an undetermined time sufficiently far downstream to allow development through flight testing of the smallest on limit condition tail. However, as the study progressed, the worsening economic environment made it more important for airlines to operate at a profit, thus increasing the urgency for incorporating major performance improvements into new derivative aircraft. Consequently, the objective was established to incorporate a small horizontal tail in near-term L-1011 derivative aircraft; and in order to accommodate all L-1011 derivatives, it became necessary to design a common-size small horizontal tail for both short-body and long-body derivatives.

4.1 Final Sizing Analysis

In resizing the small horizontal tail, a number of new requirements were recognized:

- Possible future use of the small horizontal tail on L-1011-500 short-body derivatives.
- Decreased stabilizer/elevator throw limits for the increased area tail with fixed fuselage cutout available; δ_H/δ_e = +2 deg/+5 deg to -15 deg/-30 deg.
- An $0.12\bar{c}$ forward c.g. limit was used in conjunction with the takeoff and landing flaps deflection limits defined for the dash 500 airplanes: 27 degrees and 33 degrees, respectively. A landing flaps deflection of 42 degrees was used in the initial tail sizing analysis (Section 1.2).

The small horizontal tail resizing analysis was based on a maximum lift coefficient capability of -1.4 This value was selected based on the premise that the H_{17} tail low-speed $C_{L_{MAX}}$ of -1.25 at wind-tunnel scale Reynolds number would grow to -1.4 at full scale flight conditions.

Calculations were based on the same c.g. range used in the previous analysis: 0.12 to 0.35 $\bar{c}$ for weights less than 338,000 pounds.

Results of the resizing analysis are illustrated in Figures 27 and 28. These figures show that a tail size of 898 square feet is required to achieve nosewheel liftoff (Figure 27) and control-to-stall (Figure 28) at the forward c.g. limit. Figure 28 also shows that this tail area satisfies the stall recovery and stability requirements at aft c.g. This final small tail size still represents an area reduction of 30 percent from the standard tail.

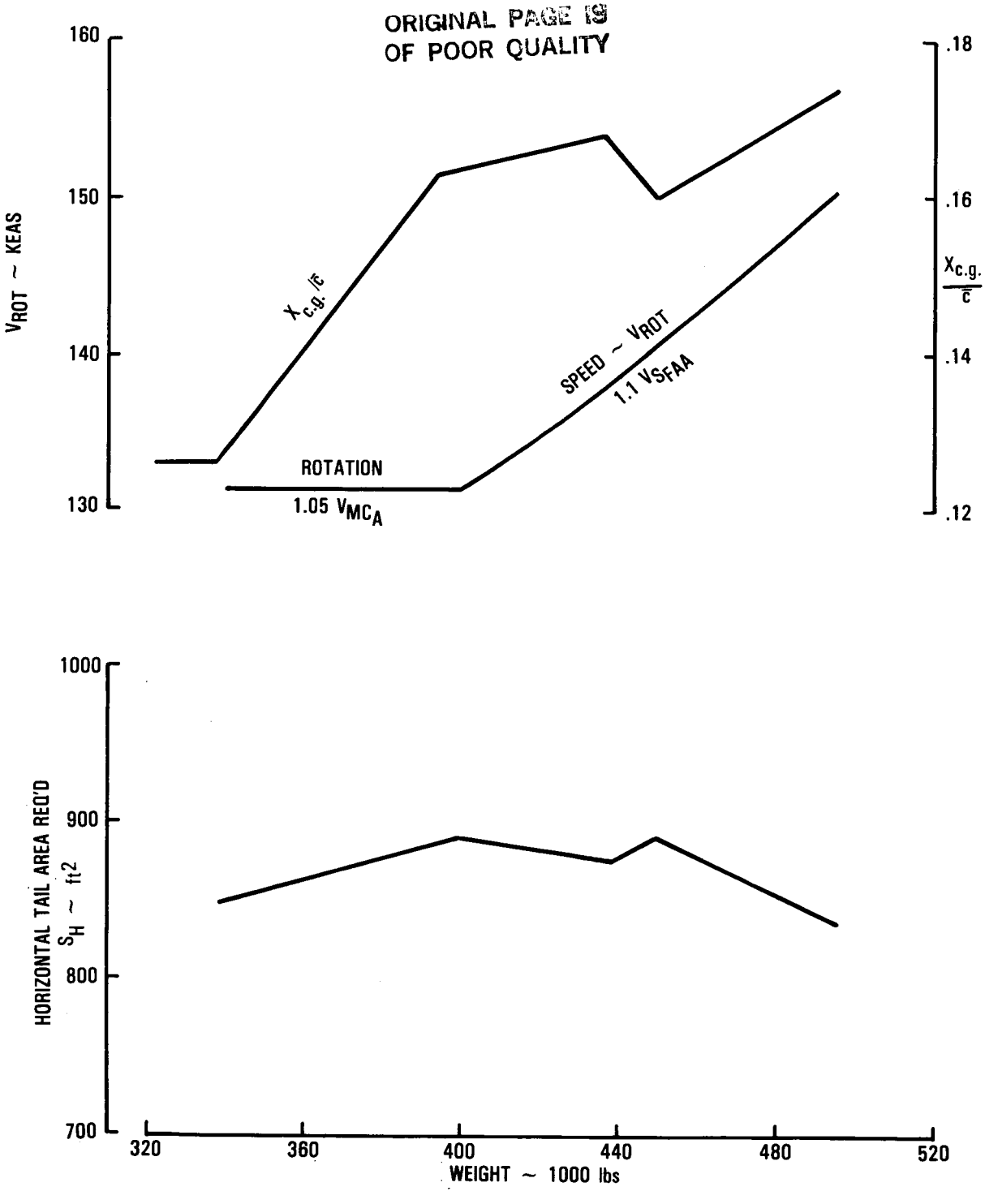

Figure 27. - Horizontal tail area required for takeoff nosewheel-liftoff.

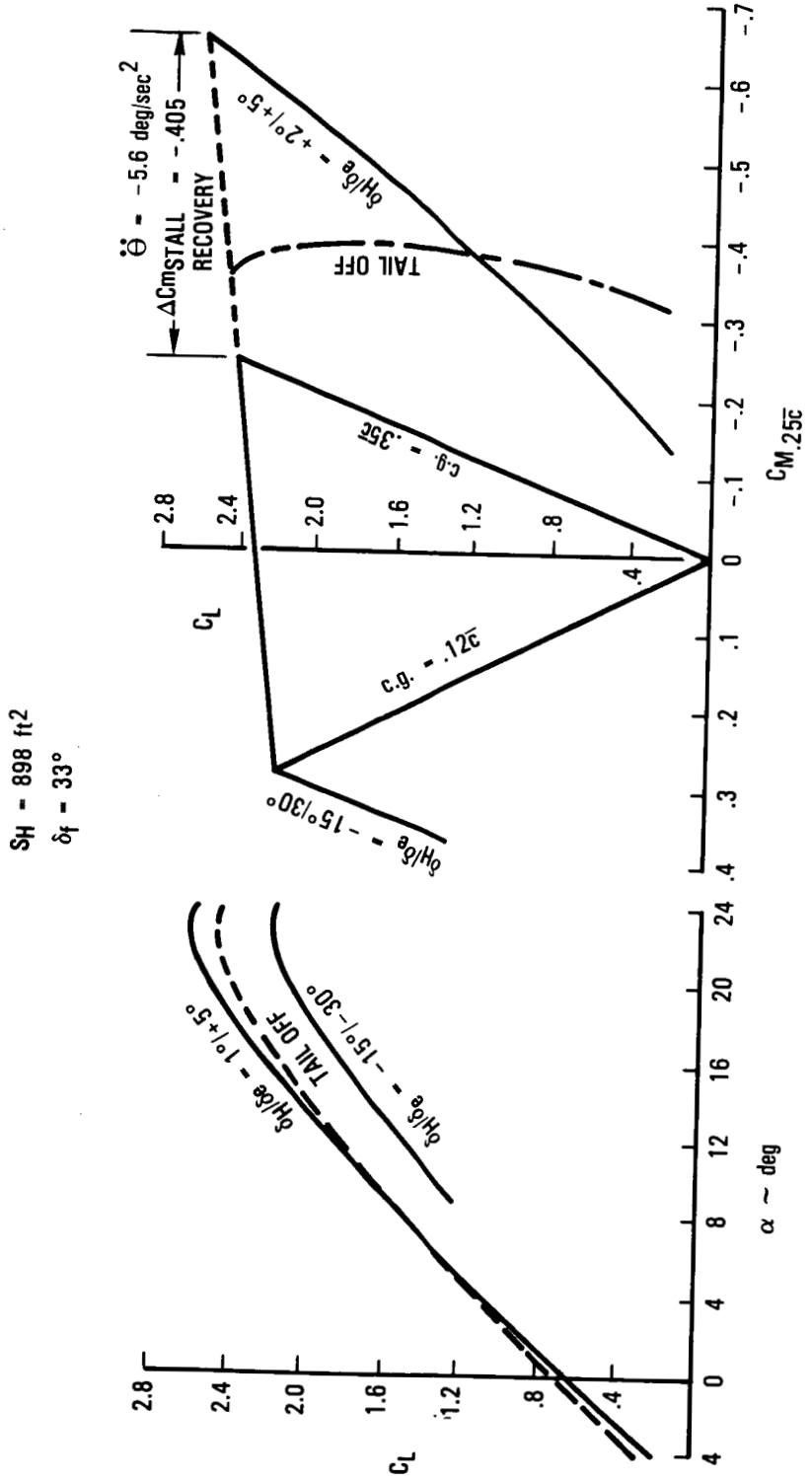

Figure 28. - Horizontal tail area required for landing configuration control to stall.

4.2 Common-Size Small Tail Design - H_{18}

A layout of the small horizontal tail suitable for all L-1011 derivatives is shown in Figure 29. The wind-tunnel model designation for this tail is H_{18}. In designing this tail the aspect ratio was increased from 4.0 to 4.5 to further enhance the lift slope characteristics of the surface. The design also features a hyperbolic tip which is intended to benefit high-speed drag characteristics. The design retains the quarter chord sweep angle and RSS2 airfoil section of the previous tail (H_{17}). Characteristics of the H_{18} tail compare with the previous designs as shown in Table 3.

4.3 Estimated Cruise Drag Reduction

Existing handbook methods do not accurately predict the drag characteristics of advanced technology airfoils. In fact, preliminary estimates for the original small tail (H_{16}) were found to be 27 percent too low, while estimates for the standard tail (H_{8c}) were accurate. Recognizing these deficiencies, a standard handbook estimates of the H_{18} drag was not made. Instead, since there was no airfoil change from the H_{17} tail, the potential cruise drag reduction for the H_{18} tail was estimated by applying an exposed area correction to previous wind-tunnel test results. Recall the H_{17} tail was designed to have essentially the same cruise drag characteristics as the H_{16} tail, but a quantitative evaluation of the H_{17} tail cruise drag was not performed due to its low speed lift deficiencies. Therefore, the H_{18} drag benefit was estimated based on data for the H_{16} tail in Figure 5. By applying an exposed area correction factor to data in Figure 5, it was estimated that the H_{18} small horizontal tail would reduce the drag of the L-1011 about 6 counts at wind-tunnel conditions for an overall cruise L/D benefit of about 2 percent, including the weight reduction of the smaller tail.

4.4 Wind-Tunnel Test Results

4.4.1 Low speed.- A model of the H_{18} small horizontal tail was constructed for an existing 1/20th scale model of an L-1011 for testing in the NASA/Ames Research Laboratory 12 foot Pressure Tunnel. The purpose of the test was to determine the effects of the H_{18} tail on the low-speed longitudinal stability and control characteristics of an L-1011-1, with emphasis on defining small horizontal tail control capability. The primary objective was to obtain low-speed, high Reynolds number data for the configuration with flap deflection angle at the maximum takeoff setting, which defines the tail size requirement for takeoff rotation.

Testing was conducted during the period from 15 through 22 January 1980. Complete configuration six-component forces and moments were measured with horizontal tail on and off.

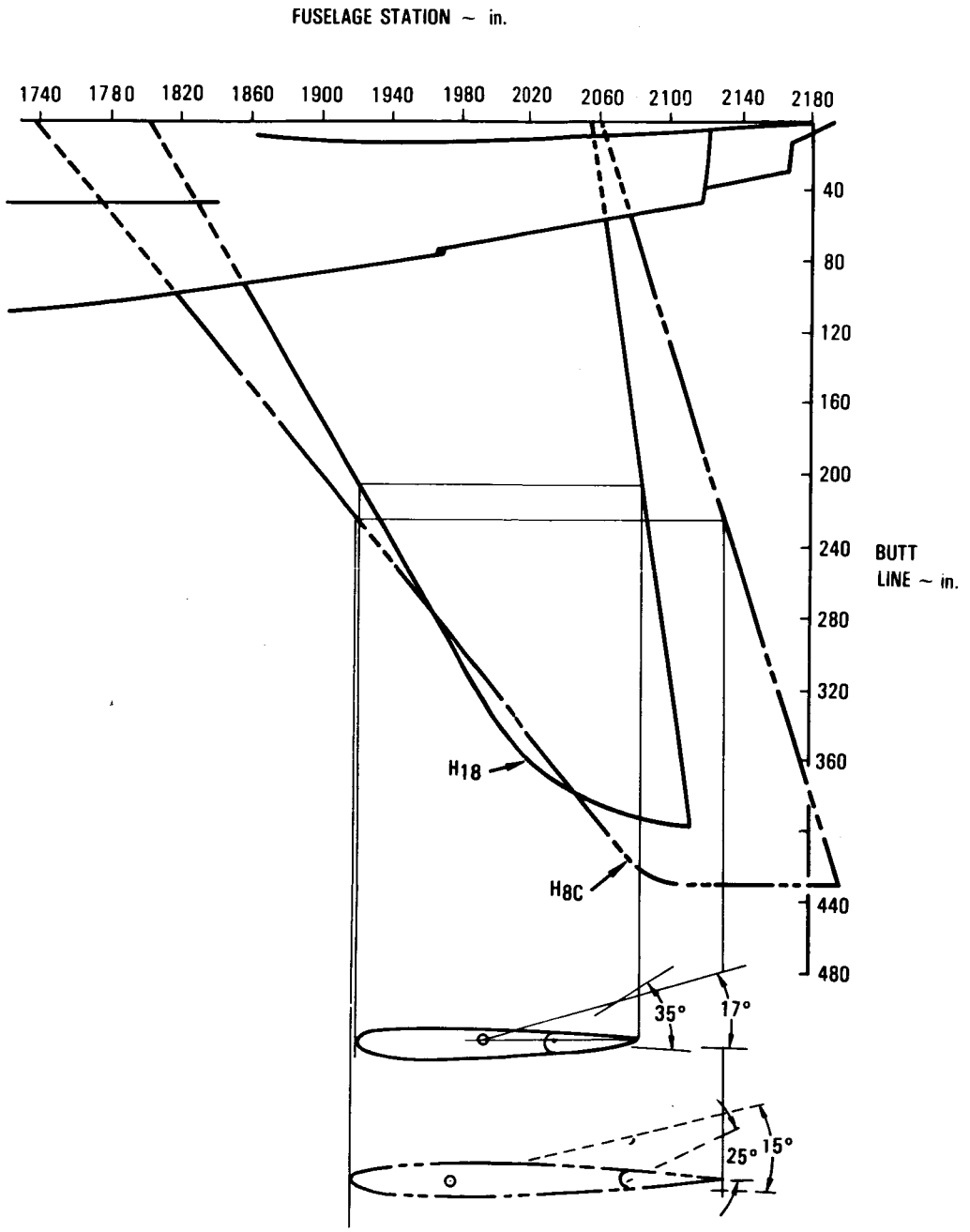

Figure 29. - H_{18} small horizontal tail compared with the H_{8c} standard tail.

TABLE 3. - H_{18} SMALL TAIL COMPARATIVE DATA

	H_{8c} Standard	H_{16} Small	H_{17} Small	H_{18} Small
Aspect ratio	4	4	4	4.5
Taper ratio	0.33	0.33	0.33	0.33
Camber	0	0.013c	0.016c	0.016c
Leading-edge radius	0.0089c	0.006c	0.036c	0.036c
Thickness ratio	0.09	0.09	0.1045	0.1045
Quarter chord sweep	35^0	28^0	25^0	25^0
Area, ft^2				
Total	1282	800	800	898
Exposed	960	552	552	652
Exposed/Total	0.75	0.69	0.69	0.73
Elevator chord ratio	0.25c	0.3c	0.3c	0.3c
Stabilizer throw	15^0 ($+1^0$ to -14^0)	20^0 ($+2^0$ to -18^0)	20^0 ($+2^0$ to -18^0)	17^0 ($+2^0$ to -15^0)
Elevator throw	25^0 (0^0 to -25^0)	40^0 ($+10^0$ to -30^0)	40^0 ($+10^0$ to -30^0)	35^0 ($+5^0$ to -30^0)

The lift and pitching moment data obtained during the test exhibited a "bubble" characteristic which had not been observed in any previous L-1011 wind-tunnel entry. The problem was encountered only at high Reynolds number 5.6×10^6/ft. and only with the wing flaps and slats deployed.

During a brief investigation of the problem, wind-tunnel balance, instrumentation, and data reduction were eliminated as possible causes. This led to the conclusion that the phenomenon was related to the wing high-lift system, since the problem did not occur with the clean wing. Insufficient test time to explore this problem led to the decision to remove the wing to determine the small horizontal tail control effectiveness. The problem did not occur with the wing off.

The incremental difference between horizontal tail on and off pitching moment data were used as a basis for extracting the lift characteristics of the the H_{18} tail. This was done both with wing-on and wing-off data. A geometric tail arm from the wing-to-tail $0.25\bar{c}$ was used in the data reduction.

The wind-tunnel extracted lift characteristics of the H_{18} tail are shown in Figure 30. This figure shows excellent correlation of the wing-on and wing-off data for the horizontal tail, adding credibility to the wing-on data. Most importantly, these data show that the H_{18} tail achieved a maximum lift coefficient of -1.4, which was the design target value used in the H_{18} tail sizing exercise.

It was thus established that the low-speed design objectives of the H_{18} tail had been achieved. However, some doubt was cast on this favorable result when it was later discovered that the bubble phenomenon was caused by a problem with either the N1 balance gage or the balance conditioning instrumentation, which caused the output to consistently jump from 4500 to 6300 counts. As a result, NASA/Ames wind-tunnel personnel advised that the data were highly questionable. All of this considered, it is believed that the data which were extracted for the tail alone may still be realistic in view of the fact that the problem did not occur with the wing off, yet the tail lift characteristics were essentially the same.

4.4.2 High speed.- A model of the H_{18} small horizontal tail was constructed for the existing 1/30th scale high-speed model. This model was designed for: 1) complete airplane model force tests to determine the longitudinal stability and control characteristics of the L-1011 with small tail, and 2) for horizontal tail pressure measurements to define the airloads required for structural analysis and control system design. The right-hand panel of the horizontal tail was instrumented with 102 pressure taps (51 top and bottom) distributed along the chord at four spanwise locations as shown in Figure 31. The left-hand panel of the small tail was equipped with a strain gaged beam to measure elevator hinge moments.

The objective of the high-speed test were to:

- Determine the incremental drag of the H_{18} small horizontal tail.
- Obtain pressure data on the exposed portion of the small horizontal tail surface to determine airloads distributions, and obtain total pivot moment characteristics of the stabilizer.
- Record strain gage measurements of total elevator hinge moments.
- Measure six-component forces and moments with the small tail on and off to determine complete configuration lift, drag, and pitching moment characteristics as well as the total control capability of the small horizontal tail.
- Obtain six-component force and moment measurements with standard-size tail on for comparison with the small tail results.

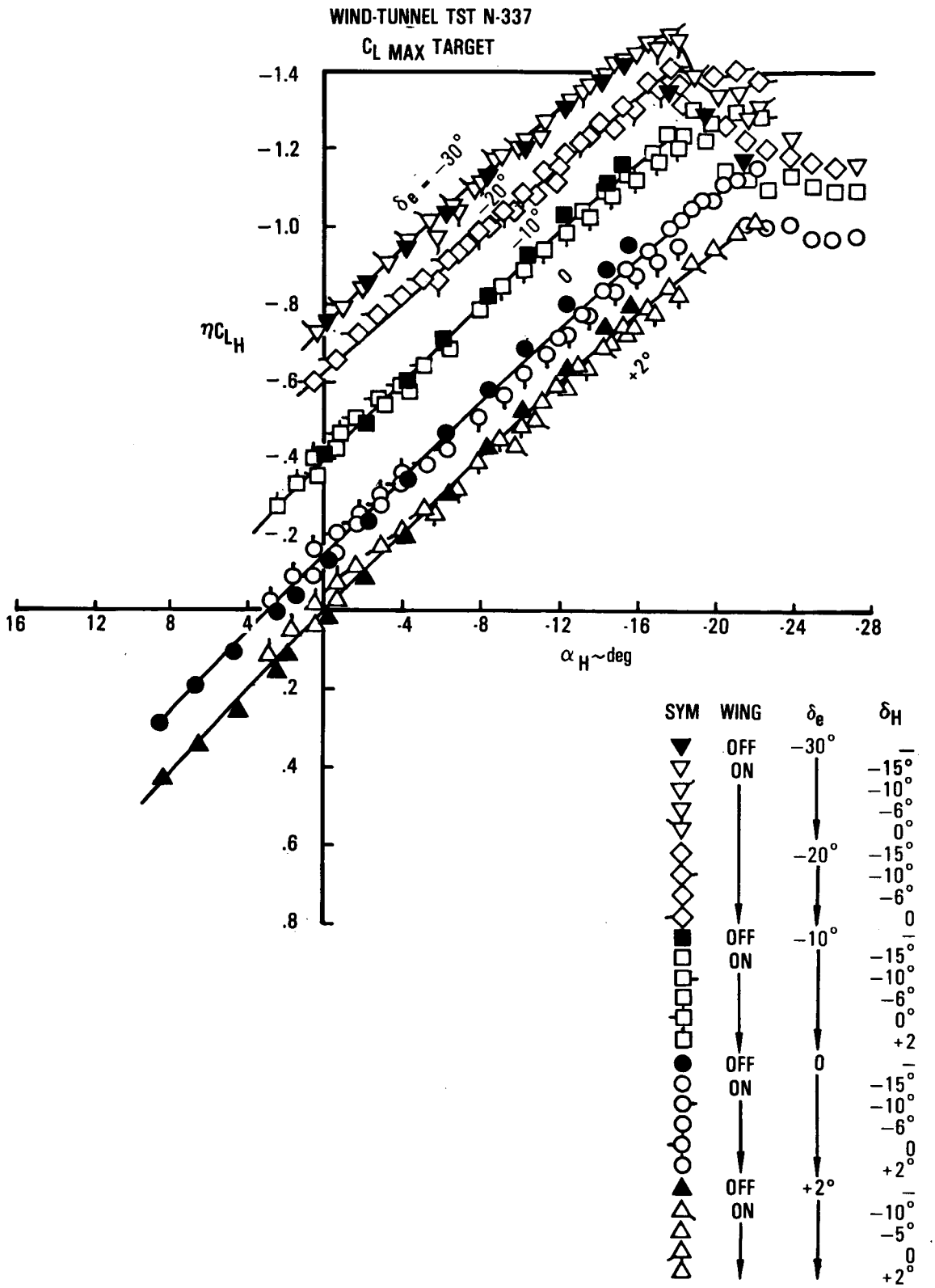

Figure 30. - H_{18} small horizontal tail high-lift characteristics.

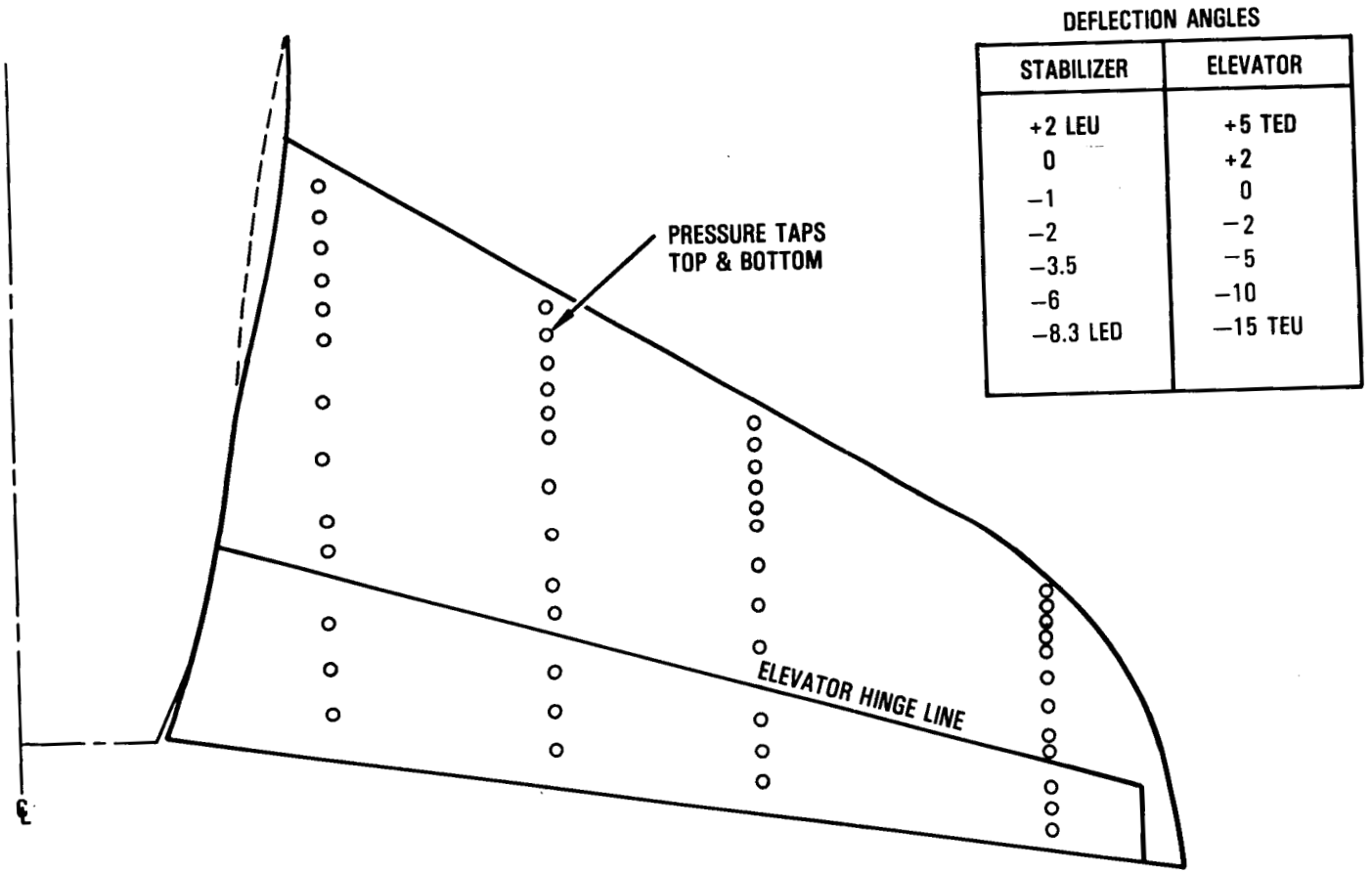

Figure 31. - H_{18} horizontal tail high-speed pressure model.

The first high-speed wind-tunnel test was conducted in the NASA/Langley 8 ft Transonic Pressure Tunnel during the period 24 through 31 July 1979. Figure 32 shows the L-1011 1/30th scale force model with pressure instrumented horizontal tail in the Langley 8 ft Transonic Pressure Tunnel. The test concentrated on the Mach number range 0.5 to 0.95 and at angles of attack extending to the limit determined by model dynamics. Specific Mach number conditions were as follows:

$$M = 0.5,\ 0.8,\ 0.83,\ 0.86,\ 0.9,\ 0.95$$

the corresponding Reynolds number was 3×10^6 per foot. The test angle of attack range varied with Mach number generally as follows:

M	Test α
0.5	0, 2, 3, 4, 5, 6, 8, 10
0.8	0, 2, 3, 4, 5,,6, 7
0.83	0, 2, 3, 4, 5,,6, 7
0.86	0, 2, 3, 4, 5,,6, 7
0.9	0, 2, 3, 4, 5,,6
0.95	0, 2, 3, 4, 5,,6

A record of configurations and conditions tested is presented in Table 4. This record shows a total of 84 actual data runs subdivided as follows:

Tail Configuration	Runs
Small	62
Off	6
Standard	16
	Total 84

The Langley high-speed wind tunnel test data revealed some unexpected results pertaining to the longitudinal static stability derivative, the control effectiveness derivative, and the drag polar.

The longitudinal static stability data for the L-1011 with standard-size tail showed some sharp variations from Mach 0.86 to 0.95 that had not been seen in previous wind-tunnel or flight tests. These data are presented in Figure 33A. The sharp increase of the stability derivative from M = 0.86 to M = 0.90 show the neutral point moving swiftly forward and the sharp decrease from M = 0.90 to M = 0.95 show the neutral point moving swiftly aft. A similar variation in stability occurred for the small horizontal tail model as shown in Figure 33B.

The control effectiveness derivative extracted from the wind-tunnel test for the standard-size tail showed the tail effectiveness to be less than previous wind-tunnel and flight test data as shown in Figure 34A. However, the

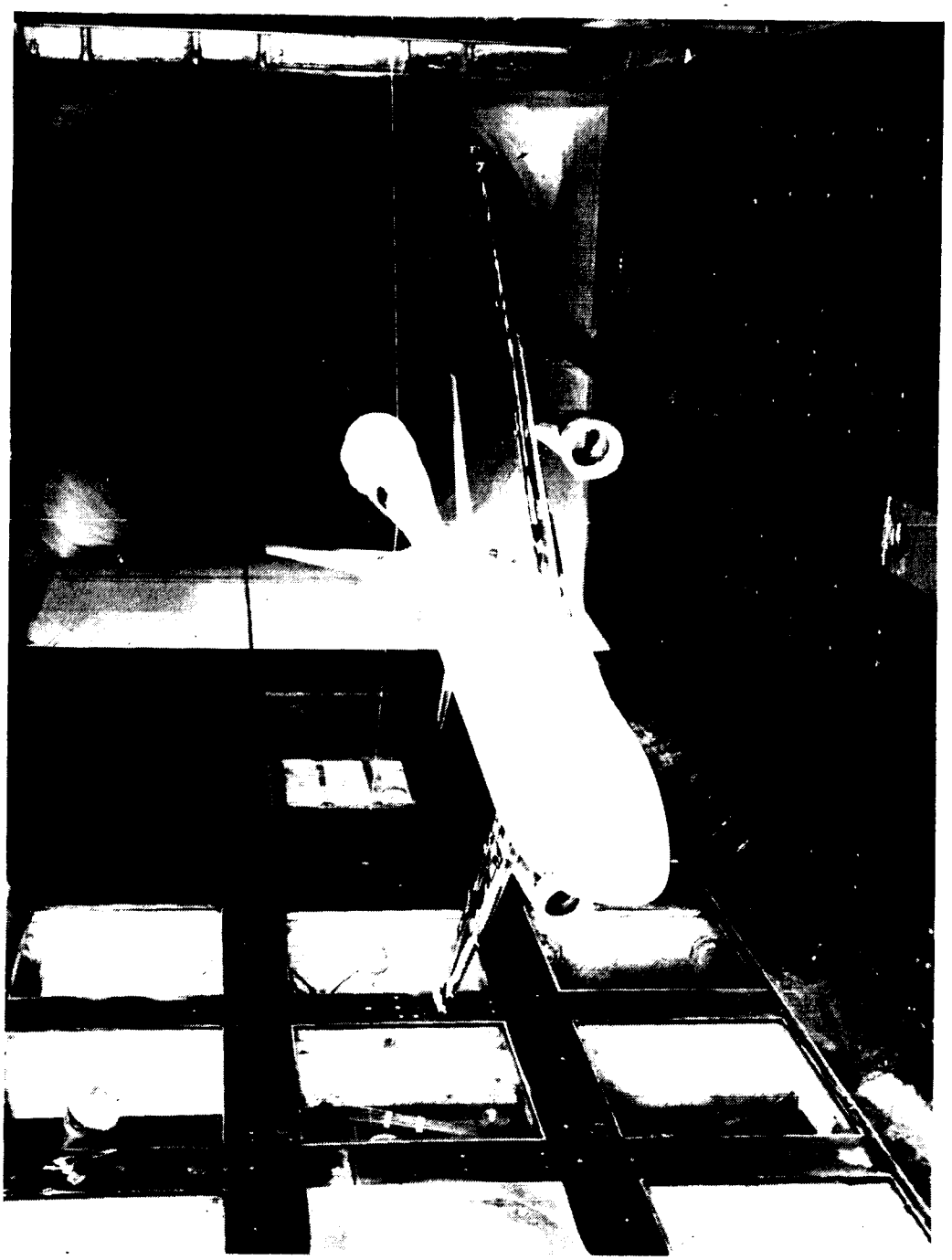

Figure 32. - L-1011 baseline model in LRC 8-foot transonic pressure tunnel.

TABLE 4. - NASA/LANGLEY 8-FOOT TRANSONIC PRESSURE TUNNEL TEST RUN RECORD

Configuration	Tail	Angles	M Series						Remarks
	δ_H	δ_e	.5	.8	.83	.86	.90	.95	
$S_{25}V_9H_{18}^{-2}$ e^0	-2	0	6	5	4	3	2	1	Inverted
			12	11	10	9	8	7	Upright
e^{-2}		-2	17	16	15	14	13		
H_{18}^{+2} e^{+5}	+2	+5	27	26	25	24	23		
e^0		0	22	21	20	19	18		
$H_{18}^{-3.5}$ e^{-5}	-3.5	-5	31	30	29	28			
H_{18}^{-6} e^{-10}	-6	-10	35	34	33	32			
e^0		0	40	39	38	37	36		Model Fouling
H_{18}^0	0	0	49	48	47	46	45	44	
+ Fillet				43	42	41			
e^{-10}		-10	53	52	51	50			Tail Fillet On
e^{+5}		+5	59	58	57	56			
e^{-5}		-5							
e^{+2}		+2		62	61	60			
Off Off	Off	Off	68	67	66	65	64	63	
H_{8C}^{+1} e^0	+1	0	72	71	70	69			Tail Off
H_{8C}^0	0		78	77	76	75	74	73	Std. Tail
H_{8C}^{-1}	-1		84	83	82	81	80	79	

S_{25} – L-1011-1 model with standard wing (w/o ext. tips) and with tails off

V_9 – Vertical tail

H_{8c}, H_{18}– Horizontal tail – e – Horizontal tail elevator.

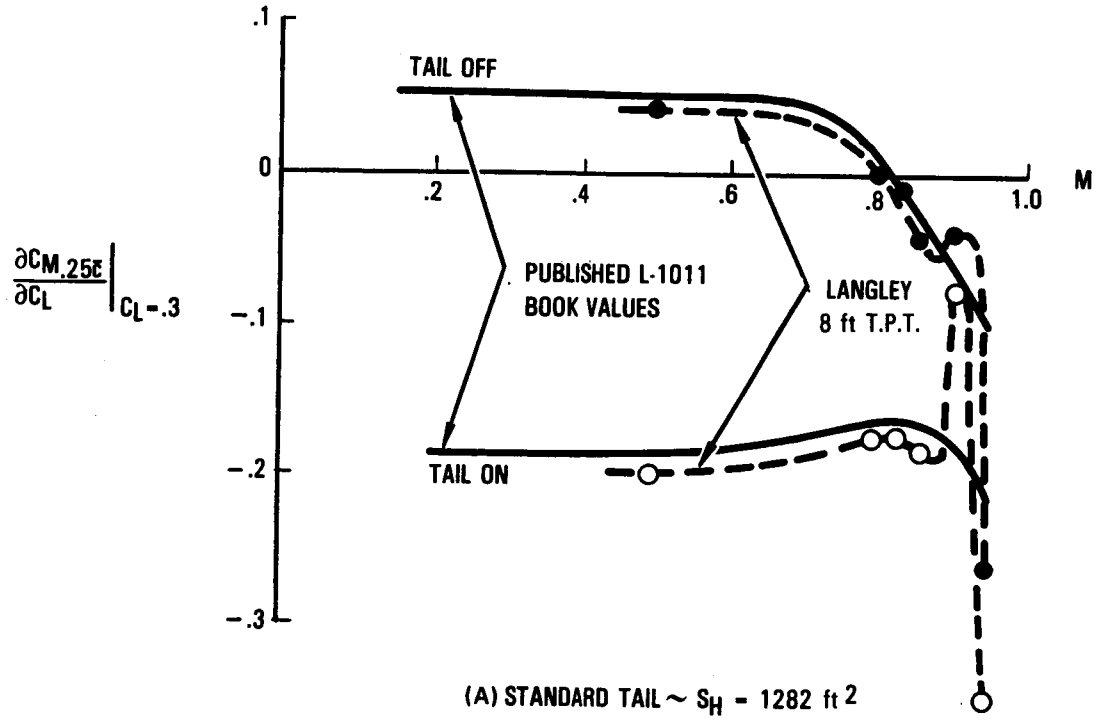

(A) STANDARD TAIL ~ S_H = 1282 ft^2

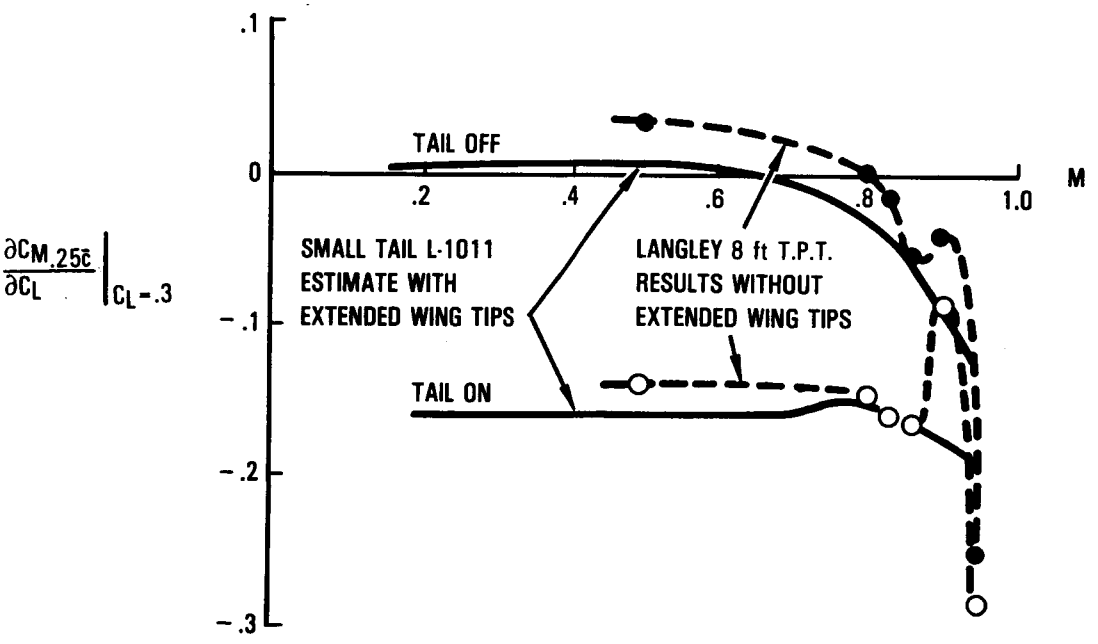

(B) SMALL TAIL ~ S_H = 898 ft^2

Figure 33. - Comparison of L-1011 and NASA/Langley 8 foot T.P.T. ongitudinal static stability derivatives

S_{REF} = 3456 ft^2

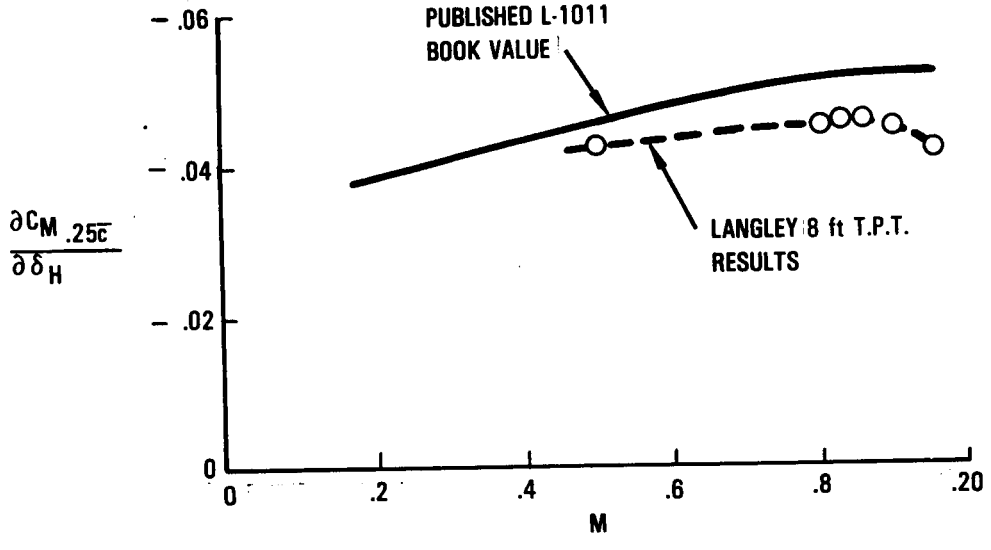

(A) STANDARD TAIL ~ S_H = 1282 ft^2

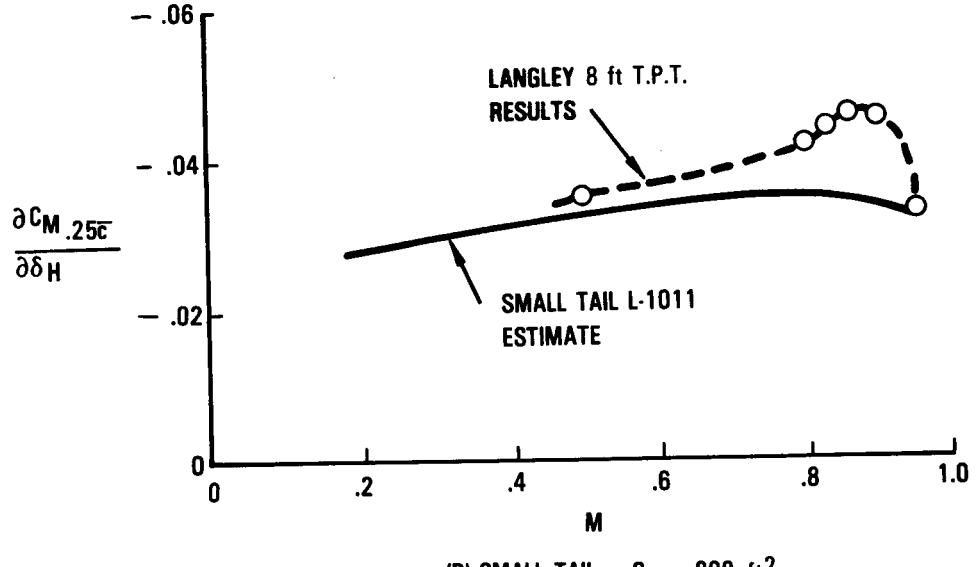

(B) SMALL TAIL ~ S_H = 898 ft^2

Figure 34. - Comparison of L-1011 Control effectiveness and NASA/Langley 8 foot T.P.T. horizontal tail

small tail effectiveness shown in Figure 34B was greater than and had a much sharper peak in the cruise Mach number range than the estimated effectiveness for the L-1011. Note that at a Mach number of 0.86 the test results show the small tail to be as effective as the standard tail.

The small incremental difference between the small and standard-size tails test results is shown in Figure 35. This difference was smaller than expected.

A review of the differences in the Langley wind-tunnel data and previous test data led to the conclusion that wall interference or blockage effects occurred in the Langley tunnel because of the relative size of the model to the tunnel test section. The 1/30th scale test model had a 62 inch wing span, and the tunnel width was 85 inches. The previous L-1011 wind tunnel tests had been performed in the Calspan Corporation transonic facility which had a slightly larger width (96 inches). Consequently, a brief test was scheduled in the Calspan tunnel to resolve the model wing span versus tunnel width question and obtain test data for some additional flight conditions.

The additional wind-tunnel testing in the Calspan 8 foot Transonic Facility was performed from 26 through 28 September, 1979. A record of configurations and conditions tested is presented in Table 5. This record shows a total of 108 actual data runs subdivided as follows:

Tail Configuration	Runs
Small	87
Off	12
Standard	9
Total	108

This test differed from the previous test in that force and moment data and horizontal tail pressures were obtained with the wing off, and with boundary layer transition grit on and off the horizontal tail to determine the effect of grit on shock wave location. The model was also tested with boundary layer transition grit on and off the wing, both with horizontal tail on and off.

Because of the larger dimensions of the Carlspan wind tunnel relative to the Langley wind tunnel, it was possible to add the L-1011 wing tip extension to the model; the wing span was 65.6 inches instead of 62 inches.

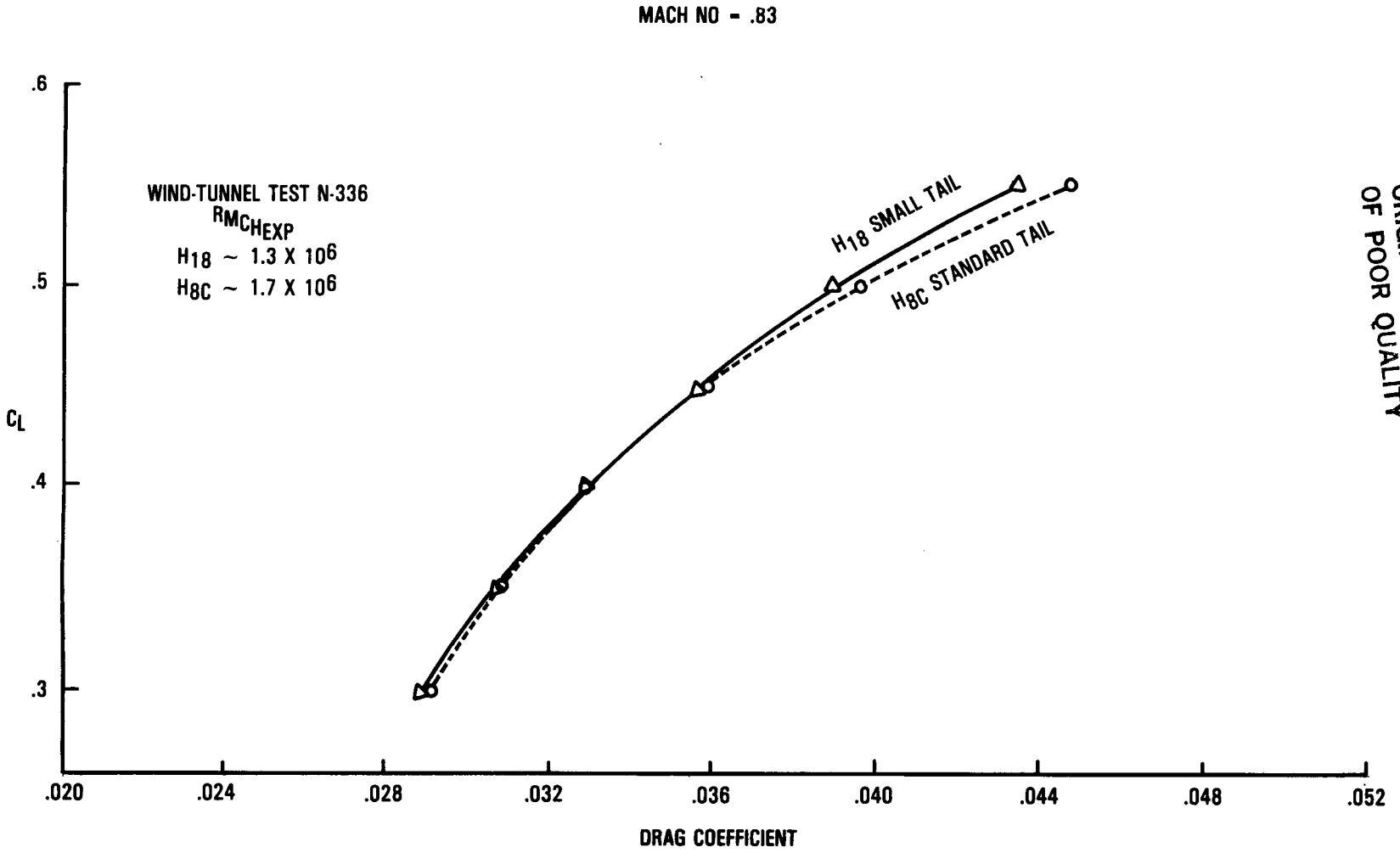

Figure 35. - Zero trim drag polar characteristics of the L-1011 with H_{18} small and H_{8c} standard horizontal tails - Langley test results.

TABLE 5 - CALSPAN 8 FOOT TRANSONIC WIND-TUNNEL TEST RUN RECORD

Configuration	Tail Angles δ_H	Tail Angles δ_e	R_N/FT X 10^{-6}	α	M Series 0.7	0.8	0.83	0.86	0.9	0.95	Remarks
$S_{25}V_9H_{18}^{-3.5}$ e^0 - W_{27B}	-3.5	0	3.5	α_1		10		7	8	7	Wing off; grit off H_{18}
H_{18}^0	0					14	13		12	11	↓
						18	17		16	15	Grit on H_{18}
$H_{18}^{-3.5}$	-3.5					22	21		20	19	all remaining runs.
H_{18}^0 e^{+5}	0	+5				26	25		24	23	
		-10				30	29		28	27	
H_{18}^{-1} e^0	-1	0		α_2	37	36	35	34	33	32	Wing on; W/O grit; Inverted
					44	43	42	41	40	39	Upright
					50	49	48	47	46	45	Wing grit on
$H_{18}^{-3.5}$	-3.5				56	55	54	53	52	51	Stabilizer
H_{18}^{+2}	+2				62	61	60	59	58	57	↓
e^{+5}		+5		α_3		67	66	65	64	63	Gearing
H_{18}^{-2} e^{-2}	-2	-2				72	71	70	69	68	↓ ↓
H_{18}^0 e^0	0	0		α_2	78	77	76	75	74	73	↓
e^{+2}		+2		α_3		83	82	81	80	79	↓
e^{+5}		+5		α_2	89	88	87	86	85	84	Elevator
		-10			95	94	93	92	91	90	↓
H_{8c}^0	0			α_3		99	98	97			Std. Tail
H_{8c}^{-1}	-1					102	101	100			↓
H_{8c}^{-2}	-2					105	104	103			
				α_2	112	111	110	109	108	107	Tail off; wing grit ON
					118	117	116	115	114	113	OFF

α_1 = -6, -4, -2, 0 2 4 6; α_2 = -8, -6, -4, -2, 0 1, 2, 3, 4, 5, 6, 8, 10, 12; α_3 = -2, 0, 1, 1.5, 2.0, 2.5, 3.0, 3.5, 4.0, 4.5, 5, 6, 8

A comparison of the NASA Langley and Calspan high-speed wind-tunnel tests results shows:

- Longitudinal static stability data from the Langley and Calspan tests (Figure 36) are in generally good agreement for Mach numbers less than 0.86. Between Mach 0.86 and 0.90 the Langley stability derivatives increase and decrease as was shown in Figure 33, whereas the Calspan derivatives fall below the predicted values. Further investigations are required to explain the descrepancy between predictions and test results in the Mach number range from 0.86 to 0.90.

- A comparison of the Langley and Calspan longitudinal control effectiveness for the H_{18} horizontal tail stabilizer and elevator are shown in Figures 37 and 38 respectively. The test results from the two tunnels was in excellent agreement. However, control effectiveness of the stabilizer was considerably more effective than predicted in the cruise Mach number range. This is due to higher than predicted lift slope characteristics of the surface. The elevator effectiveness was slightly less than predicted.

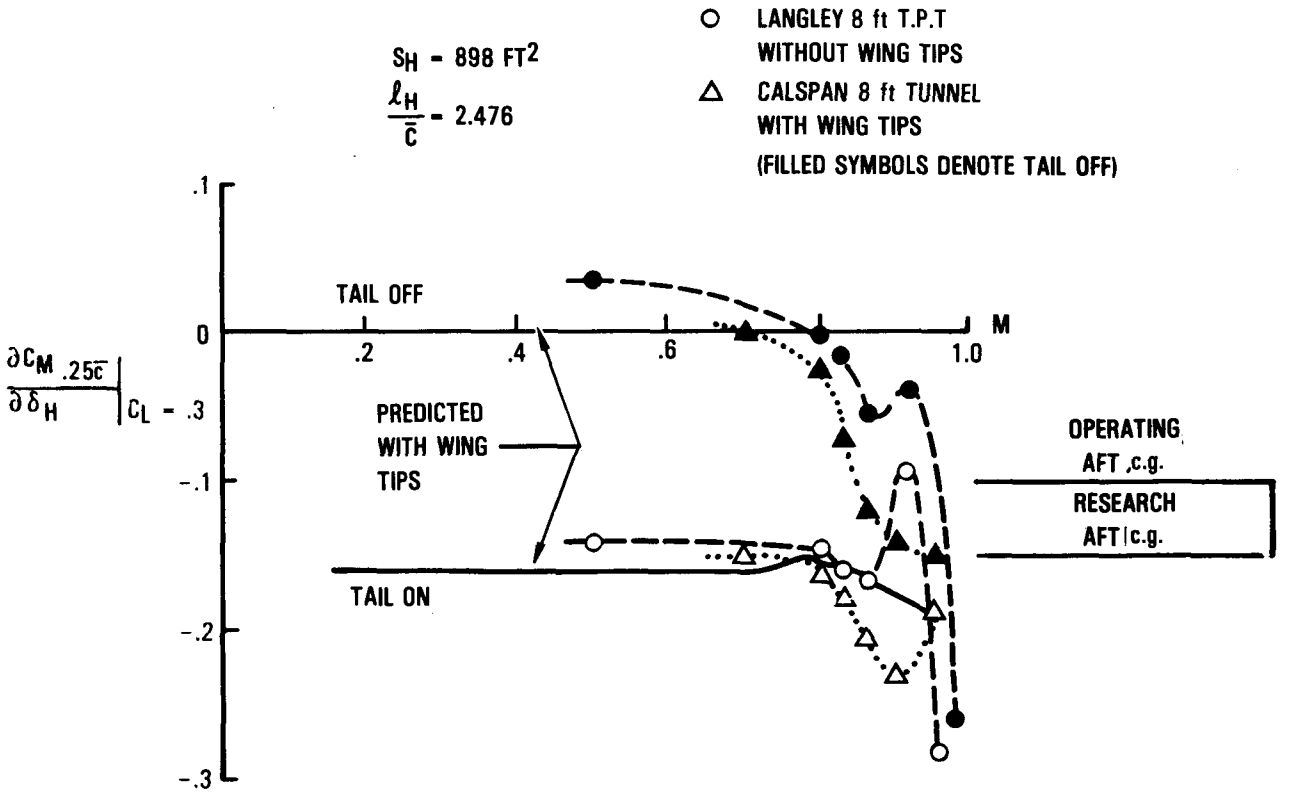

Figure 36. - Longitudinal static stability derivatives with the H_{18} small tail.

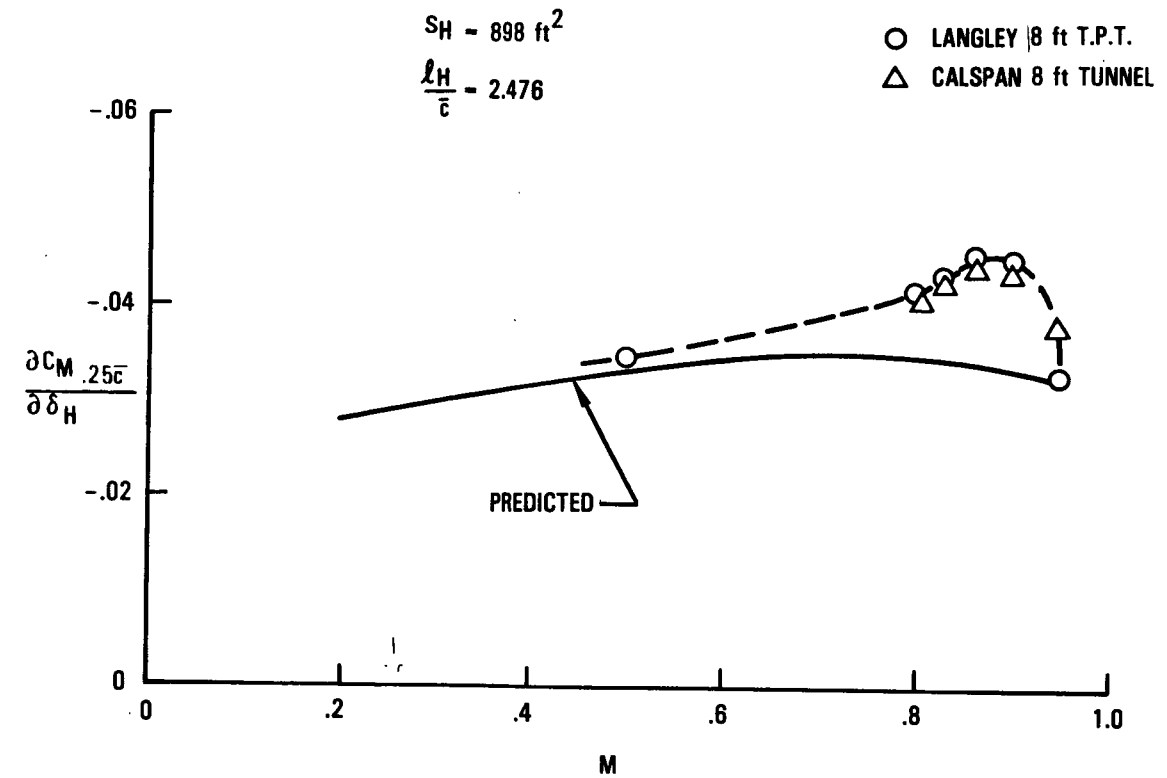

Figure 37. - Longitudinal control effectiveness of the H_{18} stabilizer.

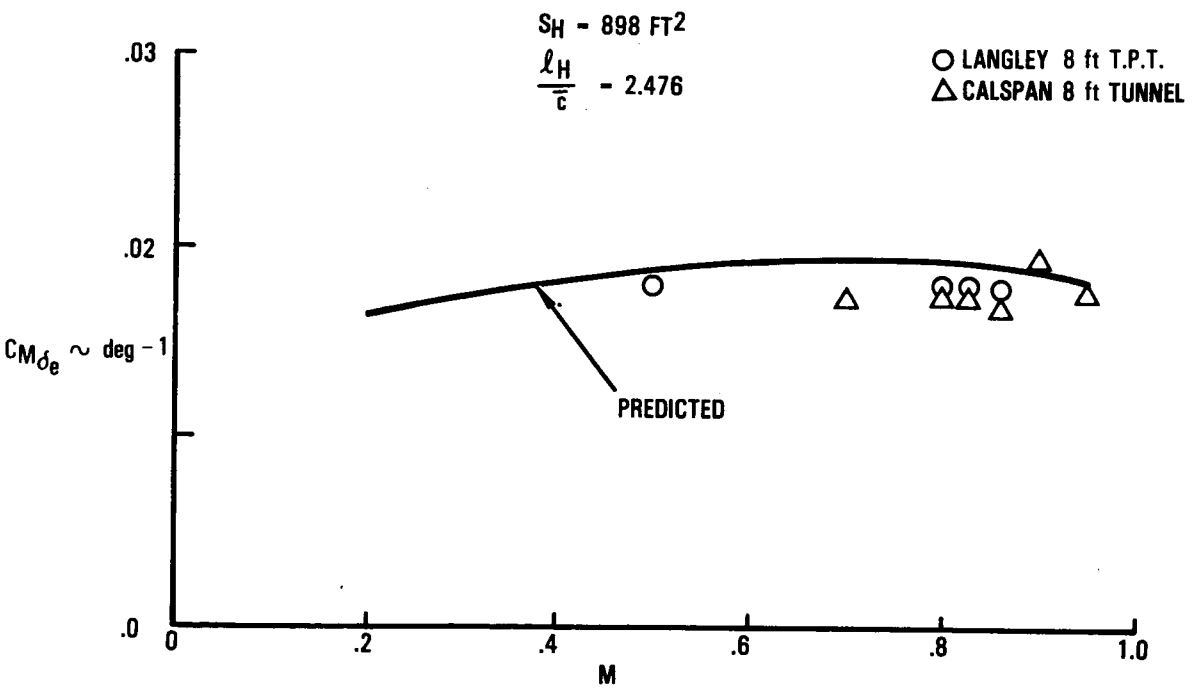

Figure 38. - Longitudinal control effectiveness of H_{18} elevator.

- A comparison of Figures 35 and 39 shows the difference in the Langley and Calspan tests drag data. The Langley data shows a good match at low lift coefficients, but the Calspan data show less drag at high lift coefficients due to the effect of extended wing-tips (lower induced drag). The significant finding from the Calspan test, which confirmed the Langley test results, was that there is very little drag benefit due to the smaller tail.

Pressure distributions.- The pressure distribution data were used to integrate stabilizer pivot moments. These data were also compared with theoretically computed pressures to show the accuracy of current analytical techniques. Pressure data from the Calspan test were used for this comparison, since wing-off, horizontal tail pressure data were not obtained from the Langley test; it was not possible to compare wing-on horizontal tail pressures with theory because of the unknown spanwise distribution of downwash from the wing onto the tail. For a cruise Mach number of 0.83, Figure 40 shows a comparison of wind-tunnel measured pressure data on the tail compared with viscous Jameson-Caughey FLO 22.5 theory. Data in Figure 40 for a tail angle of attack of -3.36 degrees with elevator undeflected show pretty good agreement, particularly at the outboard stations away from the influence of the boattail which is difficult to model. Figure 41 for -2 degrees tail angle of attack with elevator deflected -10 degrees show similarly good agreement except in the region of the elevator where it is difficult to model the turbulent boundary layer separation characteristics.

Stabilizer pivot moments.- Stabilizer pivot moment data were integrated from pressure data and reduced to fit the following linearized equation

$$C_{h_H} = C_{h_{H_O}} + (C_{h_H}/\alpha_H)\ \alpha_H + (C_{h_H}/\delta_e)\ \delta_e$$

Reduced data from the two high-speed tests are shown in Figure 42. There is excellent agreement between data for the two tests except at zero lift, $C_{h_{H_O}}$, where the differences are significant. These differences are attributed to the use of wing-on data from the Langley test and wing-off data from the Calspan test.

Elevator hinge moments.- Elevator hinge moments were determined directly from strain gage measurements. These data were also reduced to fit the linearized equation.

$$c_{h_e} = c_{h_{e_o}} + (c_{h_e}/\delta_e)\ \delta_e + (C_{h_e}/\alpha_H)\alpha_H$$

Reduced data from the two high-speed tests are shown in Figure 43. Here again the data show good agreement except for some differences between the tail hinge moment derivatives due to angle of attack, C_{h_e}/α_H.

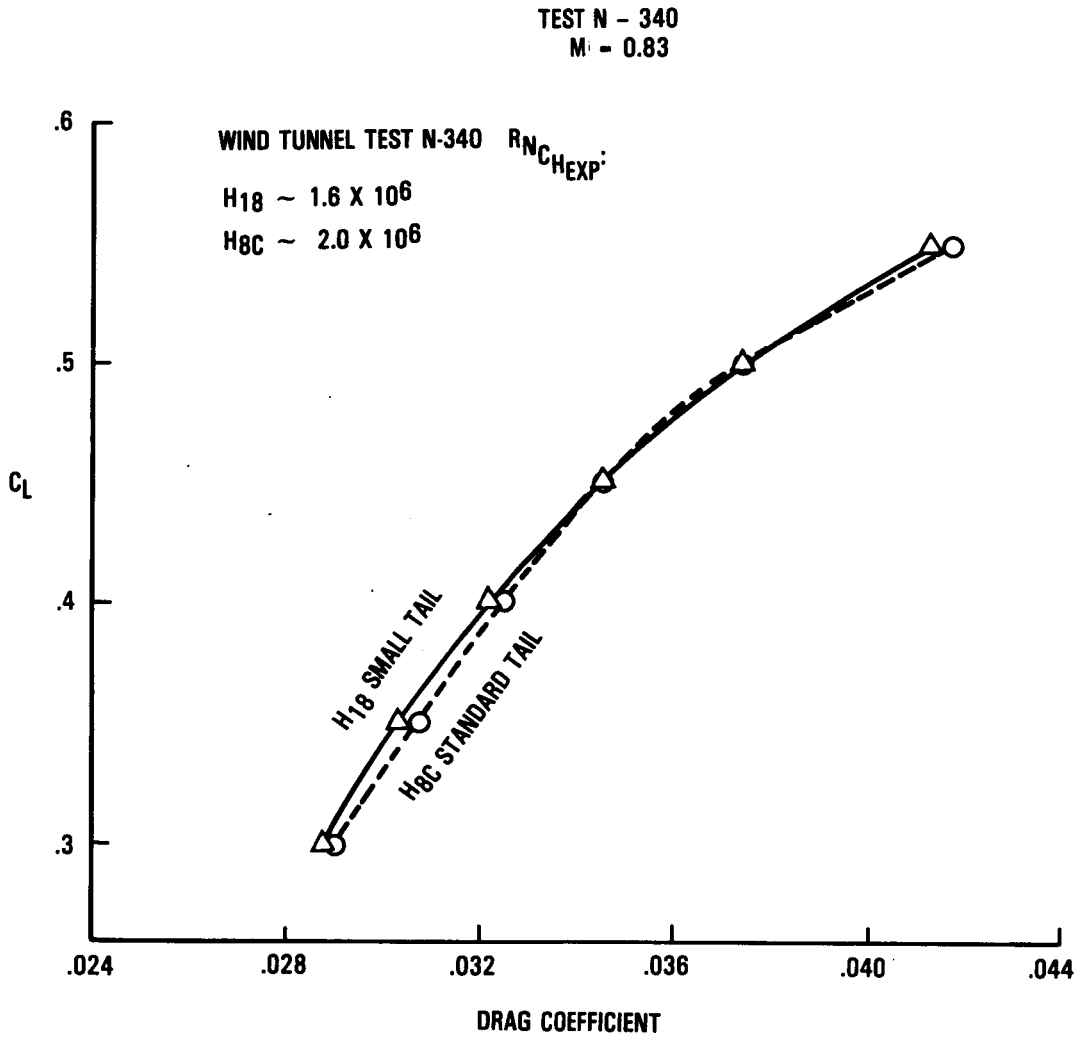

Figure 39. - Zero trim drag polar characteristics of the L-1011 with H_{18} small and H_{8c} horizontal tails - Calspan test results.

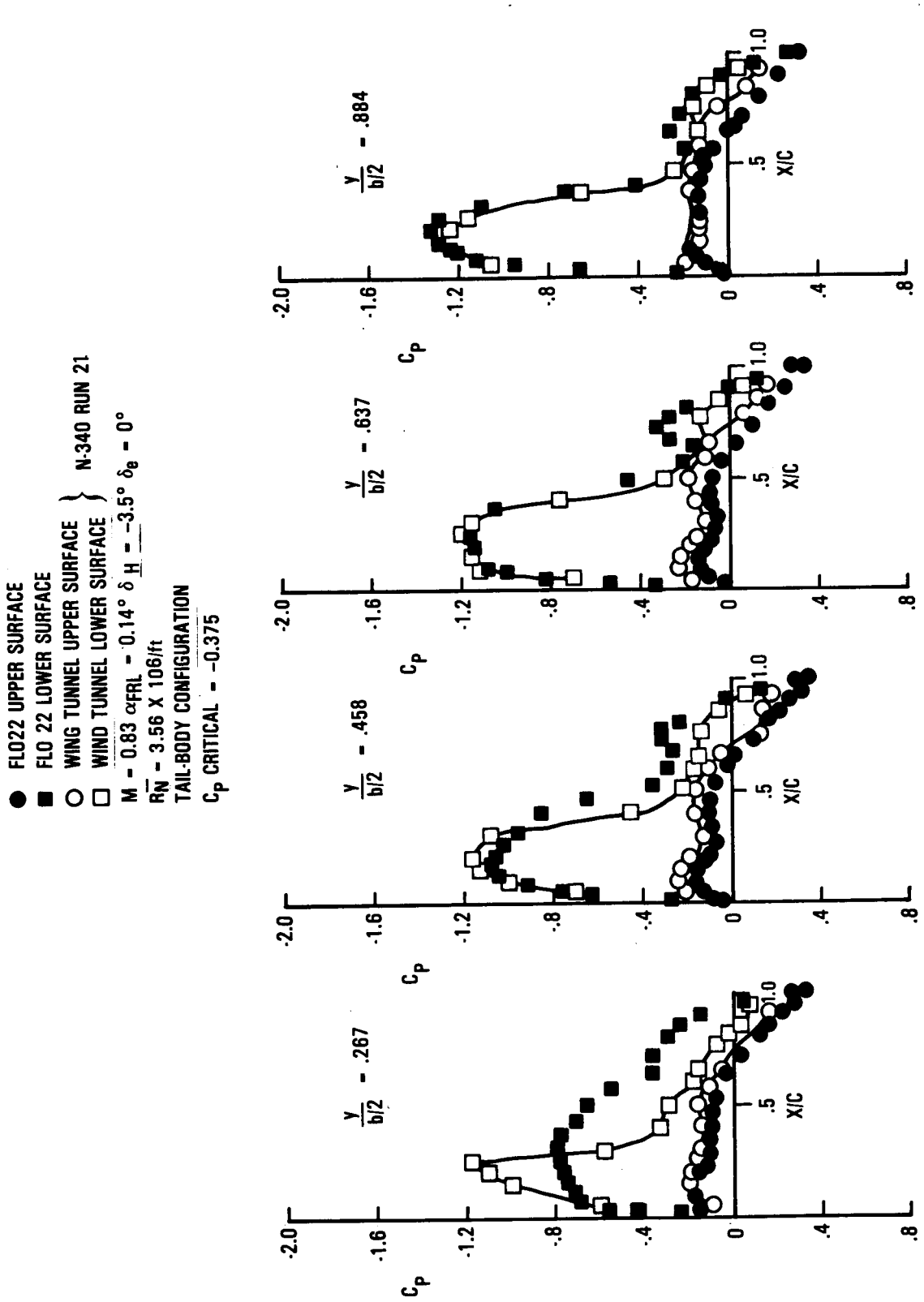

Figure 40. - Theory to experiment pressure distribution comparison.

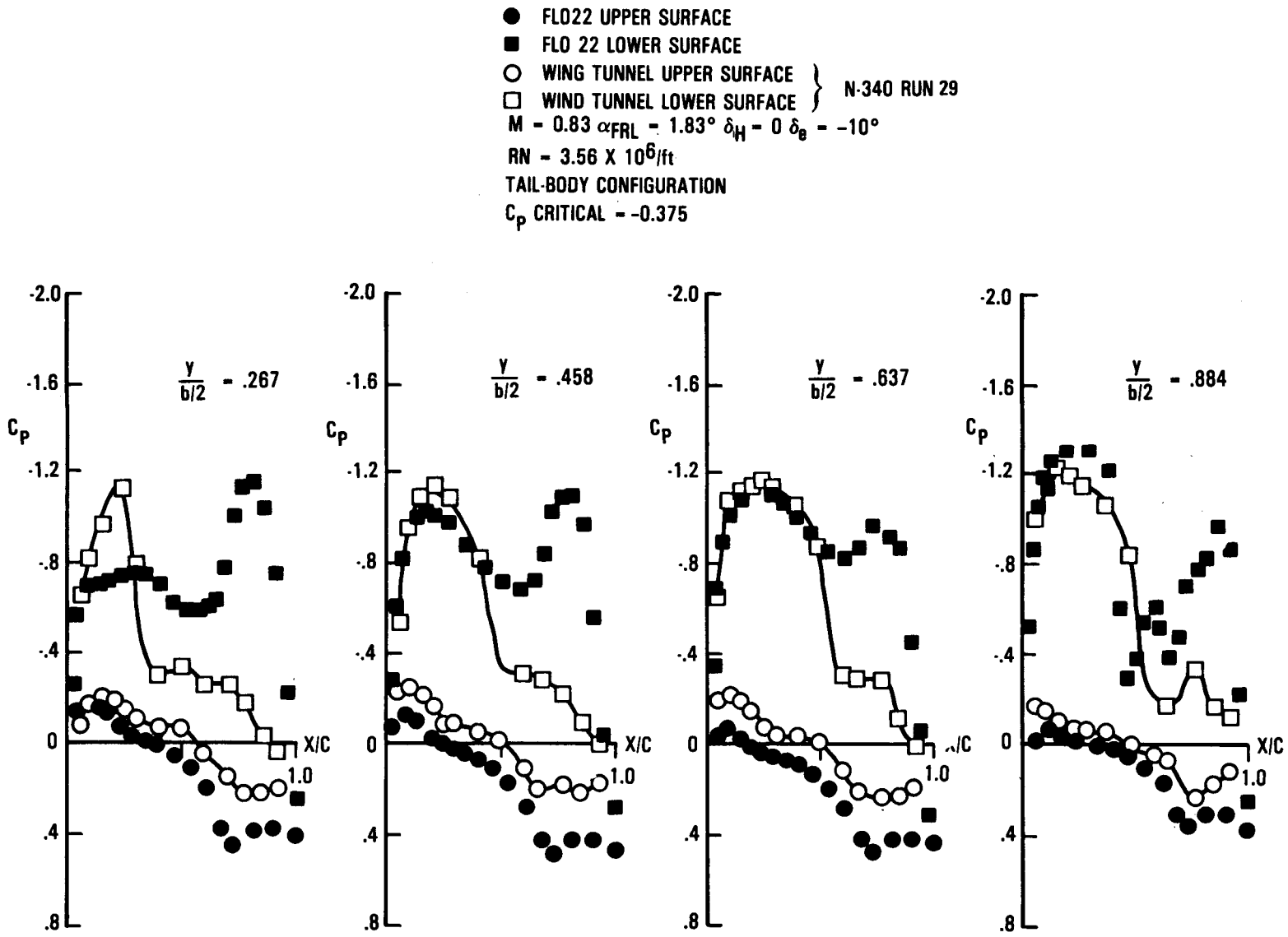

Figure 41. - Theory to experiment pressure distribution comparison - 10° upper elevator.

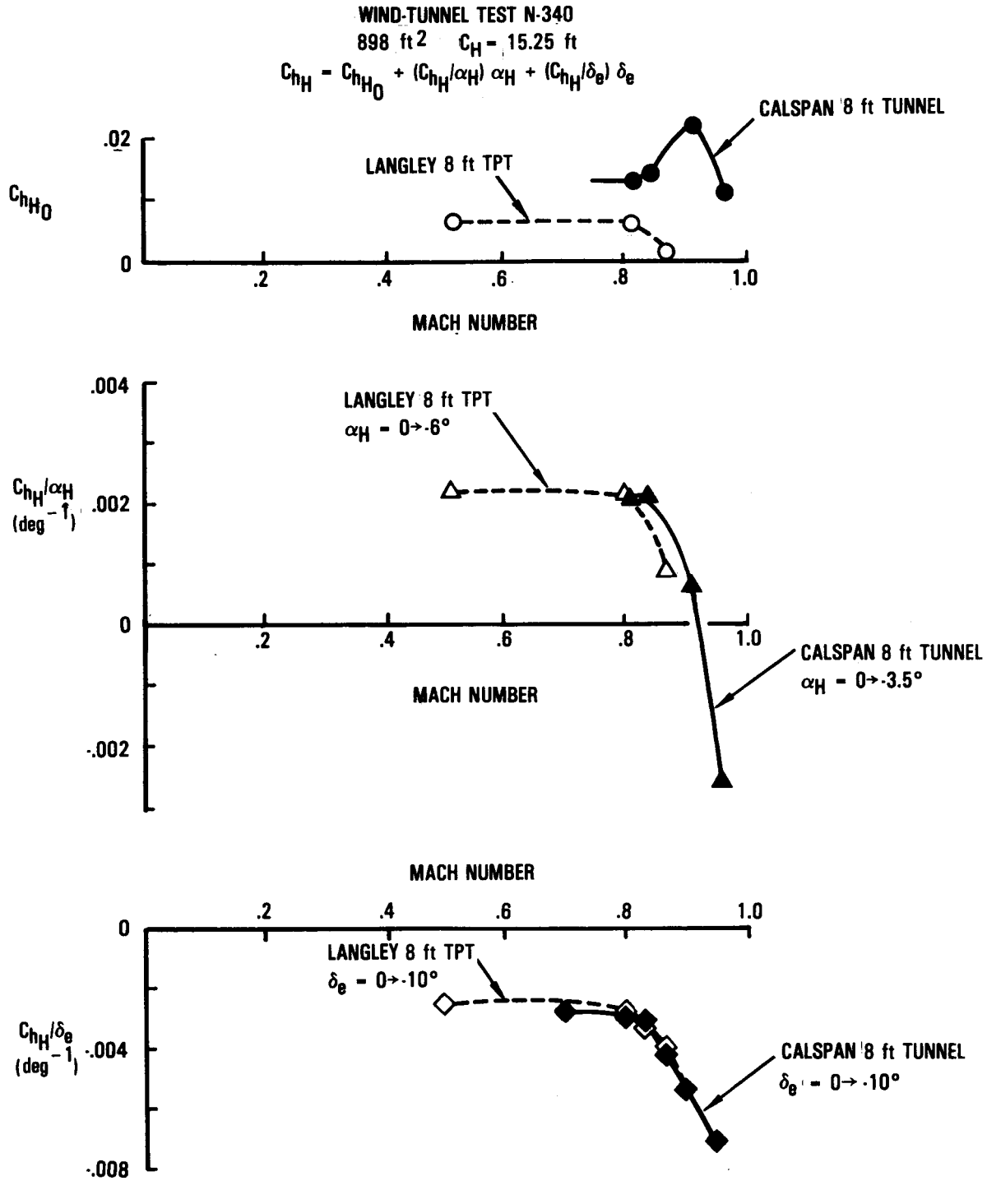

Figure 42. - Linearized stabilizer pivot moment coefficients for the H_{18} small horizontal tail.

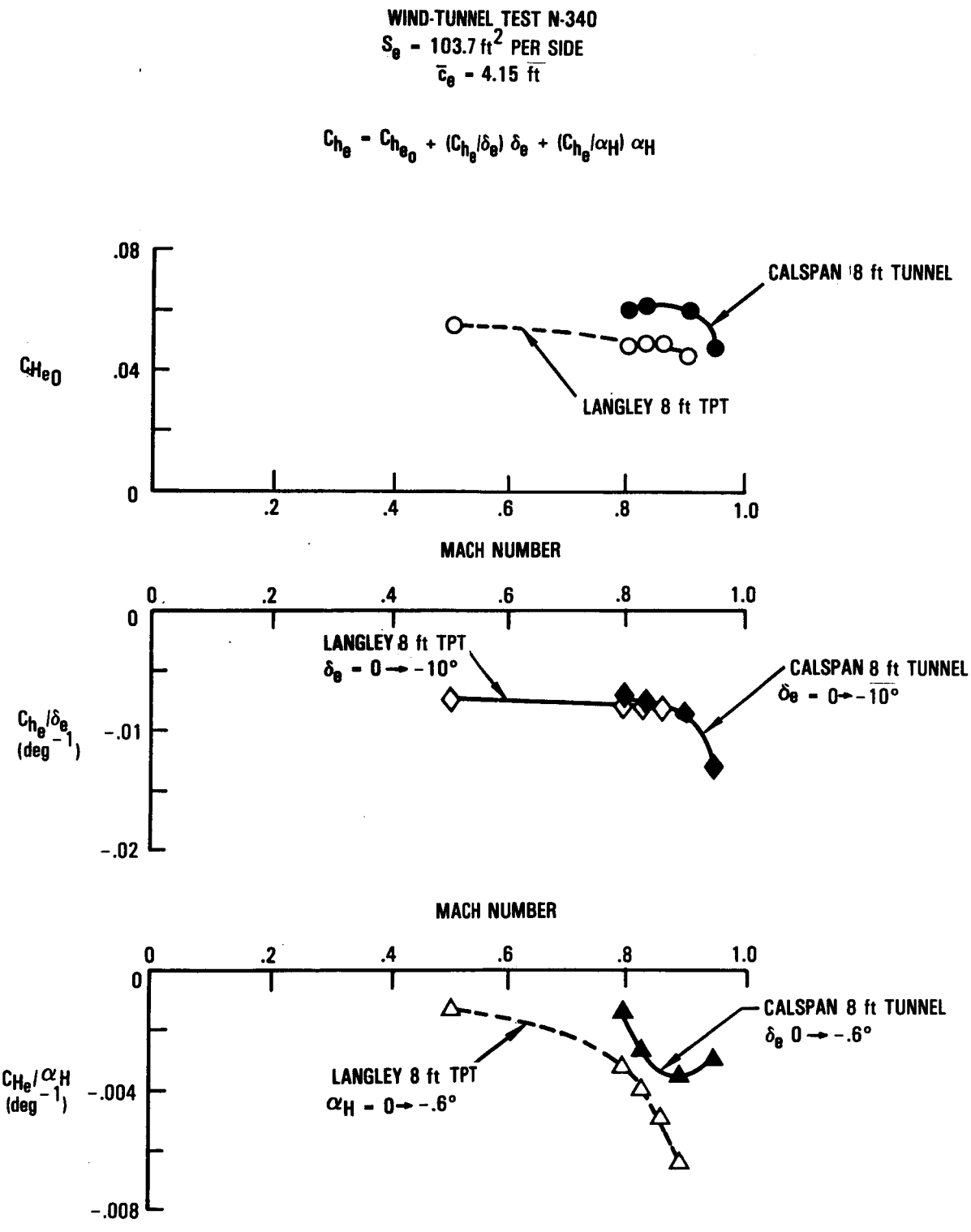

Figure 43. - Linearized elevator hinge moment coefficients for the H_{18} small horizontal tail.

Drag creep.- Upon closer examination of the Calspan data, a tail drag creep problem was discovered going from M = 0.80 to 0.83. This is illustrated by wind-tunnel extracted zero-lift tail drag characteristics shown in Figure 44. This premature drag rise was attributed to premature shock formation on the tail surface compared to that which was predicted by the inviscid Jameson-Caughey transonic code FLO-22 method used to design the airfoil.

Another brief high-speed wind-tunnel test was conducted for final confirmation of the drag characteristics of the H_{18} tail. This test was performed in the Lockheed (4 ft Trisonic Wind Tunnel. This test focused on the comparative drag characteristics of the various tail configurations which had been previously tested. In addition to the 898 ft^2 tail model (H_{18}), the previous 800 ft^2 models (H_{16} and H_{17}) were also tested and compared with the standard 1282 ft^2 tail (H_{8_c}). For this test the tails were mounted alone (i.e., without wing) on a simple test body, so that drag differences between tails represented a significant fraction of total model drag and therefore of balance scale.

A simple wind-tunnel test model, requiring minimal new parts, was devised to maximize the sensitivity to measurement of small differences between characteristics of the various tail configurations. Existing L-1011 fuselage nose and tail sections were attached by means of a short adapter. This test body was mounted on the sting through a six component task balance located in the tail section. The balance center was approximately at 0.25$\bar{c}$ of the horizontal tail. Full span tail surfaces were then attached to their normal mounting trunions on the precision incidence setting device. A tail fairing was added to reduce overall drag level by lessening base drag. This model configuration is shown in Figure 45.

Specific objectives of this test were to:

- Obtain timely verification of recent test results.
- Get comparative horizontal tail drag for all configurations from a single wind-tunnel entry.
- Measure horizontal tail drag on a test configuration where tail increments were significant in terms of balance scale and sensitivity.
- Obtain data at higher Reynolds numbers than in previous tests.

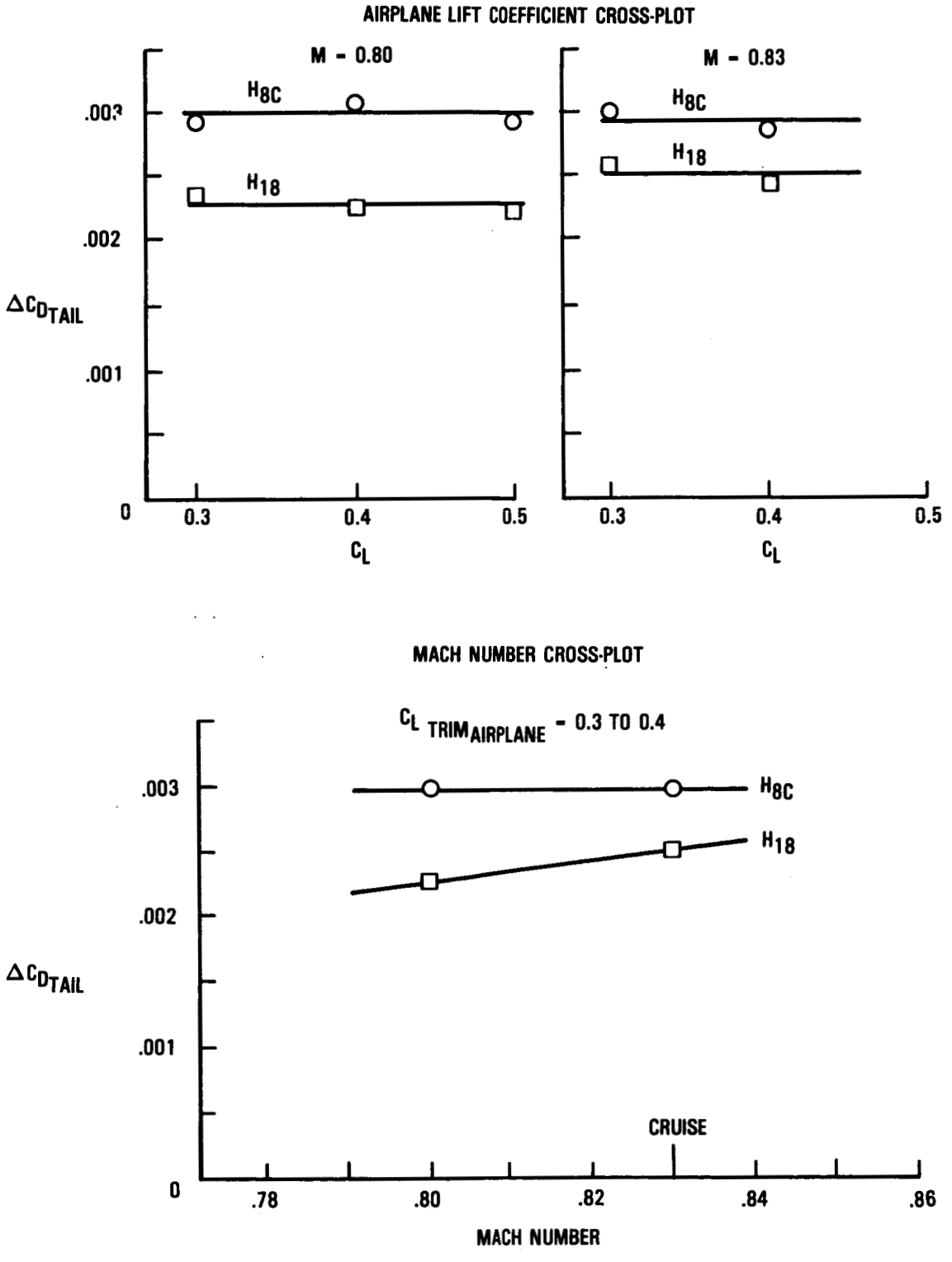

Figure 44. - Wind-tunnel extracted zero lift drag characteristics of the H_{18} small and H_{8c} standard tails.

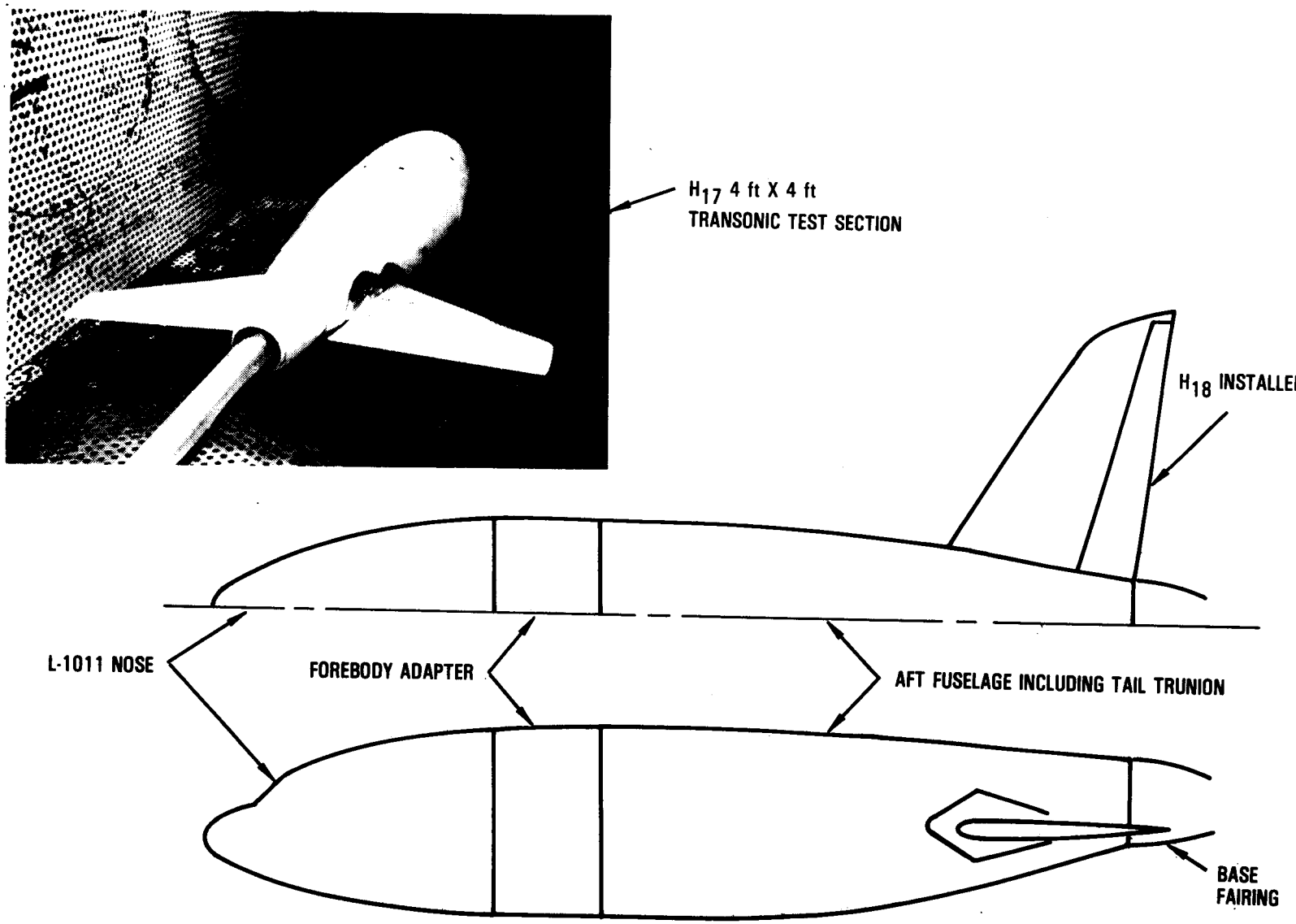

Figure 45. - Horizontal tail test configuration.

Results of this test confirmed the results from all previous tests. These data are shown in Figure 46. The zero-tail-load drag characteristics of the H_{18} small tail show no drag improvement compared to the standard tail (H_{8C}) in the cruise Mach number range (0.80 to 0.83), despite being 30 percent smaller in total area. These results generally agree with data from the Langley and Calspan tests, although the drag levels are generally lower due to the higher Reynolds numbers of the test. Data for the H_{17} and H_{18} tails show that in terms of area differences there is a disproportionate increase in drag going from the 800 to 898 square-foot tail; these tails both have the same airfoil section and, aside from the increase in area, the only differences in geometry were an increase in aspect ratio from 4 to 4.5 and a hyperbolic tip instead of trapezoidal.

4.5 Reconciliation and New Directions

In an attempt to determine the cause for the disproportionate increase in measured drag going from the H_{17} to H_{18} tail, the wind-tunnel models were reinspected to determine if the airfoil contours conformed to specifications. This was done by using a digital height gage to measure actual airfoil ordinates. Measurements were made at span stations where the chords of the two tails were equal. The error from specified airfoil ordinates in terms of height/chord fraction is shown in Figure 47. Overall, H_{17} is slightly thin

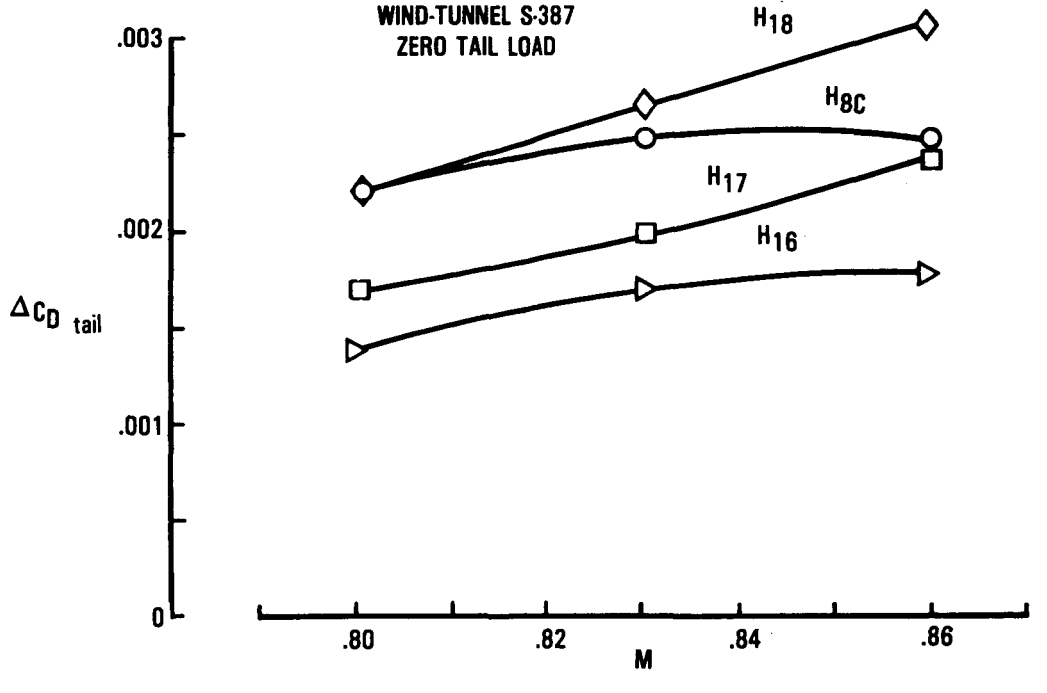

Figure 46. A comparison of the zero-lift drag characteristics of the various horizontal tail designs.

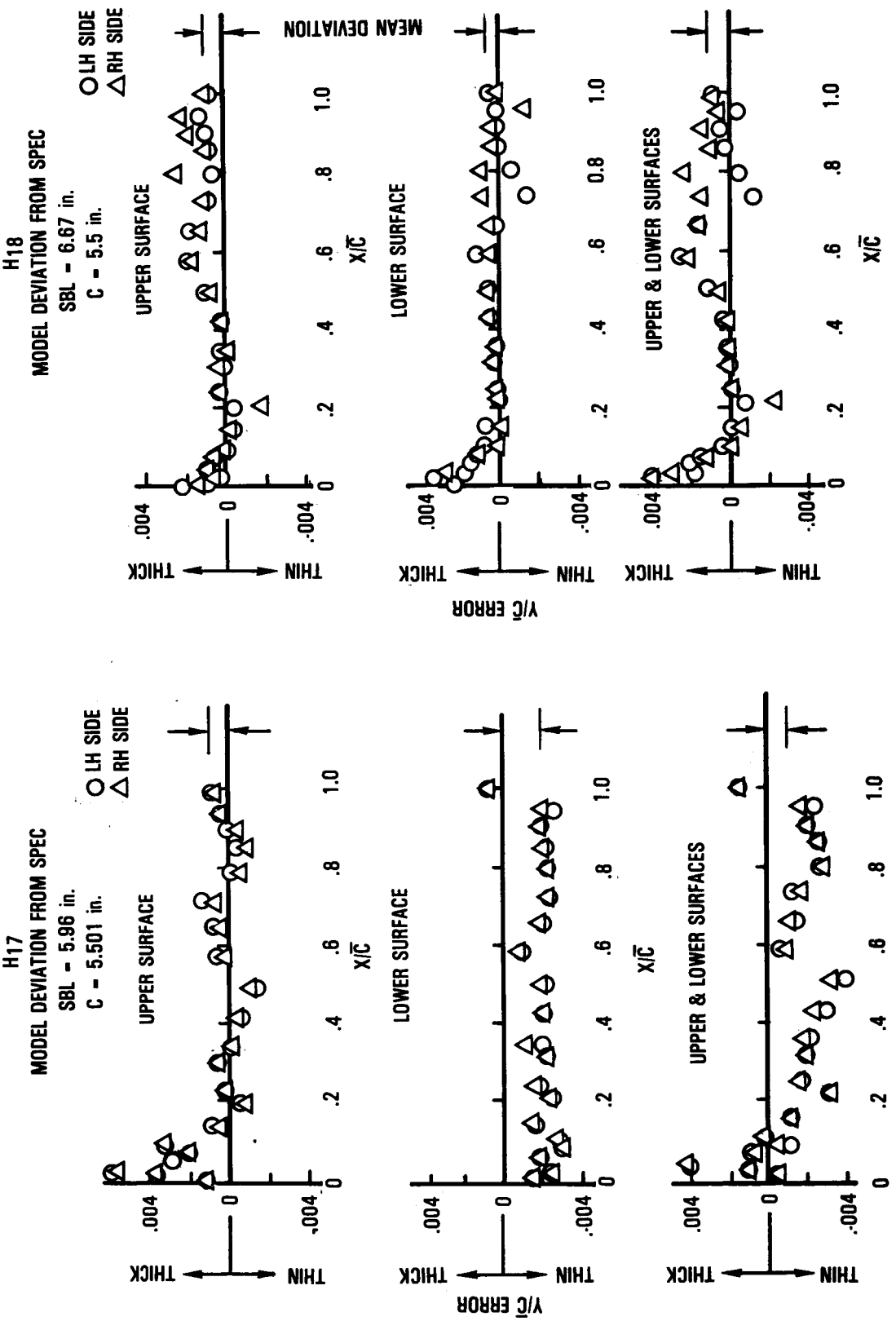

Figure 47. - Model airfoil ordinates deviation from SPE.

and H_{18} slightly thick, however, not an amount that could affect form factor enough to cause a measurable difference in drag coefficient. The mean deviation of ordinates over the whole chord of H_{18} is quite low on both upper and lower surfaces.

Resolution of the drag discrepancy between H_{17} and H_{18} tails was hindered by the fact that the complete airplane model with H_{17} was not tested under contract, and the brief testing that was done did not have a duplicate series of runs with the standard tail (H_{8c}) installed. Testing of H_{17} was performed with limited Lockheed Independent Development funding in conjunction with the L-1011-500 development program. During this test, data for the standard tail were obtained with a wing-body fillet installed, but it had been removed by the time the small tail was tested. Therefore, it was impossible to determine the absolute drag benefits of H_{17} compared to the standard tail.

The H_{18} small horizontal tail is simply an increased area version of the H_{17} configuration for which the design basis was a detailed inviscid Jameson-Caughey transonic flow code 22 analysis (Section 3.2.1). The inviscid version of this program was the only one available at the time for three-dimensional analysis of lifting surfaces. In the meantime, a new viscous version of the program was made available, called FLO 22.5, which incorporated the effects of boundary layer including a separation criterion to flag the point of expected separation, although the effects of separation could not be computed.

With the availability of this improved program, some additional analysis was performed in an attempt to find a technique of predicting the unexpected drag characteristics of the H_{18} tail. This would then provide a method of determining revisions to the tail design which would result in satisfactory cruise drag characteristics.

In performing this analysis, it was found necessary to model the fuselage effect on horizontal tail airflow, because of the significant boattail effect on the inboard section pressures of the tail. Modeling of the fuselage/tail combination is illustrated in Figure 48.

Results of the analysis with and without the fuselage boattail effect are shown in Figure 49. These data show that a good correlation of analysis with wind-tunnel data is obtained, including the drag "creep" effect, by properly modeling the fuselage boattail effect. This finding was significant in that a method was now available for analytically determining modifications to the H_{18} design to eliminate its undesirable drag characteristics.

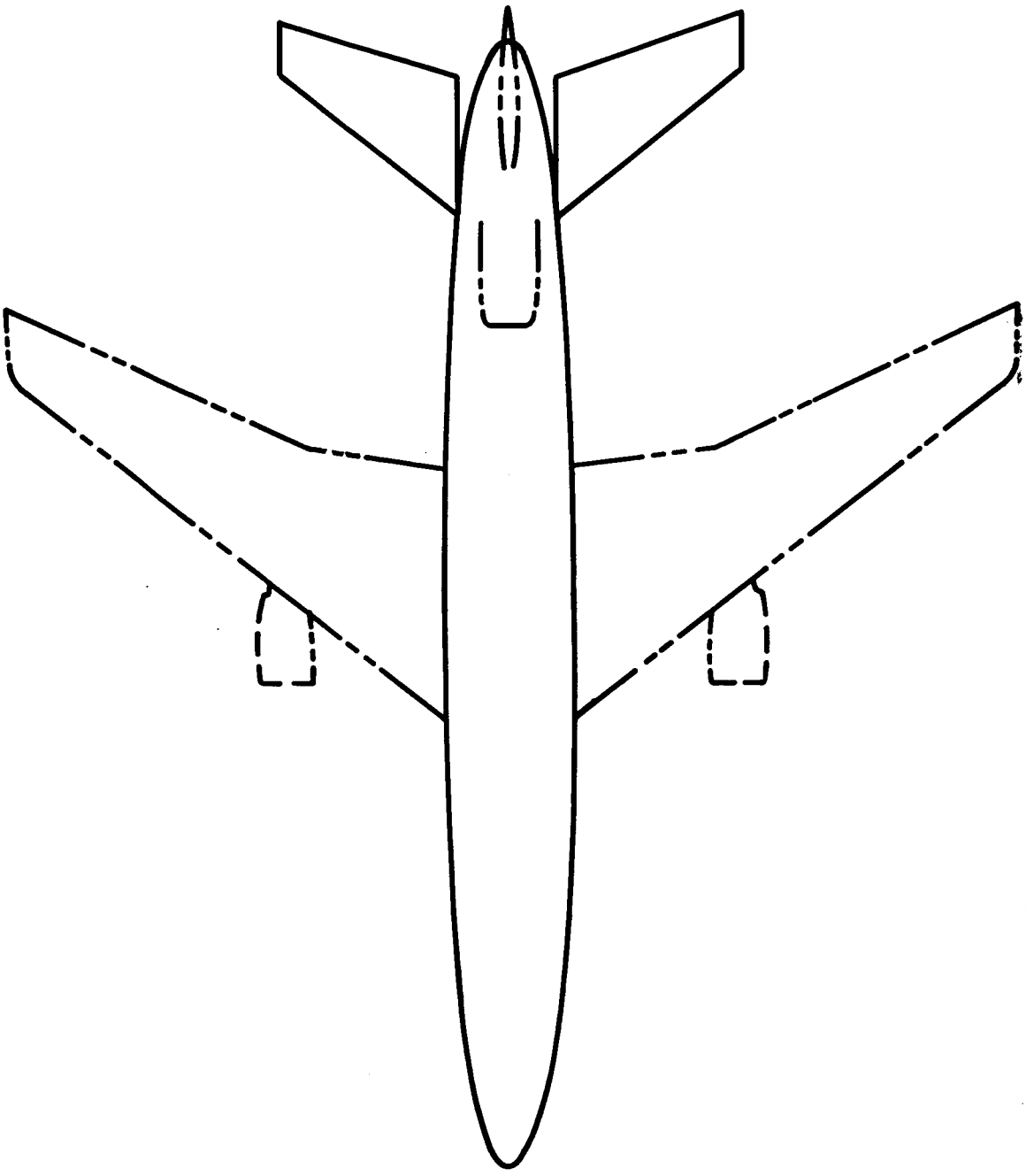

Figure 48. - H_{18} small horizontal tail flow model for viscous Jameson - Caughey FLO 22.5 drag analysis.

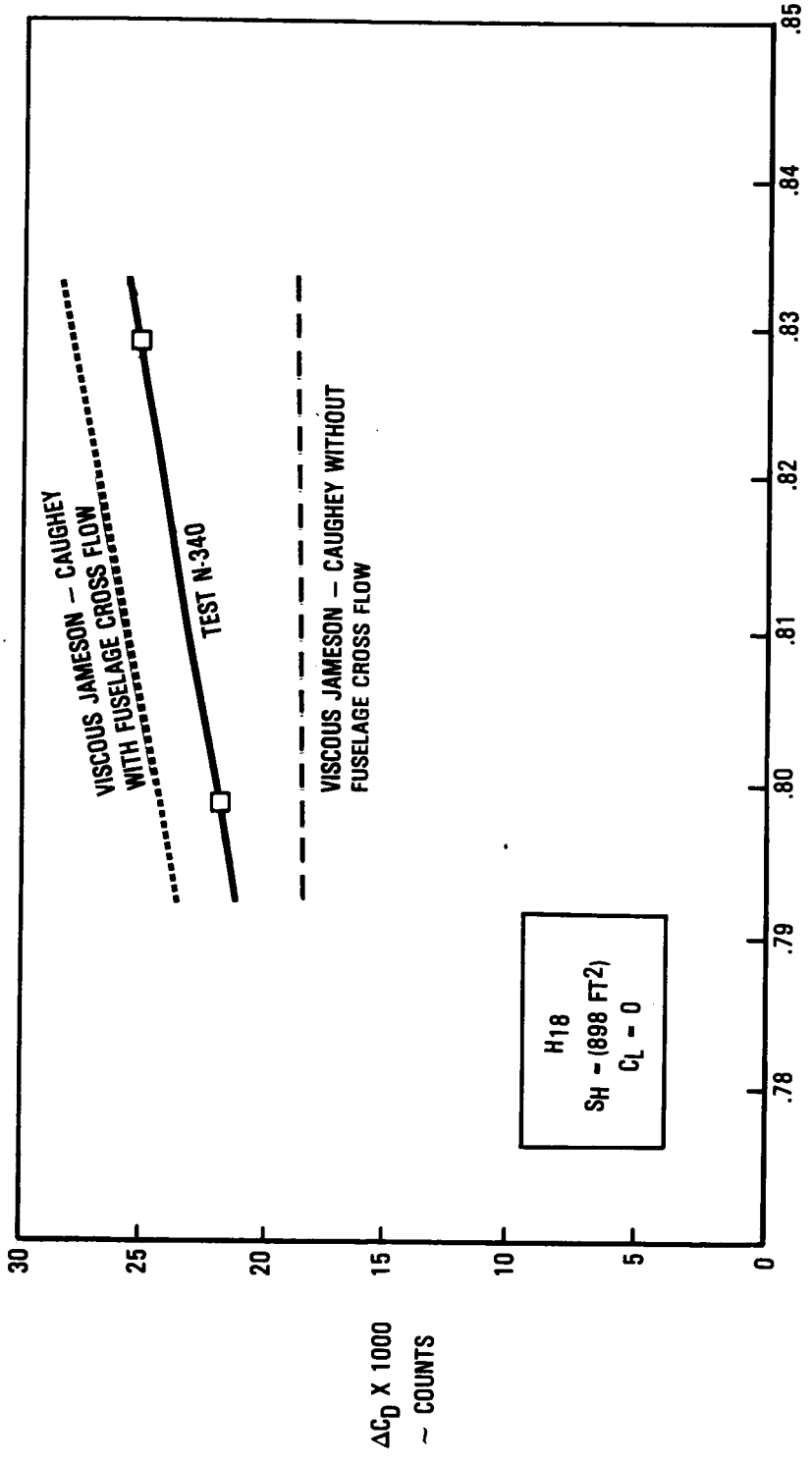

Figure 49.- Comparison of theory with wind tunnel data.

5. FINAL SMALL TAIL DESIGN

5.1 Planform/Airfoil Modification

After the disappointing results which emerged from the H_{18} high-speed test program, a review was held with NASA contract monitors and technical specialists to decide upon an appropriate course of action for determining a satisfactory small horizontal tail design. A review of the results of independent development of small horizontal tail designs by NASA, including wind-tunnel test data, revealed significant differences between NASA and Lockheed designs. The following differences were identified:

	NASA	Lockheed
Sweep Angle ($\bar{c}/4$)	32.5^{o}	25^{o}
Aspect Ratio	3.0	4.5
Airfoil Sections	NASA developed inverse camber & symmetrical	Lockheed Developed inverse camber
Airfoil Thickness	10%	10.5%

After reviewing the data it was concluded that the drag creep problem encountered with the Lockheed configuration could be eliminated by: 1) increasing the sweep angle of the tail, 2) using one of the NASA airfoil sections which is one-half percent thinner, and 3) retaining the 4.5 aspect ratio planform. Of the two NASA airfoils, the symmetrical section was selected because of its good low-speed properties. Ordinates of this airfoil section are shown in Figure 50.

It was further decided to determine an appropriate sweep angle for the horizontal tail by means of viscous Jameson-Caughey analysis, and based on the results of that analysis to proceed with high-speed model construction and testing at Calspan. A decision on low-speed model construction and wind-tunnel testing was delayed until after the results of the high-speed test could be reviewed.

Figure 51 shows the effect of sweep angle on small horizontal tail zero-lift drag, as determined by viscous Jameson-Caughey FLO 22.5 analysis. Based on these results, a sweep angle of 35 degrees was selected for the wind-tunnel model.

5.2 H_{19} Design Layout

A layout of the final small horizontal tail design is shown in Figure 52. The wind-tunnel model designation for this tail is H_{19}. Characteristics of the H_{19} tail compare with the previous designs as shown in Table 6.

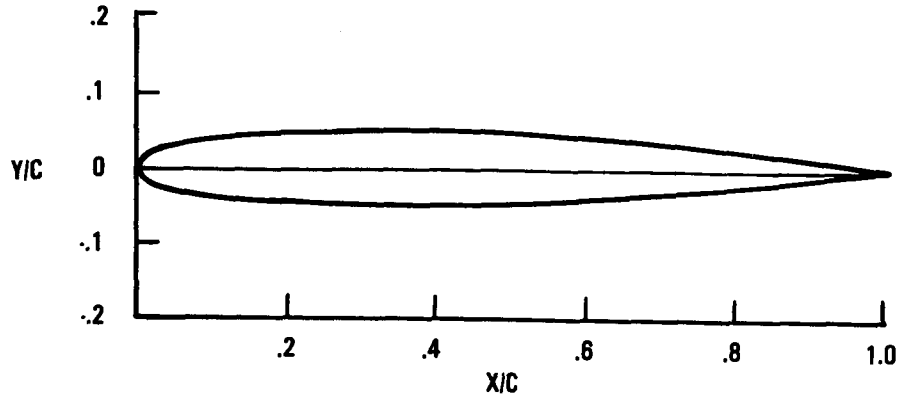

X/C		Y/C	
0.0000	.5600	0.0000	±.0460
.0020	.6000	±.0076	±.0436
.0050	.6400	±.0116	±.0402
.0100	.6800	±.0155	±.0361
.0200	.7200	±.0207	±.0319
.0400	.7800	±.0270	±.0256
.0800	.8000	±.0343	±.0235
.1200	.8200	±.0390	±.0214
.1600	.8400	±.0425	±.0193
.2000	.8600	±.0451	±.0172
.2400	.8800	±.0470	±.0151
.2800	.9000	±.0484	±.0130
.3200	.9200	±.0494	±.0109
.3600	.9400	±.0499	±.0088
.4000	.9600	±.0500	±.0067
.4400	.9800	±.0497	±.0046
.4800	1.0000	±.0490	±.0025
.5200		±.0478	

Figure 50. - NASA symmetrical airfoil section.

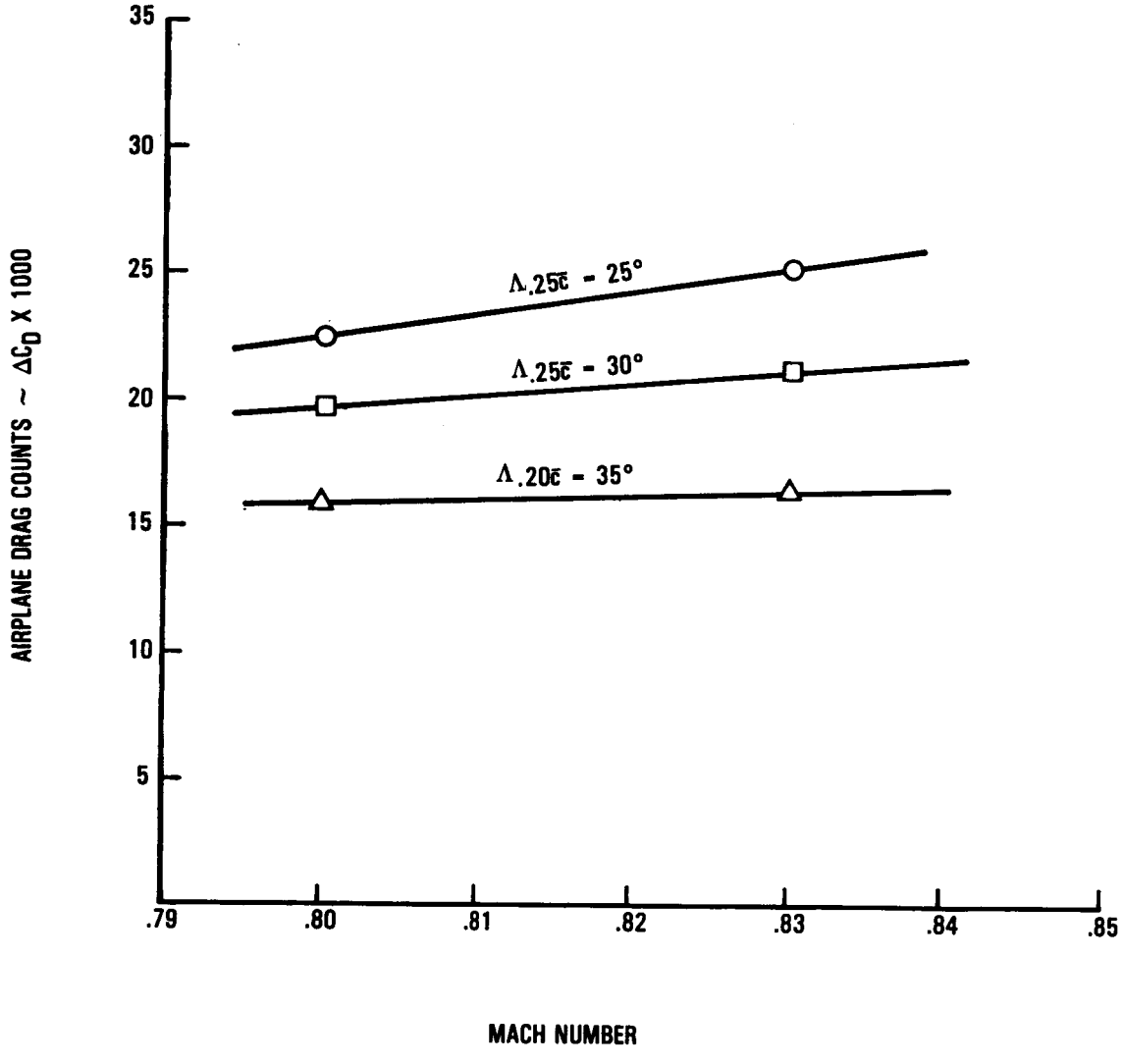

Figure 51. - Viscous Jameson-Caughey H_{19} small horizontal tail zero-lift drag.

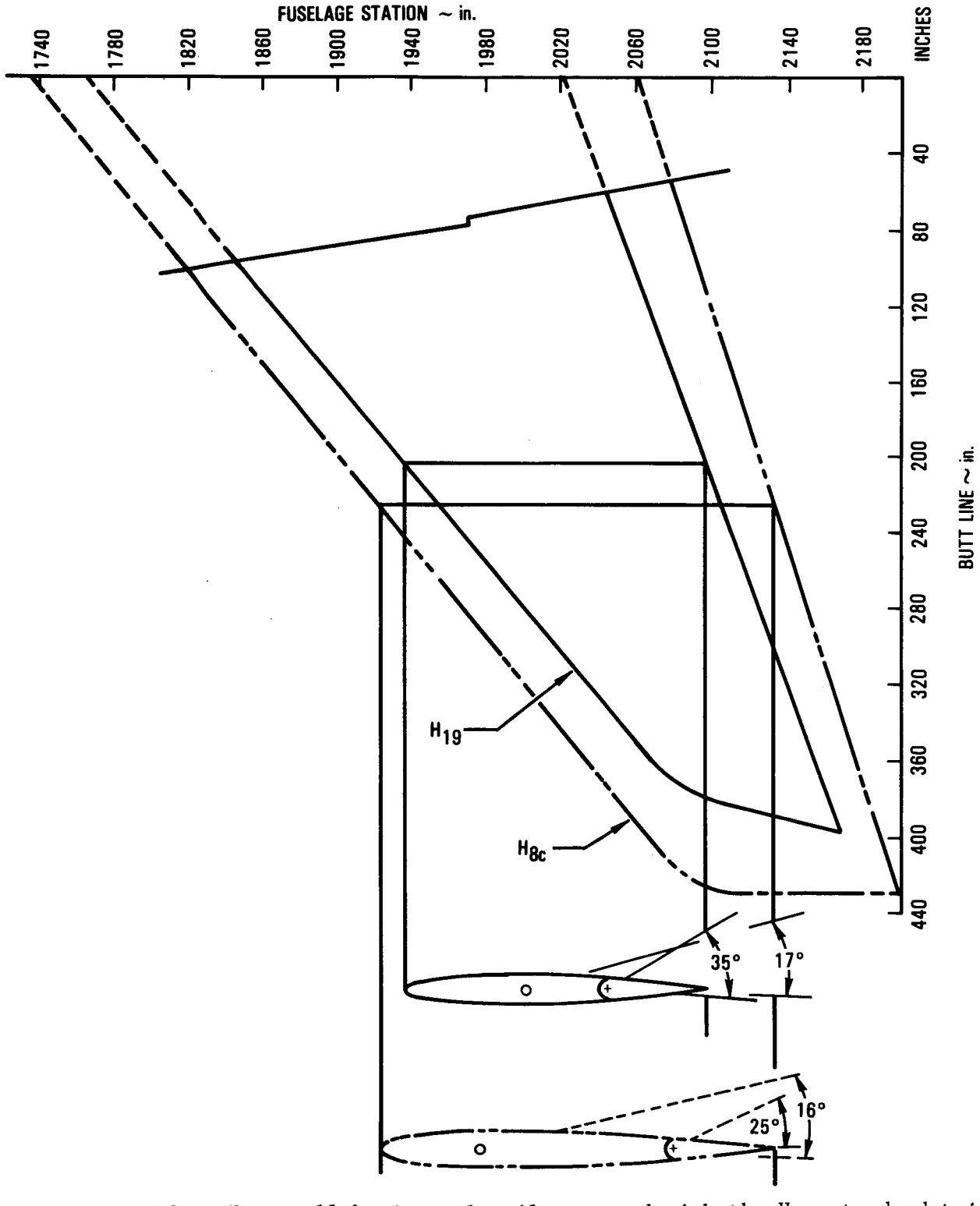

Figure 52. - H_{19} small horizontal tail compared with the H_{8c} standard tail.

Table 6. - H_{19} SMALL TAIL COMPARATIVE DATA

	H_{8c} Standard	H_{16} Small	H_{17} Small	H_{18} Small	H_{19} Small
Aspect ratio	4	4	4	4.5	4.5
Taper ratio	0.33	0.33	0.33	0.33	0.33
Camber	0	0.013c	0.016c	0.016c	0
Leading-edge radius	0.0089c	0.006c	0.036c	0.036c	0.015c
Thickness ratio	0.09	0.09	0.1045	0.1045	0.10
Quarter chord sweep	35^0	28^0	25^0	25^0	35^0
Area, (ft^2)					
Total	1282	800	800	898	898
Exposed	960	552	552	652	644
Exposed/Total	0.75	0.69	0.69	0.73	0.72
Elevator chord ratio	0.25c	0.3c	0.3c	0.3c	0.3c
Stabilizer throw	15^0	20^0	20^0	17^0	17^0
Elevator throw	25^0	40^0	40^0	35^0	35^0

5.3 Wind-Tunnel Test Results

5.3.1 High speed. - High-speed force tests of the H_{19} small horizontal tail were performed during the period 20 to 26 August 1981 in the Calspan 8-Foot Transonic Wind Tunnel. Complete configuration six-component forces and moments were obtained in the Mach number range of 0.70 to 0.95 at angles of attack extending to the limit determined by model dynamics.

The primary purpose of this test was to define the zero trim drag polar characteristics of the L-1011 with H_{19} small and H_{8c} standard horizontal tails. Data for a Mach number of 0.83 are shown in Figure 53. Figure 54 shows the incremental drag characteristics of the H_{19} and H_{8c} tails cross-plotted as a function of airplane lift coefficient. Generally these test results confirm that the desired high-speed drag improvements of the H_{19} small tail were achieved; i.e., the drag was further reduced and the Mach number creep eliminated, compared to previous results for the H_{18} tail (Figure 44). For a cruise condition of 0.4 lift coefficient and 0.83 Mach number, the zero-lift drag for the H_{19} tail is 20 counts and for the standard tail (H_{8c}) 26 counts. The difference of 6 counts at wind-tunnel scale is equal to the drag benefit that was originally predicted for the H_{18} (Section 3.3.3). This translates into an overall cruise L/D benefit of about 2 percent, including the weight reduction of the smaller tail.

Thus having achieved the long sought-after cruise drag benefits of a smaller tail, its acceptability was now dependent on results of low-speed control effectiveness tests.

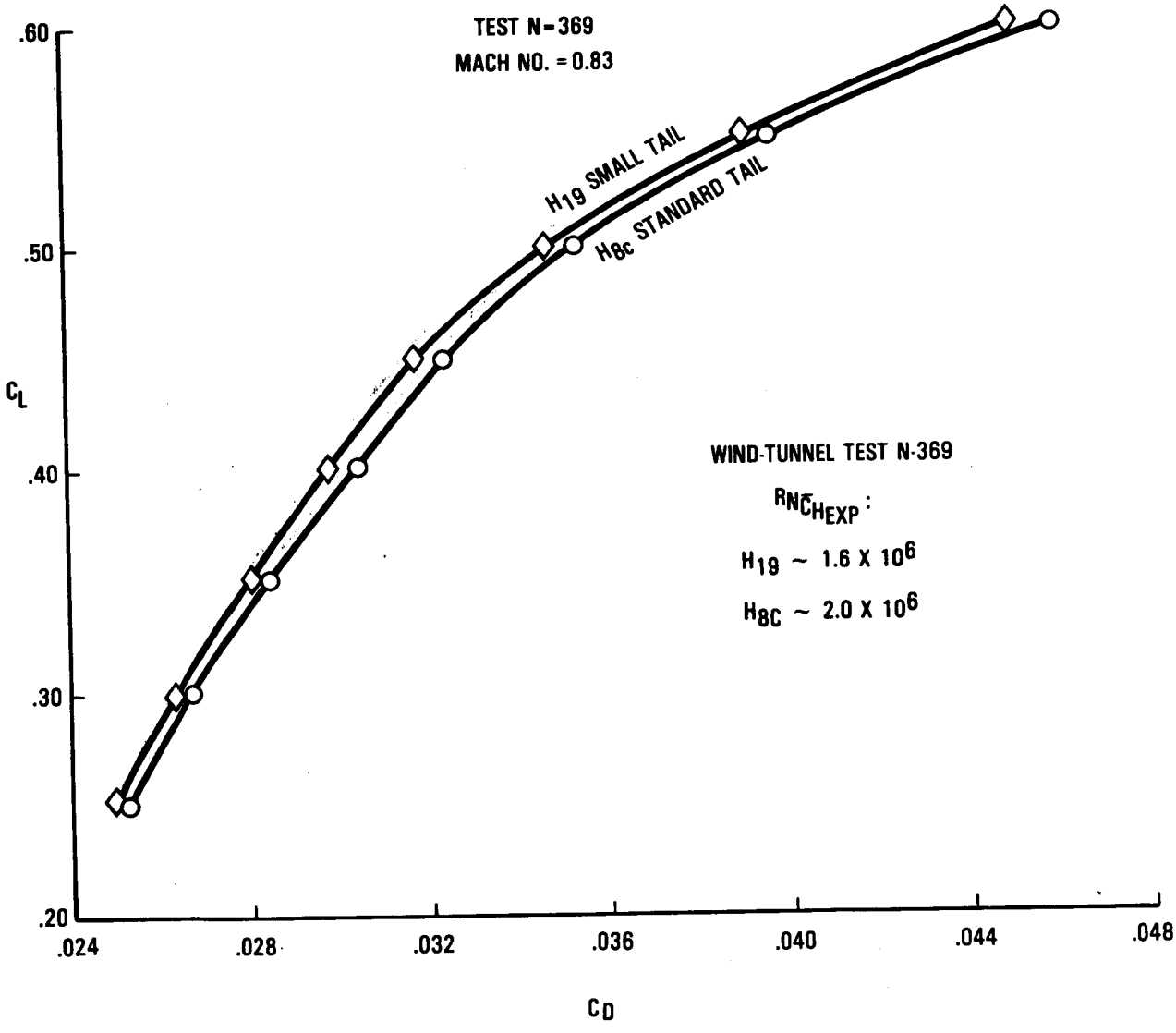

Figure 53. - Zero trim drag polar characteristics of the L-1011 with H_{19} small and H_{8c} standard horizontal tails - Calspan test results.

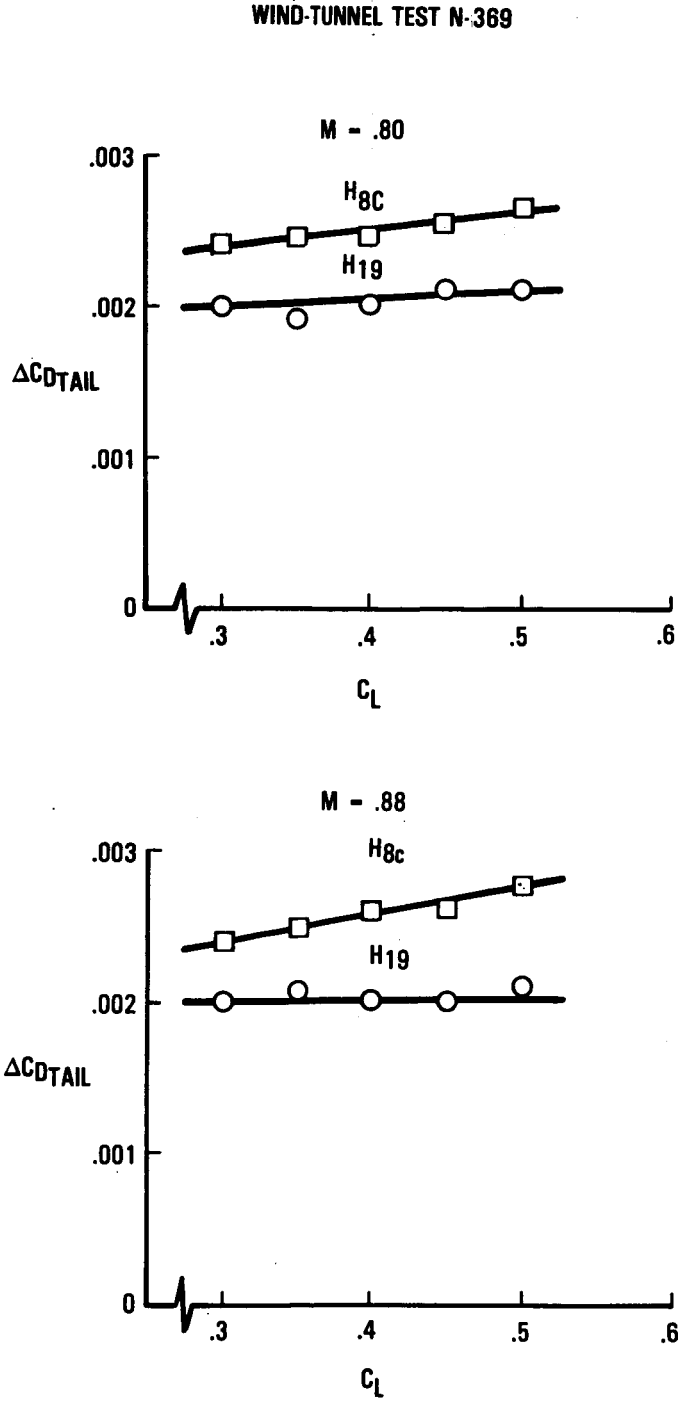

Figure 54. - Zero lift drag characteristics of the H_{19} small and H_{8c} standard horizontal tails.

5.3.2 Low speed. - The H_{19} small horizontal tail configuration was wind-tunnel tested in the NASA/Ames 12-Foot Pressure Tunnel during the period from 4 through 15 January 1982. This was a low-speed, high Reynolds number test designed to obtain the control effectiveness of the small horizontal tail with wing flaps at the maximum takeoff setting 26 degrees, which defines the tail size requirement for takeoff rotation.

Results of this test were used to extract the maximum lift characteristics in Figure 55 and 56 for the H_{19} small and H_{8c} standard horizontal tails. These data show that the H_{19} tail achieved a lift coefficient of -1.26, which is 10 percent below the target value of -1.4. However, the data also show that the small tail design was partially successful in that it obtained a $C_{L_{max}}$ 11 percent higher than the standard tail, even though a much higher percentage of the tail is embedded in the fuselage. Still, the small tail design did not meet the requirement of obtaining the same control power as the standard tail for nose-wheel lift-off at the forward center-of-gravity limit, which implies some restriction of c.g. range for this design to be usable.

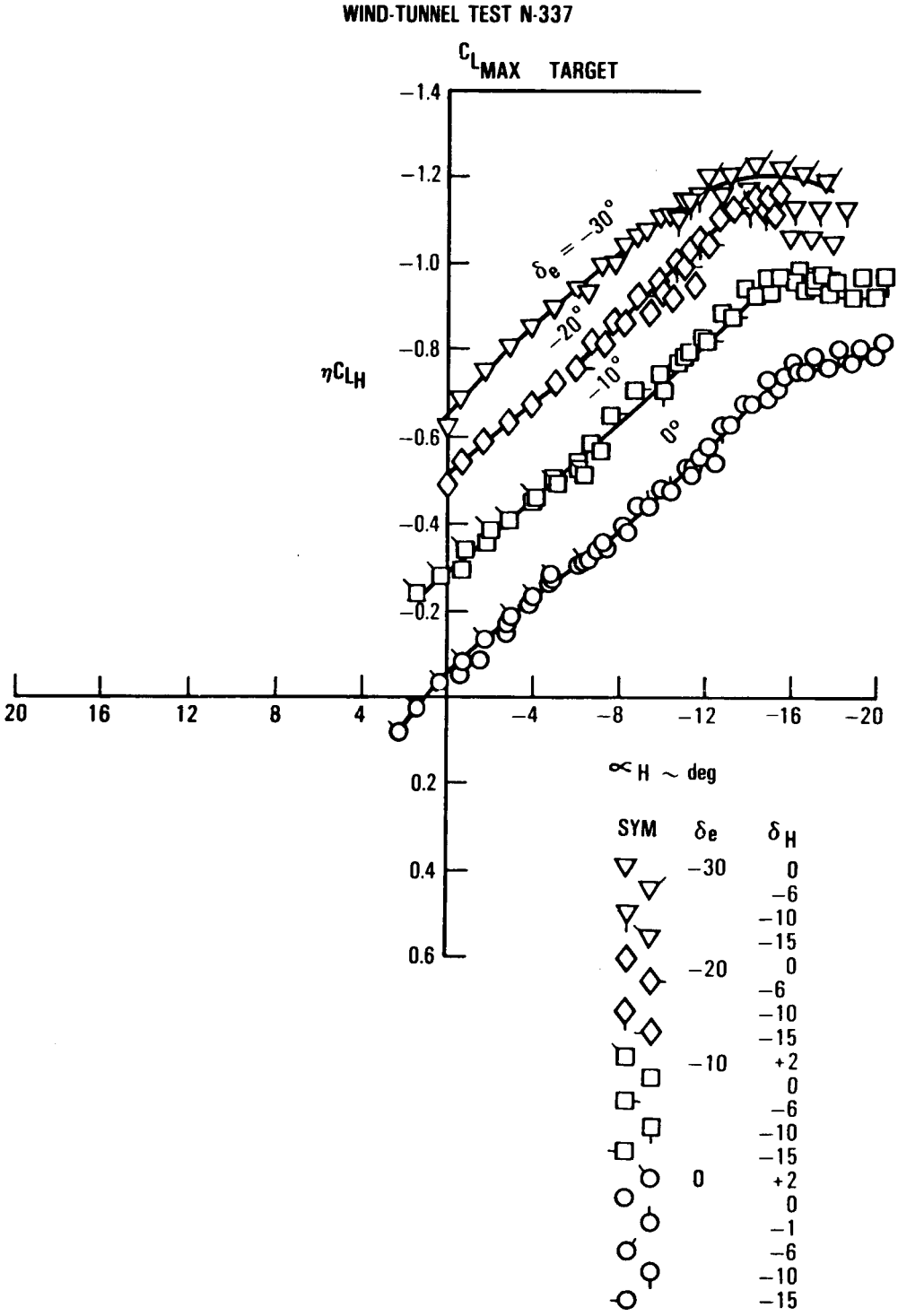

Figure 55. H_{19} small tail high-lift characteristics.

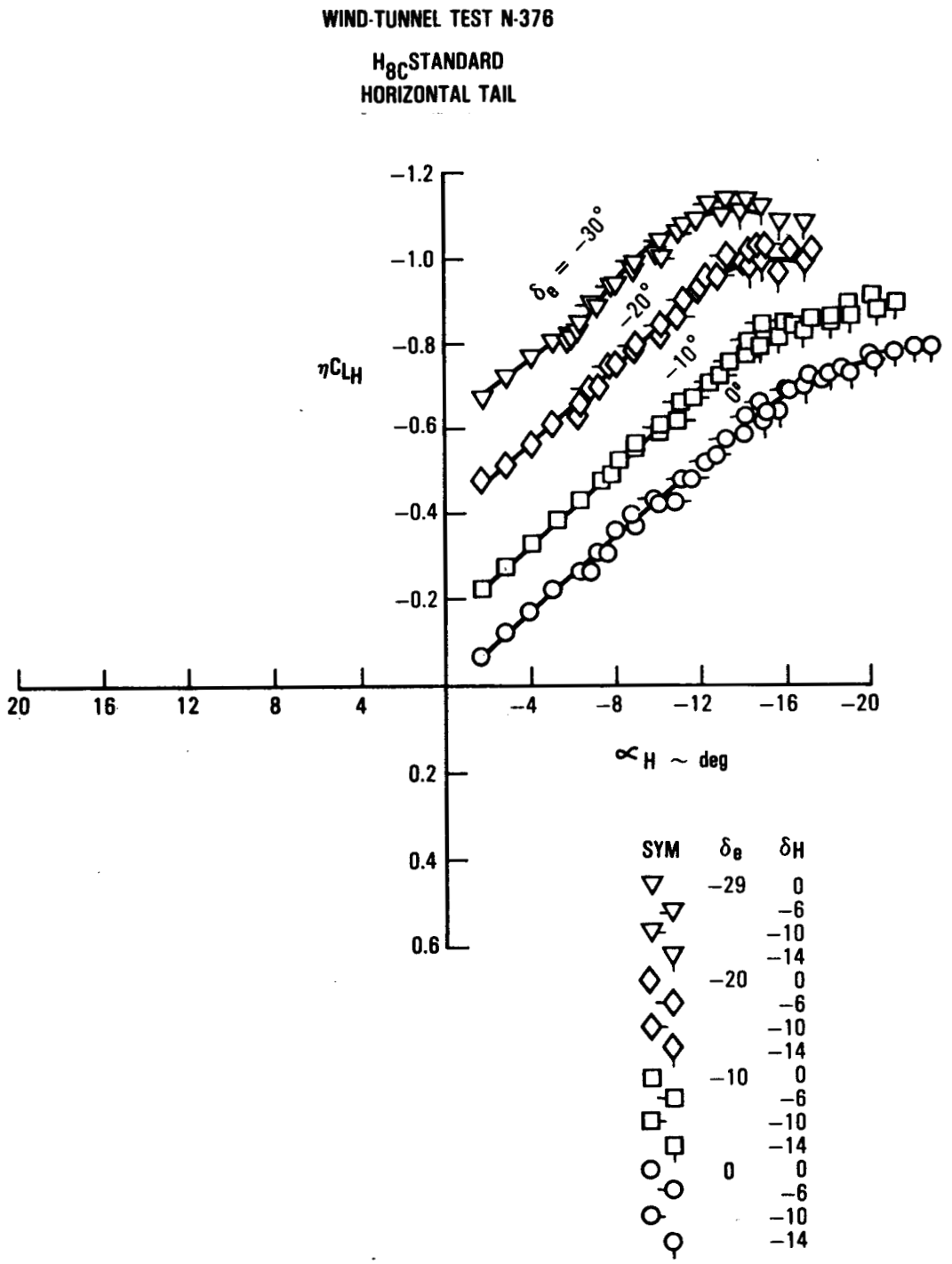

Figure 56. H_{8c} standard horizontal tail high-lift characteristics.

CONCLUSIONS

In addition to longitudinal stability requirements, horizontal tails are sized to meet certain control requirements for a specified center-of-gravity range. Therefore, in order to reduce tail size by using active controls to provide stability augmentation, it is necessary to proportionally enhance the aerodynamic effectiveness of the surface to retain the same control power capability.

This study has shown that by designing the tail to achieve the desired high-speed drag benefits, it was not possible to achieve the required low-speed control capability without resorting to sophisticated high-lift devices (leading-edge flaps, slats, etc.). This introduces an unwanted additional complexity in horizontal tail design which would require extensive development and testing to ensure reliability and flight safety in the event of a system failure.

The alternative would be to manage the center-of-gravity location of the airplane more carefully, either by loading or fuel pumping, to reduce the range of c.g. movement, thus decreasing the control requirements of the tail. If this could be accomplished, and by adhering to the criterion that at least neutral stability be retained, then the results of this study show that an active control small horizontal tail could be designed for next generation transport aircraft to reduce cruise drag by 2 to 3 percent.

REFERENCES

1. Urie, D.M., and Passer, J.S. "Aerodynamic Development of a Small Horizontal Tail for an Active Control Released Stability Transport Application," AIAA Paper 79-1653, 1979.

2. Bingham, Gene J. and Noonan, Kevin W., "Low Speed Aerodynamic Characteristics of Five Helicopter Blade Sections at Reynolds Numbers from 2.4×10^6 to 8.4×10^6," NASA TMX-2467, 1972.

3. Jameson, A., Caughey, D.A., Newman, P.A., and Davis, R.M., "A Brief Description of the Jameson-Caughey NYU Transonic Computer Program - FLO 22," NASA TM-73996, 1976.

4. Jameson, A., Caughey, D.A., "Numerical Calculation of the Transonic Flow Pact a Swept Wing," NASA-CR-153297, 1977.

1. Report No.	2. Government Accession No.	3. Recipient's Catalog No.
NASA CR-172278		

4. Title and Subtitle	5. Report Date
Development of a Reduced Area Horizontal Tail for a Wide Body Jet Aircraft	February 1, 1984
	6. Performing Organization Code
7. Author(s)	8. Performing Organization Report No.
Jerry J. Rising	LR 30645
	10. Work Unit No.
9. Performing Organization Name and Address	
Lockheed California Company Burbank, California	11. Contract or Grant No. NAS1 - 15326
	13. Type of Report and Period Covered Contractor Report Jan 1982 - Dec 1982
12. Sponsoring Agency Name and Address	14. Sponsoring Agency Code
National Aeronautics and Space Administration Washington, DC 20546	

15. Supplementary Notes

Langley technical monitor: Dennis W. Bartlett,
Final Report

16. Abstract

A research program was performed to develop a reduced area horizontal tail configuration for the L-1011 that would provide fuel savings of approximately two to three percent. The scope of the program included design criteria definition, aerodynamic analysis, tail configuration development, and wind tunnel tests.

Three planform configurations were evaluated: one with a reduced area of 38 percent and two with a reduced area of 30 percent relative to a Lockheed L-1011 standard tail. Principal planform parameters evaluated were aspect ratio and quarter chord sweep angle. The airfoil parameters evaluated included camber, leading edge radius, and thickness ratio. The L-1011 has a flying stabilizer with a geared elevator. Consequently, stabilizer/elevator throw was included in the evaluation.

High speed wind tunnel tests showed drag reductions of approximately twenty percent for the 38 percent small tail and for the 30 percent small tail with the best airfoil. However, the tails did not achieve the low speed maximum lift characteristics required for the L-1011 without resorting to sophisticated high-lift devices. Thus, a forward c.g. limitation would have to be imposed on the airplane. On a new aircraft design, optimum landing gear location, controlled c.g. range, and increased stabilizer/elevator throws could possibly solve the lift deficiency problem, and it would be feasible to utilize the small tail to realize significant fuel savings.

17. Key Words (Suggested by Author(s))	18. Distribution Statement
Longitudinal Control, Horizontal Tail Design, Aerodynamic Efficiency, Drag Reduction	[redacted]

19. Security Classif. (of this report)	20. Security Classif. (of this page)	21. No. of Pages	22. Price*
Unclassified	Unclassified	98	